

**THE ANTIMICROBIAL ACTIVITY OF ZINC OXIDE NANOPARTICLES
SYNTHESIZED WITH PLANT EXTRACTS AGAINST *STAPHYLOCOCCUS
AUREUS***



GISELA KRIEK

UNIVERSITY *of the*
WESTERN CAPE

A thesis submitted in partial fulfilment of the requirements for the degree of Magister
Scientiae in the Department of Biotechnology, University of the Western Cape

23rd July 2019

**THE ANTIMICROBIAL ACTIVITY OF ZINC OXIDE NANOPARTICLES
SYNTHESIZED WITH PLANT EXTRACTS AGAINST *STAPHYLOCOCCUS
AUREUS***

Gisela Kriek

KEYWORDS

Nanoscience

Calendula officinalis

Zinc oxide nanoparticles

Green synthesis

Antimicrobial resistance

Methicillin resistant *Staphylococcus aureus*



Abstract

THE ANTIMICROBIAL ACTIVITY OF ZINC OXIDE NANOPARTICLES SYNTHESIZED WITH PLANT EXTRACTS AGAINST *STAPHYLOCOCCUS AUREUS*

G. Kriek

M.Sc Thesis, Department of Biotechnology, University of the Western Cape

Nanoparticles using a green synthesis production method is of increasing interest for biomedical applications. Zinc oxide is currently used in medicinal and cosmetic formulations, and zinc oxide nanoparticles have potential in biomedical applications. Antibiotic-resistant bacterial infections are of growing concern globally, and novel antimicrobial agents are drastically needed. In this work, zinc oxide nanoparticles were synthesized using *Calendula officinalis* flowers aqueous extract and zinc nitrate hexahydrate using a single-pot green synthesis approach. The synthesized particles were calcined and characterised using UV-Vis spectrophotometry, Dynamic Light Scattering (DLS), X-Ray Diffraction (XRD), Transmission Electron Microscopy (TEM), Scanning Electron Microscopy (SEM), Thermogravimetric Analysis (TGA), Fourier-Transform Infrared Spectroscopy (FTIR) and Nuclear Magnetic Resonance Imaging (NMR). Quasi-spherical, hexagonal phase zinc oxide nanoparticles with core size <10nm according to TEM and average size of ~53nm according to XRD were successfully synthesized. The particles tended towards agglomeration. Antioxidant assays were run to determine the reducing power, antioxidant activity, and presence of polyphenols in the final products. The final product possessed antioxidant activity, polyphenols and had reducing power, confirming the constituents from *Calendula officinalis* playing a role in the reduction of the zinc ions and capping of the zinc oxide nanoparticles. Minimum inhibitory concentration of the samples by tube dilution was conducted to determine potential of the samples as antimicrobial agent against methicillin-resistant *Staphylococcus aureus*, using Clindamycin as control. Results of antimicrobial studies indicate the need for investigation of MIC using a variety of concentrations of the samples, and a variety of solvents, in order to determine exact MIC values. Further work is needed to improve the methodology to obtain particles that have a narrow size distribution, that are well dispersed, and are of higher concentration to be considered for antimicrobial use in the biomedical field.

Declaration

I declare that *The antimicrobial activity of zinc oxide nanoparticles synthesized with plant extracts against Staphylococcus aureus* is my own work; that it has not been submitted for any degree or examination in any other university, and that all the sources I have used or quoted have been indicated and acknowledged by complete references.

Gisela Kriek

Date: 23 July 2019

Signed:



UNIVERSITY *of the*
WESTERN CAPE

Acknowledgements

I would like to express my sincerest gratitude to my supervisor, Prof. Edith Antunes, who has been an unwavering pillar of support and guidance. Your encouragement and efforts are appreciated immensely. A special note of thank you to my co-supervisor, Prof. Mervin Meyer, who assisted me greatly at the start of my research program.

This work was performed in part at the Melbourne Centre for Nanofabrication (MCN) in the Victorian Node of the Australian National Fabrication Facility (ANFF). To Dr. John Zhu, Dr. Hemayet Uddin, Dr. Abu Sadek, and Dr. Paul Spirizzi and the rest of the team at the Melbourne Centre for Nanofabrication, thank you for all your help and assistance during the time I was at the MCN. I would also like to express my gratitude to Mrs. Valencia Jamali and Prof. Dirk Knoesen for all your assistance and accommodating me.

Eldon and Franklin at UWC, thank you for your assistance with the research and the results.

My family deserve acknowledgement for encouraging me to push through. My loving husband, Richard, thank you for your patience and support throughout this marathon.

I dedicate this thesis to my late grandfather Johan Christiaan Kriek who never had the opportunity to pursue tertiary education formally but always continued to learn. He always encouraged us to pursue knowledge and to get involved in life, and I strive to uphold that.

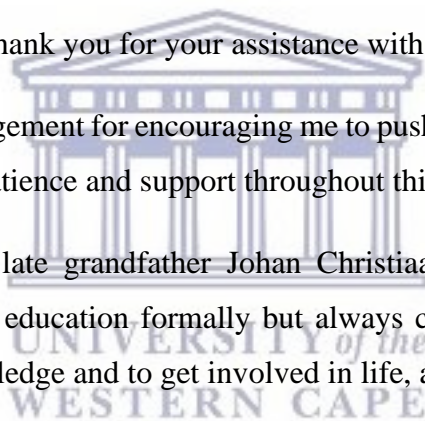


TABLE OF CONTENTS

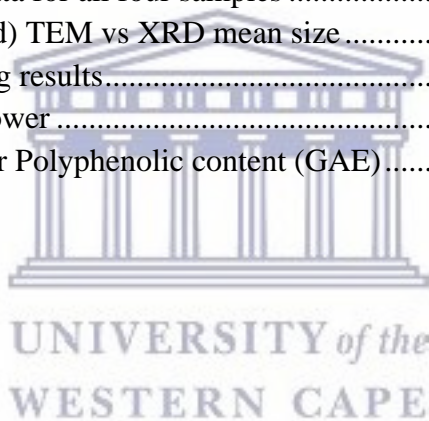
Abstract.....	ii
Declaration.....	iii
Acknowledgements.....	iv
List of tables.....	vii
List of figures.....	viii
List of abbreviations.....	ix
CHAPTER 1: GENERAL INTRODUCTION.....	1
CHAPTER 2: LITERATURE REVIEW.....	3
2.1. Herbs.....	3
2.1.1. <i>Hydrastis canadensis</i>	3
2.1.2. <i>Calendula officinalis</i>	5
2.1.3. <i>Hamamelis virginiana</i>	8
2.2. Nanomaterials.....	9
2.2.1. General overview.....	9
2.2.2. Metallic Nanoparticles.....	10
2.2.3 Negative effects of ZnO Nanoparticles.....	12
2.2.4. Application of nanoparticles.....	13
2.2.5. Synthesis.....	13
2.3 Characterisation.....	21
2.3.1 UV-Vis spectroscopy.....	22
2.3.2. DLS and Zeta potential measurements.....	23
2.3.3. X-Ray Diffraction (XRD).....	24
2.3.4. Transmission Electron Microscopy (TEM).....	24
2.3.5. Scanning Electron Microscopy (SEM).....	24
2.3.6. Fourier Transform Infrared (FTIR) Spectroscopy.....	25
2.3.7. Thermogravimetric analysis (TGA).....	25
2.3.8. Nuclear Magnetic Resonance (NMR) Spectroscopy.....	25
2.4. Antimicrobial studies.....	26
2.4.1. <i>Staphylococcus aureus</i>	29
2.4.2. Multidrug resistance.....	29
Discussion.....	30
CHAPTER 3: RESEARCH DESIGN AND METHODOLOGY.....	31
3.1. Aims, objectives and hypothesis of study.....	31
3.2. Research questions.....	31
3.3. Characterization of nanoparticles.....	32
3.4 Materials & methods.....	32

3.4.1. Chemicals and reagents.....	32
3.4.2. <i>Calendula officinalis</i> extract preparation.....	33
3.4.3. Synthesis of zinc oxide nanoparticles.....	33
3.4.4. Characterisation of nanoparticles.....	34
3.4.5. Antioxidant studies.....	36
3.4.6. Antimicrobial studies.....	38
3.5 Potential limitations and gaps.....	38
CHAPTER 4: RESULTS AND DISCUSSION.....	40
4.1. UV-Visible spectroscopy.....	40
4.2. Dynamic Light Scattering (DLS) and Zeta potential measurements.....	43
4.3. X-Ray Powder diffraction.....	44
4.4. TEM and EDX analyses.....	47
4.5. SEM analyses.....	54
4.6. FT-IR spectroscopy.....	59
4.7. TG analysis (Thermogravimetric data).....	62
4.8. NMR data.....	63
4.9. Discussion of results.....	67
4.10. Antioxidant assays.....	68
4.10.1. Radical scavenging.....	68
4.10.2. Total reducing power.....	70
4.10.3. Polyphenolic content.....	72
4.11. Antimicrobial assays.....	74
CHAPTER 5: CONCLUSIONS AND FUTURE RECOMMENDATIONS.....	76
REFERENCES.....	78



List of tables

Table 2.1 Constituents found in <i>Calendula officinalis</i>	6
Table 2.2 Structure of selected constituents found in <i>Calendula officinalis</i>	8
Table 2.3: Synthetic methods employed for nanoparticles	14
Table 2.4: 12 Principles of Green Chemistry	16
Table 2.5: Phytochemical methods to produce zinc oxide nanoparticles	18
Table 3.1: Characterisation techniques and main characteristics evaluated	32
Table 4.1: Summary of DLS results	43
Table 4.2: Zeta potential readings.....	44
Table 4.3: XRD data measured compared to expected Zincite values	47
Table 4.4: ZnO NPs size summary data obtained from TEM.....	52
Table 4.5: Weight % and atomic % of ZnO NPs (calcined) and ZnO NPs (uncalcined)	57
Table 4.6: EDX data obtained for the <i>Calendula officinalis</i> aqueous extract	58
Table 4.7: Weight % zinc nitrate hexahydrate.....	59
Table 4.8: EDX analysis summary TEM vs. SEM analysis	59
Table 4.9: FTIR Summary Table	61
Table 4.10: Tabulated TGA data for all four samples	63
Table 4.11: ZnO NPs (calcined) TEM vs XRD mean size	67
Table 4.12: Radical scavenging results.....	68
Table 4.13: Total Reducing Power	70
Table 4.14: Average results for Polyphenolic content (GAE).....	73



List of figures

Figure 2.1: Structure of berberine (1) and hydrastine (2)	4
Figure 2.2 Crystal structure of zinc oxide (Diebold et al. (2004)).....	12
Figure 2.3 Scheme showing in vitro mechanism of green nanoparticle synthesis (Marslin et al., 2018).	21
Figure 2.4: TEM images showing effect of zinc oxide nanoparticles on <i>Salmonella typhimurium</i> cells (Siddiqi et al., 2018).....	27
Figure 4.1: UV-Vis spectra of zinc nitrate hexahydrate and the <i>Calendula</i> aqueous extract in distilled water.....	40
Figure 4.2: UV-Vis Spectra obtained at various time intervals for a) Method A, b) Method B, c) Method C and d) Method D in water.	42
Figure 4.3: XRD diffractograms for the Zn salt, <i>Calendula</i> extract, uncalcined and calcined ZnO NP samples.....	46
Figure 4.4 XRD pattern of ZnO nanoparticles synthesized using Neem extract ((Bhuyan, Mishra, Khanuja, Prasad, & Varma, 2015)	46
Figure 4.5: TEM images and EDX data obtained for <i>Calendula officinalis</i> extracts	48
Figure 4.6: TEM images for the ZnO NPs (uncalcined) and the histogram obtained for the size distribution.	49
Figure 4.7: TEM Images ZnO NPs (calcined)	50
Figure 4.8: EDX ZnO NPs uncalcined a) and calcined b)	51
Figure 4.9: Hexagonal image - FFT filter applied	52
Figure 4.10: TEM images obtained from Zinc nitrate hexahydrate salt	53
Figure 4.11: EDX data obtained from zinc nitrate hexahydrate sample	53
Figure 4.12: SEM images obtained for the uncalcined ZnO NPs	54
Figure 4.13: SEM images obtained for the calcined ZnO NP sample	55
Figure 4.14: Magnified SEM image obtained for the calcined ZnO NPs	56
Figure 4.15: EDX data obtained for the uncalcined ZnO NPs.....	57
Figure 4.16: EDX data obtained for the calcined ZnO NPs.....	57
Figure 4.17: EDX <i>Calendula officinalis</i> aqueous extract	58
Figure 4.18: EDX data obtained for the zinc nitrate hexahydrate salt	58
Figure 4.19: FTIR spectral data with labelled peaks.....	60
Figure 4.20: TGA data obtained for all four samples	62
Figure 4.21: ¹ H NMR data obtained for the <i>Calendula extract</i> and the calcined ZnO NPs in DMSO- <i>d</i> ₆ at 333K (500 MHz).....	64
Figure 4.22: HSQC NMR (500 MHz) spectra acquired in DMSO- <i>d</i> ₆ at 333K for the aqueous extract of <i>Calendula officinalis</i>	65
Figure 4.23: HSQC NMR (500 MHz) spectra acquired in DMSO- <i>d</i> ₆ at 333K for the ZnO NPs (uncalcined sample) synthesised with the aqueous extract of <i>Calendula officinalis</i>	66

List of abbreviations

DW = Distilled water

EDX = Energy Dispersive X-ray

F-C = Folin-Ciocalteu

FTIR = Fourier Transform Infrared (spectroscopy)

hMSC = human Mesenchymal Stem Cells

IR = Infrared

NMR = Nuclear Magnetic Resonance

NPs = Nanoparticles

SEM = Scanning Electron Microscopy

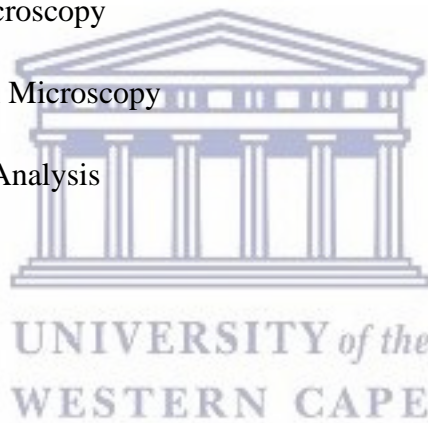
TEM = Transmission Electron Microscopy

TGA = Thermal Gravimetric Analysis

UV-Vis = Ultraviolet-visible

XRD = X-Ray Diffraction

ZnO = Zinc oxide



CHAPTER 1: GENERAL INTRODUCTION

Nobel Prize Laureate, Richard Feynman, has had the concept of “nanoscience” attributed to him after delivery of a visionary talk in 1959 (Schaming & Remita, 2015). However, it was Norio Taniguchi who in 1974 had first employed the word “nanotechnology” in 1974 (Schaming & Remita, 2015). The origin of the word “nano” comes from the Greek word meaning “dwarf” which is “nanos” (Schaming & Remita, 2015). Enabling of nanotechnologies occurred thanks to the development of technologies that changed how nanoscaled objects could be imaged and manipulated (Schaming & Remita, 2015). The two tools that caused this revolutionary shift were the Scanning Tunnel Microscope (STM) and the Atomic Force Microscope (AFM) (Schaming & Remita, 2015). STM was invented in 1981 by Binnig and Rohrer (Binnig & Rohrer, 1987) and AFM was invented in 1986 by Binnig, Quate and Gerber (Kumar, Chaudhury, Sen, & Guha, 2005). These tools allowed scientists to obtain atomic resolution images of surfaces, and also to move individual atoms (Schaming & Remita, 2015). Extensive detail on nanomaterials and nanotechnologies is not provided in this thesis, but the article by Schaming and Remita (2015) can be consulted for an overview of nanomaterials and nanotechnologies. Chapter 2 provides arguments about the toxicological concern surrounding nanoparticle preparation, the environment and the limitation this creates for biomedical applications. “Green chemistry” is an area that is developing due to these concerns. Phytosynthetic (i.e. produced with the help of plants) approaches are of interest and are discussed in Chapter 2.

Antimicrobial resistance is a global concern, and novel therapeutic agents are required to address this concern. Zinc oxide is frequently encountered in topical preparations – both medicinal and cosmetic. *Calendula officinalis* has a rich history of medicinal use and is easily acquired. The combination of these factors formed the basis of this work.

The thesis aims to report on a novel phytosynthetic method using *Calendula officinalis* to obtain zinc oxide nanoparticles and their antimicrobial potential against *Staphylococcus aureus*.

The rest of the thesis is structured as follows:

Chapter 2: Literature review covering *Calendula officinalis*, nanomaterials, synthesis, characterisation and antimicrobial studies.

Chapter 3: Research Design and Methodology

Chapter 4: Results and Discussion

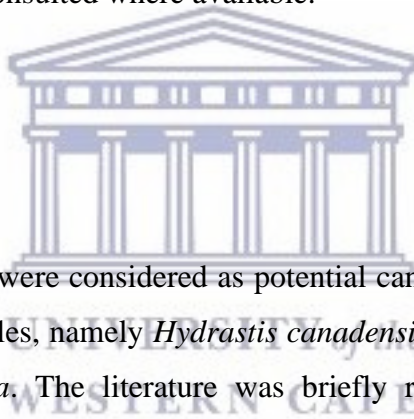
Chapter 5: Conclusion and Future Recommendations



CHAPTER 2: LITERATURE REVIEW

This chapter summarizes the literature reviewed throughout the course of this research. In this chapter an overview of three herbs is provided with the main focus on *Calendula officinalis*. Nanomaterials are briefly reviewed, with a focus on metallic nanoparticles, the negative effects of ZnO nanoparticles, the biomedical applications of nanoparticles and the synthesis of nanoparticles. Characterisation techniques of nanoparticles are reviewed, and antimicrobial studies related to *Staphylococcus aureus* are discussed.

The literature reviewed included publications in English found using the search engines EbscoHost, PubMed central, Science Direct and Google Scholar. Academic textbooks were also consulted where available.



2.1. Herbs

Three different herbs were considered as potential candidates for the synthesis of Zinc oxide nanoparticles, namely *Hydrastis canadensis*, *Calendula officinalis* and *Hamamelis virginiana*. The literature was briefly reviewed, with a focus on phytochemical constituents of the herbs, antimicrobial activity of the herb, availability of the herb, and toxicity of the herb.

2.1.1. *Hydrastis canadensis*

Hydrastis canadensis is commonly known as Goldenseal. It is a perennial plant belonging to the Ranunculaceae family and it is a North American native plant (Villinski, Dumas, Chai, Pezzuto, Angerhofer, Gafner, 2003).

Native Americans used the roots in the treatment of various conditions such as for wounds and local inflammation, indigestion, diarrhoea and fever (Villinski, et al., 2003). In Ayurvedic and Chinese medicine, berberine (one of the constituents in *Hydrastis canadensis*) has a 3000 years long usage as antimicrobial, antiprotozoal, and antidiarrheal, amongst other uses (Kumar, Chopra, Mukherjee, Pottabathini, &

Dhull, 2015). Berberine (compound **1**) and hydrastine (compound **2**) (Figure 2.1) are some of the alkaloids contained within goldenseal and contribute to the intense bitterness of the powdered root of this plant (Villinski, et al., 2003). The molecular structure of these two compounds can be seen in figure 2.1. Berberine is a quaternary benzyloisoquinoline, non-basic plant alkaloid (Kumar, et al., 2015; Tillhon, Ortiz, Lombardi, & Scovassi, 2012). Broad antimicrobial activity due to the alkaloid content of goldenseal has been investigated (Villinski, et al., 2003). The antimicrobial effects of berberine are due to it being a NorA substrate that is capable of being accumulated in the cells of bacteria and binding to DNA, both single-stranded and double-stranded, causing DNA damage which leads to bacterial death (Tillhon, et al., 2012). Berberine has activity against gram-positive bacteria such as Methicillin-Resistant *Staphylococcus aureus* (MRSA) by NorA inhibiting the MDR pump (Tillhon, et al., 2012). Berberine inhibits tumour necrosis factor- α (TNF- α), interleukin-6 (IL-6), and monocyte chemo-attractant protein 1 (MCP-1) giving it anti-inflammatory properties (Tillhon, et al., 2012). Berberine has various molecular targets interacting directly with nucleic acids and proteins such as telomerase, DNA topoisomerase, p53m NF-kB, MMPs, and oestrogen receptors (Tillhon, et al., 2012). The combination of antimicrobial and anti-inflammatory activity makes berberine containing herbs, such as Goldenseal, particularly interesting for biomedical applications.

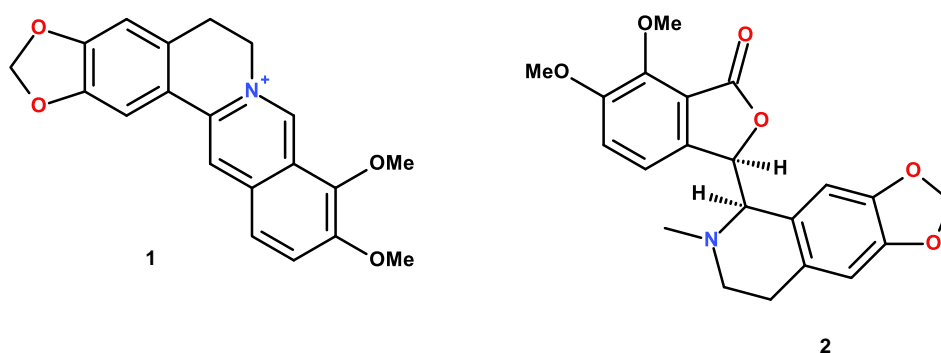


Figure 2.1: Structure of berberine (1) and hydrastine (2)

The decision against using *Hydrastis canadensis* in this research was based on the fact that Goldenseal is difficult to obtain due to rising popularity in previous years.

It is difficult to cultivate, difficult to obtain and is costly. When approaching suppliers, most did not have stock, and those that had stock could only provide quantities that were insufficient for research requirements.

2.1.2. *Calendula officinalis*

Calendula officinalis belongs to the Asteraceae family with yellow to orange flowers (Efstratiou, et al., 2012; Heinrich, Barnes, Prieto Garcia, Williamson, 2018, p. 320). It has been cultivated for centuries and has a long history of being used in pharmacy (Efstratiou, et al., 2012; Heinrich et al., 2018, p.320). “Calendula” is derived from the latin word *Calendae*, meaning ‘first day of each month’ (Gomes Honório et al., 2016). The botanical variability of *Calendula officinalis* has increased due to its use as an ornament (Heinrich et al., 2018, p.320). Commonly known as Marigold, this annual plant does well in different soils (Safdar et al., 2010), making it an easily cultivated plant.

Arora, Rani, & Sharma (2013) published a review on the *Calendula* species with emphasis on the traditional uses as well as the clinical potential. Traditionally, *Calendula officinalis* has been used for inflammatory conditions of the internal organs, dysmenorrhea and gastrointestinal ulcers (Arora, et al., 2013). It has also been used traditionally in convulsions as a diuretic and diaphoretic (Arora, et al., 2013). It has been used in skin conditions where inflammation and wounds has been a concern, and it has also been used as a colourant for foods, fabrics and cosmetics (Efstratiou, et al., 2012). The antimicrobial activity of *Calendula officinalis* is well documented (Goktas, Sahin, Yigitarslan, 2015). The microbes that extracts of *Calendula officinalis* have shown activity against, include bacteria (Gram-positive and Gram-negative bacteria) and fungi (Efstratiou, et al., 2012). The anti-inflammatory properties are attributed to the lipophilic triterpene alcohols (Heinrich et al., 2018, p.320).

The flowerheads of *Calendula officinalis* contains saponins, triterpene pentacyclic alcohols, flavonoids, sesquiterpene and ionone glycosides, volatile oil, polysaccharides and chlorogenic acid (Heinrich et al., 2018, p. 320). Some of the included constituents are summarised in table 2.1 below, as adapted from the information in Heinrich et al. (2018) and Verma et al. (2018).

Table 2.1 Constituents found in *Calendula officinalis*

Class	Description	Names
Saponins	Oleanolic acid type	Calendasaponins A, B, C, D (refer to 1 – 4 in table 2.2)
Alcohols	Triterpene pentacyclic	Faradol Arnidiol Erythrodiol Calenduladiol Heliantriols A1, B0, B1, B2 Taraxasterol Lupeol Ursatriol
Flavonoids		Hyperoside Rutin Isorhamnetin Quercetin Isoquercetin Calendoflavoside Isorhamnetin-3-O- β -D glycoside Narcissin
Glycosides	Sesquiterpene and ionone	Officinosides A, B, C, D Lolioside Arvoside A
Terpenoids		Lupeol Ψ -taraxasteol Erythrodiol Calenduloside

		Calendulaglycoside A Calendulaglycoside B Cornulacic acid acetate
Volatile oil		Cubenol α -cadinol Oplopanone Methylnoleate Sabinene Limonene α -pinene p-cymene nonanal Carvacrol Geraniol Nerolidol t-muurolol, Palustron
Polysaccharides		PS-1, PS-11, PS-iii

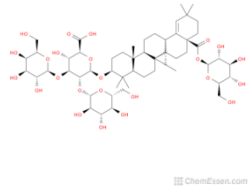
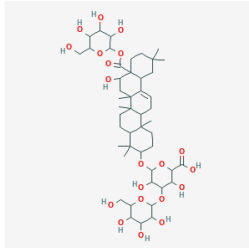
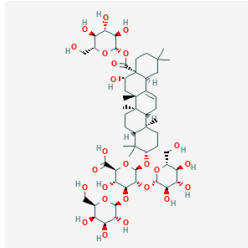
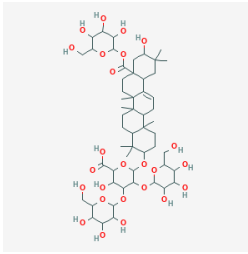
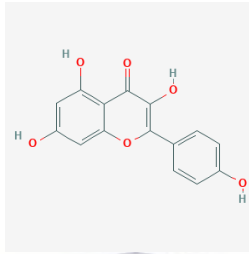
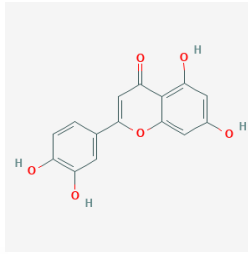
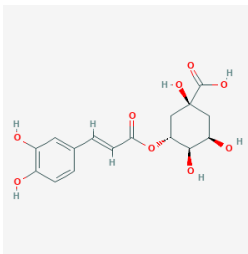
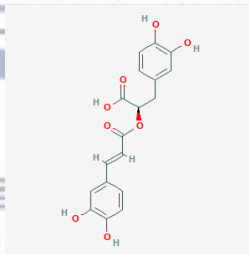
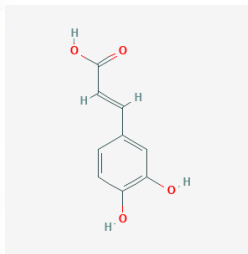
UNIVERSITY of the
WESTERN CAPE

Maximum extraction of flavonoids is possible with ethanolic extracts (Verma et al., 2018). Factors such as choice of solvent, solid-to-liquid ratio, extraction time and temperature, all have an impact in the constituents in the final extract.

As stated, *Calendula officinalis* is a widely used herb medicinally. There is literature available on the antimicrobial activity of extracts from *Calendula officinalis*, however literature on particularly aqueous extracts made from the flowers and the antimicrobial activity against *Staphylococcus aureus* is limited.

The structure of some of the constituents that were of interest in this work are given in table 2.2 below.

Table 2.2 Structure of selected constituents found in *Calendula officinalis*

<p>Calendasaponin A¹ (3)</p> 	<p>Calendasaponin B² (4)</p> 	<p>Calendasaponin C³ (5)</p> 
<p>Calendasaponin D⁴ (6)</p> 	<p>Kaempferol⁵ (7)</p> 	<p>Luteolin⁶ (8)</p> 
<p>Chlorogenic acid⁷ (9)</p> 	<p>Rosmarinic acid⁸ (10)</p> 	<p>Caffeic acid⁹ (11)</p> 
<p>*References for images</p> <p>1: https://www.molinstincts.com/structure/Calendasaponin-A-cstr-CT1102508707.html</p> <p>2: https://pubchem.ncbi.nlm.nih.gov/compound/85099152</p> <p>3: https://pubchem.ncbi.nlm.nih.gov/compound/101105717</p> <p>4: https://pubchem.ncbi.nlm.nih.gov/compound/73120628#section=Structures</p> <p>5: https://pubchem.ncbi.nlm.nih.gov/compound/kaempferol#section=2D-Structure</p> <p>6: https://pubchem.ncbi.nlm.nih.gov/compound/luteolin#section=2D-Structure</p> <p>7: https://pubchem.ncbi.nlm.nih.gov/compound/chlorogenic_acid</p> <p>8: https://pubchem.ncbi.nlm.nih.gov/compound/rosmarinic_acid#section=Structures</p> <p>9: https://pubchem.ncbi.nlm.nih.gov/compound/caffeic_acid#section=Structures</p>		

2.1.3. *Hamamelis virginiana*

Hamamelis virginiana is commonly known as witch hazel and belongs to the Hamamelidaceae family (Heinrich et al., 2018, p. 321). It is found indigenously in North America and Canada and the distilled extract is used in inflammation of the skin or the eyes due to its astringent properties (Heinrich et al., 2018, p.321). The constituents contained in the leaves and barks are tannins, predominantly gallotannins, alongside proanthocyanins and condensed catechins (Heinrich et al.,

2018, p.321). Due to its astringent properties, witch hazel was also considered for the phytosynthesis of zinc oxide nanoparticles. In initial trial experiments, there was a lack of formation of zinc oxide nanoparticles as determined by UV-vis and formation of precipitate, and it was decided to not pursue the use of *Hamamelis virginiana* in the phytosynthesis of zinc oxide nanoparticles.

2.2. Nanomaterials

2.2.1. General overview

Nanomaterials are those that have a size of up to 100nm (Guo, Yao, Lin, & Nan, 2015; Siddiqi, ur Rahman, Tajuddin, & Husen, 2018). Generally, three different morphologies are exhibited by nanostructures, namely zero-dimensional, one-dimensional, and two-dimensional structures (Guo et al., 2015). Methods of synthesis of nanoparticles include chemical, physical, biogenic and phytosynthesis (or so called 'green' synthesis). Nanoparticles produced through chemical and physical methods are precluded from application in biomedical and clinical fields due to the toxic chemicals and nonpolar solvents used in their synthesis (Akhtar, Panwar, & Yun, 2013, p. 591; Kumar, Smita, Cumbal, & Debut, 2014). Phytosynthesis utilizes extracts from parts of plants for the synthesis of metallic nanoparticles, and is an 'advantageous and profitable approach' according to Akhtar et al., (2013). The phytosynthesis method is simple, rapid cost effective and easily scalable compared to other methods (Akhtar et al., 2013, p. 592; Shah, Fawcett, Sharma, Tripathy, & Poinern, 2015).

Characteristic of nanomaterials is the relatively large surface area per unit of mass (Lin, Lin, Wang, & Sridhar, 2014). This increase in surface/volume ratio means that the contribution of the surface atoms becomes very important at the nanoscale. Due to the surface area of a solid being dependent on its shape, any changes in the size or shape of a nanoparticle can affect the physiological and physicochemical properties (Lin et al., 2014). Properties of materials can be dramatically altered when the size, shape, or surface chemistry of the nanoparticles are changed (Ross, Mirkin, & Schatz, 2016). This is in contrast to bulk materials.

2.2.2. Metallic Nanoparticles

Controlling the shape and size of particles in addition to achieving monodispersity in solution are the main challenges frequently encountered in the biosynthetic approach to nanoparticles (Akhtar et al., 2013, p. 595). Akhtar et al. (2013) summarised reports relating to the factors that may have a direct influence or in some way hinder the phytosynthesis of metallic nanoparticles. These include the effect of pH that may have an influence on the size and shape of the nanoparticles formed. Depending on the plant used, as well as the part of the plant used, there may be quite large differences in pH (Akhtar et al., 2013, p. 595). At a lower pH larger nanoparticles are formed, as compared to a higher pH (Akhtar et al., 2013, p. 595). The reaction temperature is another factor that can have an effect of the formation of nanoparticles (Akhtar et al., 2013, p. 596). Contact or incubation time, which is the time that is required for all the steps of the reaction to be completed, also has an effect on the formation of nanoparticles (Akhtar et al., 2013, p. 596). There is a high dependency between the optical properties of metallic nanoparticles and their proximity to other nanoparticles (Ross et al., 2016).

In the literature reviewed there was no evidence of prior synthesis of zinc oxide nanoparticles using *Calendula officinalis* flower aqueous extracts. Fierascu et al., (2014) synthesised silver nanoparticles using *Calendula officinalis* extract.

2.2.2.1. Zinc Oxide Nanoparticles Overview

Zinc is an essential trace element needed for many enzymatic reactions in the human body (Siddiqi et al., 2018). The two other elements in the same group, cadmium and mercury, have the same electronic configuration but are toxic (Siddiqi et al., 2018). The molecular formula for the inorganic compound Zinc oxide is ZnO. Zinc oxide is nearly insoluble in water and is a white powder in appearance (Sabir, Arshad, & Chaudhari, 2014). ZnO is a semiconductor that is a group II-VI binary compound whose ionicity is between ionic and covalent semiconductors (Matinise, Fuku, Kaviyarasu, Mayedwa, & Maaza, 2017; Morkoç and Özgür, 2009). ZnO is a transition-metal oxide where the s-shells of positive metallic ions are filled with electrons, but there may not be complete filling of the d-shells (Guo et al., 2015). Various unique properties can be attributed to this characteristic such as reactive

electronic transitions, wide bandgaps, and high dielectric constant (Guo et al., 2015). Zinc oxide nanoparticles are semiconductor nanoparticles that have properties between molecules and the bulk solid semiconductors, and size is a strong predictor for their physicochemical properties (Ghobadi, 2013). ZnO can be found in different crystalline structures, namely wurtzite, Zinc blende, and rocksalt (Morkoç and Özgür, 2009). The wurtzite symmetry is present under ambient conditions due to it being in a thermodynamically stable phase (Morkoç and Özgür, 2009). This wurtzite hexagonal structure of ZnO is one in which 4 cations surround each anion at the corners of the tetrahedron (Diebold, Koplitz, & Dulub, 2004; Sabir et al., 2014). The inherent defects and interstitial sites on the surface of ZnO crystals are responsible for the diverse mechanical, optical, electric and thermal properties (Kumar et al., 2017).

Nanoformulations containing zinc oxide are important in the biomedical and cosmetic industries (Shah et al., 2015). Zinc and alloys of zinc have been used in medical applications due to their low toxicity and abundance (Vimbela, Ngo, Frazee, Yang, & Stout, 2017, p. 3956). As previously mentioned, zinc is important in numerous biological functions which is one of the reasons for adding zinc into biomedical devices (Vimbela et al., 2017). Stimulation of certain enzymes in humans and plants by zinc oxide nanoparticles and suppression of disease can be achieved due to the fact that they are innocuous in low concentrations (Siddiqi et al., 2018). In research where chemical compounds have been used in the synthesis of metal oxides, applications to the biomedical field is limited (Azizi et al., 2017), thus making phytosynthetic approaches appealing. Good antibacterial activity has been displayed by ZnO nanoparticles (Shah et al., 2015; Sabir et al., 2014). This makes them of particular interest in this research and details of these antibacterial studies can be found in section 2.4, but include antimicrobial activity against *Staphylococcus aureus*, *Escherichia coli*, *Streptococcus pyogenes*, *Bacillus cereus*, *Pseudomonas aeruginosa*, and *Proteus mirabilis*.

Zinc oxide is classified as ecotoxic according to the EU hazard classification (Siddiqi et al., 2018). There is no reported demonstrated carcinogenicity, genotoxicity, and reproductive toxicity in humans (Siddiqi et al., 2018). However,

the condition known as zinc fever can be produced from the inhalation or ingestion of zinc powder (Siddiqi et al., 2018). The non-hygroscopic zinc oxide nanoparticle is economical and a safe inorganic crystalline material that is polar and has extensive applications in a variety of areas (Azizi et al., 2017).

UV reflection/absorption techniques can be used to measure the electronic core levels of zinc oxide (Morkoç and Özgür, 2009). At room temperature, ZnO nanoparticles have a wide direct band gap (3.37eV) and large exciton binding energy (60meV) (Azizi et al., 2017). This band width corresponds to 375nm (Huang, Wu, & Aronstam, 2010). The electronic band and crystal structure of zinc oxide is shown in figure 2.2 below, taken from Diebold et al. (2004).

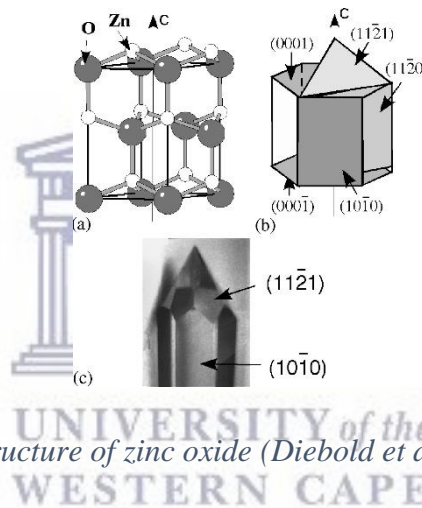


Figure 2.2 Crystal structure of zinc oxide (Diebold et al. (2004))

2.2.3 Negative effects of ZnO Nanoparticles

ZnO NPs have potential environmental and health risks (Sabir et al., 2014). Particularly interesting is the ability of ZnO NPs to penetrate the skin. Ickrath et al. (2017) reported that most of the toxicity studies done on ZnO NPs are short-term exposure experiments addressing only the acute toxic effects of nanomaterials. The authors reported the potential for genotoxic and cytotoxic risk of ZnO NPs in primary cells as in addition to several cell lines. Of concern is workers exposed to ZnO NPs via inhalation or via dermal contact. It is considered that an intact dermis gives protection against NPs, but when there are lesions the NPs may be able to extend to deeper layers in the epidermis or dermis (Ickrath et al., 2017). The concern at these levels is that proliferating cells may be in contact with NPs potentially

leading to DNA damage or induction cytotoxicity. The authors additionally state that cytotoxicity in nasal mucosa cells as well as human mesenchymal stem cells (hMSC) has been shown in their own studies after short term exposure by ZnO NPs. In their studies, Ickrath *et al.* (2017) also revealed that NPs persist in cells.

2.2.4. Application of nanoparticles

Due to diverse chemical and physical properties, zinc oxide is used widely in many areas (Kołodziejczak-Radzimska and Jesionowski, 2014). Some industries that require the use of zinc oxides are the rubber industry, pharmaceutical and cosmetic industries, textile industry, electronics and electrotechnology industries, photocatalysis (Kołodziejczak-Radzimska and Jesionowski, 2014)

Jiang, Pi, & Cai (2018) recently reviewed the synthesis and advances of ZnO nanoparticles related to the biomedical field. Due to the impact that various factors such as surface chemistry, size distribution, morphology of the particle, and reactivity of the particle in solution, have on the biological activity of nanoparticles, it is important for controlled structures to be produced for application in the biomedical field (Jiang et al., 2018). ZnO NPs are an ingredient in sunscreens and various cosmetic products due to their UV-protective value (Ickrath et al., 2017).

Biodegradability and the low toxicity of ZnO nanomaterials are important features for biomedical applications (Zhang, Nayak, Hong, & Cai, 2013). ZnO surface is rich in -OH groups and is easily functionalised (Zhang et al., 2013).

2.2.5. Synthesis

There are numerous different techniques for synthesizing nanoparticles but these can be broadly divided into two approaches: ‘top down’ or ‘bottom up’ (Shah et al., 2015). The material of interest is reduced to produce nanoparticles via chemical or physical processes in the ‘top down’ approach (Shah et al., 2015). This is in contrast to the ‘bottom up’ approach in which atoms, molecules and monomers/small particles are used to create nanoparticles (Shah et al., 2015).

The process of synthesis determines the morphology of the zinc oxide nanoparticles (Siddiqi et al., 2018). The different methods of synthesis of zinc oxide nanoparticles is covered by the review by Kołodziejczak-Radzimska and Jesionowski (2014) as

well as by Jiang et al. (2018). These include metallurgical process, chemical processes, mechanochemical, controlled precipitation, sol-gel method, solvothermal and hydrothermal method, and methods using emulsion. Some of these methods are briefly summarised in table 2.3 below using the aforementioned references:

Table 2.3: Synthetic methods employed for nanoparticles

Process & Brief description	Advantages	Disadvantages/ Challenges
Mechanochemical: Low temperature, high energy dry-milling..	Low production costs Small particle sizes Low affinity for particle agglomeration. Reproducible crystalline structure and morphology.	Uniform grinding is difficult. Greater impurities as milling time is increased.
Controlled precipitation: Fast and spontaneous reduction of solution of zinc salt using reducing agent followed by precipitation of precursor of ZnO from the solution. Precursor then undergoes thermal treatment, and then impurities are removed by milling.	Product is reproducible. Simple and easily controlled. Easily scaled.	Calcined powders have high level of agglomeration of particles.
Sol-Gel: Three steps: Preparation of zinc precursor Preparation of zinc clusters Crystal growth	Simple process Low cost Reliability Repeatability	No major challenges noted.
Hydrothermal: Mixture of substrates is heated gradually in an autoclave to a temperature of 100-300°C and left for several days.	Simple, environ-mentally friendly technique - does not involve organic solvents or additional processing (grinding or calcination). Varied crystal shapes and sizes. Depends on: starting	No major challenges noted.

	mixture composition, process temperature and pressure, high degree of crystallinity of product. High purity material obtained.	
--	---	--

2.2.4.1 Green synthesis

Green synthesis employs eco-friendly and safe solvents such as water and natural extracts in the synthesis of nanoparticles (Sabir et al., 2014). When using plant extracts, combinations of molecules act as reducing agents as well as capping agents during the synthesis of nanoparticles (Shah et al., 2015). Plants have the potential to accumulate and reduce metallic ions biologically (Shah et al., 2015). It is believed that extracts from plants that contain bioactive alkaloids, phenolic acids, polyphenols, proteins, sugars, and terpenoids play a role in the reduction and stabilisation of metallic ions (Shah et al., 2015). This process is straightforward and can occur at room temperature (Shah et al., 2015). The process is started by mixing a solution of the metal salt with the plant extract, resulting in the biochemical reduction of the salt (Shah et al., 2015). Colour changes in the reaction mixture indicates the formation of nanoparticles (Shah et al., 2015). Various morphologies can be found as growth progresses, these include spheres, cubes, triangles, hexagons, pentagons, wires and rods (Shah et al., 2015). The stabilization rendered by the plant extracts determines the morphology that is the most stable and energetically favourable (Shah et al., 2015). The quality, size and morphology of the synthesized nanoparticles are influenced significantly by the concentration of the plant extract, the concentration of the metal salt, the reaction time and the pH of the reaction solution (Shah et al., 2015). As reported in their review, Marslin et al. (2018), stated that the binding or conjugation of NPs to plant secondary metabolites could be used for the purification of compounds and for drug discovery.

Green chemistry is favourable as it prevents waste thereby reducing pollution risk at the source level, and not necessitating cleaning up of toxic waste after it has been formed (Sabir et al., 2014). The 12 principles of green chemistry as summarised on

the United States Environmental Protection Agency website (US EPA, 2013) are shown in table 2.4 below:

Table 2.4: 12 Principles of Green Chemistry

1. Prevent waste by designing chemical syntheses that leave no waste to treat or clean up
2. Maximize atom economy designing syntheses so that the end product has the maximum amount of starting materials thereby the waste contains few or no atoms
3. Design less hazardous chemical syntheses – generate substances with little/no toxicity to environment and humans
4. Design safer chemicals and products
5. Use safe reaction conditions and solvents
6. Increase energy efficiency
7. Use renewable feedstocks
8. Avoid chemical derivatives
9. Use catalysts, not stoichiometric reagents/quantities
10. Design chemicals and products that degrade after use
11. Analyze in real time to prevent pollution
12. Minimize the potential for accidents

2.2.4.2 Plant extracts

The literature reviewed was limited to the inclusion of extracts that were water based. Due to the fact that the extraction process strongly influences the type and amounts of phytochemical constituents present in the resultant extract, it is very important for this to be considered in the context of green synthesis of nanoparticles (Goktas et al., 2015). The highest yield of the desired phytochemical is what is to be considered when selecting the most appropriate extraction conditions as this determines the antibacterial and antifungal properties of the extract (Goktas et al., 2015). In their research where they were producing sterilizing agents from *Calendula officinalis*, Goktas et al., (2015) determined the optimum conditions for extraction by computer program using response surface methodology. The authors

concluded that phytochemical extraction was very sensitive to temperature as well as solid-to-liquid ratio. Different phytochemical constituents were found to be higher under different conditions. Triterpenes were dominant for extracts that had a 7h extraction at 16.5g/200ml solid-to-liquid ratio at 37.5°C. Flavonoids were highest after 7 hours of extraction at 41°C at 3.3g/200ml solid-to-liquid ratio. Saponins were higher after 1 hour of extraction at 37.5°C at 3.3g/200ml solid-to-liquid ratio.

Different parts of plants and concentrations of extract have been used in the green synthesis of metallic nanoparticles. Some of the methods that were reviewed and used to decide on the plant extract preparation and subsequent synthesis method utilised in this research are outlined below.

In the method by Supraja (2016), 10g of plant powder was mixed with 100ml of distilled water and boiled for 30 mins. This was filtered using Whatman no. 1 filter paper and stored at 4°C. 90ml of an aqueous solution of 1.0×10^{-3} M zinc nitrate was mixed with a 10ml of 10% aqueous solution of *B. ovalifoliolata* stem bark extract. Samples were centrifuged at 4000RPM to get clear supernatant.

In the method by Manokari (2016), 5g of finely chopped plant material was boiled in clean and sterilized conical flasks of desired volume with 50ml double distilled water for 5 mins for preparation of broth solutions. These were filtered. The extraction procedure was repeated 3 times (using different parts of the plant) and used for the reduction of zinc ions to zinc oxide. Zinc nitrate hexahydrate was used as the precursor. A 1mM zinc nitrate solution was prepared using zinc nitrate hexahydrate with double distilled water and stored at 4°C until further use. For the synthesis of the ZnO NPs, 3 boiling tubes were taken, one with 10ml of 1mM zinc nitrate solution as control, a second containing 10ml broth solution, and the last a 5ml of 1mM zinc nitrate solution and 5ml of plant extract as the test solution. Synthesized zinc nanoparticles were centrifuged at 10000RPM for 10min with cooling to obtain the pellet. Supernatant was discarded and pellet was redispersed in double distilled water.

In the method by Gupta, Tomar, Kaushik, Mishra, & Sharma (2018), 6g of dried ground powder from the leaves was mixed with 50ml distilled water and left at room temperature for 24 hours. After filtration, the extract was centrifuged for 30 minutes at 4000RPM. The supernatant was used for the biosynthesis of the NPs and stored at 4°C until further use.

Matinise et al. (2017) used a solid-to-liquid ratio of 30g/300ml of dried *Moringa oleifera* leaves to deionized water, and kept with magnetic stirring, for around 1 hour 45 minutes at 50°C. The authors dissolved Zinc nitrate hexahydrate in 50ml of filtered *Moringa oleifera* extract at differing concentrations. The reaction was allowed to proceed for 18h at room temperature at which time a colour change was observed but no precipitate was formed. The authors concluded that any formation of a zinc complex was in a suspended form. They proceeded to dry each concentration at 100°C in a standard oven, after which the powder was washed numerous times with deionised water in order to remove residual extract. The powders were calcined for 1 hour at 500°C.

Table 2.5 below summarizes zinc oxide nanoparticles produced using various phytochemical methods from the literature, and the obtained sizes. These did not influence the method used in this research, but the sizes produced are of interest.

Table 2.5: Phytochemical methods to produce zinc oxide nanoparticles

Size (nm)	Starting plant extract	Method	Reference
12 – 32	Aqueous extract of flowers of <i>Nyctanthes arbor-tristis</i>	0.01M zinc acetate dihydrate solution. Flower extract added. pH maintained at 12 and solution stirred continuously for 2h. Precipitate centrifuged at 15000RPM for 5 mins and dried at 60°C overnight.	Jamdagni, Khatri, & Rana (2018).
30 - 50	Aqueous extract of <i>Passiflora caeruleatae</i>	1mM zinc acetate dissolved in 50ml DW and kept in stirrer for 1 hour. NaOH solution (20ml) slowly added to zinc acetate solution and 25ml of plant extract was added. Left stirring for 3	Santhoshkumar, Kumar, & Rajeshkumar (2017).

		hours. Centrifuged at 8000RPM for 15 mins to get pellet. Dried at 80°C for 2 hours.	
20 – 60nm	Aqueous <i>Olea europaea</i> leaf extract	5g zinc nitrate in 20ml and 80ml extract and stirred at 80°C for 1 hour. The resultant dough was annealed and dried in a furnace at 400°C for 2 hours.	Hashemi, Asrar, Pourseyedi, & Nadernejad (2016).
18.97nm average, hexagonal	Aqueous extract of cottonseed	50ml 0.02M zinc acetate dihydrate in 50ml DW. 10ml cottonseed extract mixed with 50ml NaOH and then 50ml zinc acetate slowly added to that. Ultrasonic bath for 2 hours. White solid centrifuged at 15000RPM for 15 minutes. Washed with DW and ethanol. Dried overnight in oven.	Sadat-zadeh, Charati, Akbari, & Moghaddam (2018).
45-60nm Spherical and hexagonal quartzite	<i>Magnifera indica</i> leaves	80ml of 0.1M zinc nitrate added to 20ml of plant extract. Solution stirred for 6h at room temperature. Left to settle for 2h and then centrifuged at 10000RPM for 5 min. Resulting pellet washed twice with double distilled water. Dried in a hot air oven at 80°C. The pellet was calcified in a muffle furnace at 450 °C.	Rajeshkumar et al. (2018)
8-14nm Hexagonal	<i>Anchusa italica</i> flower extract	0.02M zinc acetate dihydrate dissolved in 200ml of distilled water. Magnetically stirred for few minutes. 2g of the dried <i>A. italica</i> extract was added to the above solution under magnetic stirring. After complete dissolution of the mixture, solution moved to water bath shaker. Temperature fixed at 70°C for 6h to yield white ZnO nanoparticles. The solid product was collected through centrifugation at 8000RPM for 15min and the final product was calcined at 100°C and 200°C.	Azizi et al. (2016)

50-220nm Hexagonal	Aqueous peel extract of Aloe vera	10mM solution zinc sulphate and NaOH prepared in water. 15ml A.Vera peel extract added in 100ml zinc sulphate solution, NaOH added dropwise until white suspension formed. Centrifuged at 10000RPM for 10 minutes.	Chaudhary, Kumar, Kumar, & Salar (2018).
16 – 45nm spherical size	<i>Parthenium hysterophorus</i> leaves	10g fresh leaves in 100ml double distilled water at 60°C for 15 minutes. Plant extract added to 1mM zinc nitrate solution in 9:1 ratio and mixture incubated for 24h. Sample purified by centrifugation for 15 minutes and resuspension in 1ml DW for further use	Datta et al. (2017)

2.2.4.3 Factors influencing green synthesis of metal nanoparticles

As already mentioned, there are a variety of factors that influence the green synthesis of metal nanoparticles. The concentration of the extract, reaction time, pH, temperature all would have an influence on the synthesis of the nanoparticles (Shah et al., 2015).

2.2.4.4. Possible mechanism: *Calendula officinalis* extracts in the synthesis of metallic nanoparticles via bioreduction of metal salts

The mechanism of nanoparticle synthesis during green synthesis has been summarised in the review by Marslin et al. (2018). This is briefly outlined as follows: Metallic salt disassociates into ions and the cations form hydroxyl complexes. Crystallite growth of the metals with oxygen species starts as soon as supersaturation of the hydroxyl complexes has occurred. The result of this is crystalline planes formed that have different energy levels. The capping agent from the plant extract will stop the growth, resulting in the formation of a specific type of NP. In general, there is a donation of electrons from the reducing agents to the metal ions, converting them to NPs. There is a tendency for these NPs to convert from their high-surface energy state to low-surface energy conformation leading to

aggregation. Figure 2.3 shows the scheme suggested by the authors for the *in vitro* mechanism of green nanoparticle synthesis.

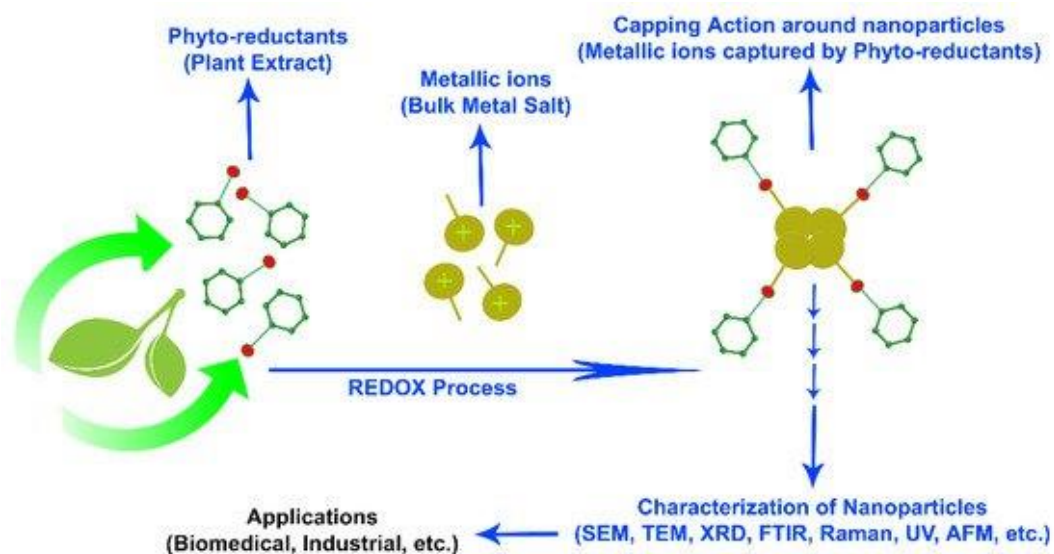


Figure 2.3 Scheme showing *in vitro* mechanism of green nanoparticle synthesis (Marstin et al., 2018).

Azizi et al. (2017) suggested the possible mechanism for ZnO-NPs formation from zinc nitrate and *Citrullus colocynthis* is as follows: “The nitrate group is a stronger oxidizer and can oxidize hydroxyl groups present in biomolecules to carbonyl groups and simultaneously Zn^{2+} ions form a complex compound inside the nanoscopic templates of metabolites through transfer of the π electrons from the carbonyl groups to the transition metal–dative coordinate bonding and finally, the ZnO-NPs formed by thermal decomposition of Zn^{2+} complex”.

2.3 Characterisation

Irrespective of how nanoparticles are produced they are characterised using various techniques to determine properties such as size of the particles, size distribution, shape of the particles as well as the surface area (Shah et al., 2015). In the synthesis of nanoparticles the metal ions from the metals salts are reduced and the reaction mixture undergoes a colour change (Shah et al., 2015). Although qualitative in nature, this is the first indication that nanoparticles have been formed (Shah et al.,

2015). Following the reaction, high speed centrifugation can be used to separate the nanoparticles from the colloid and allow characterisation using more advanced techniques (Shah et al., 2015). Direct methods for obtaining information about the nanoparticles include the microscopic techniques such as AFM, SEM and TEM which reveal information about the size and morphology of the nanoparticles (Shah et al., 2015). Indirect methods for obtaining information about the nanoparticles include spectroscopy based techniques such as UV-visible spectroscopy (UV-vis), dynamic light scattering (DLS), powder X-ray diffraction (XRD), Fourier transform infrared spectroscopy (FT-IR) and Raman spectroscopy (Shah et al., 2015). Indirect methods give data about the composition, structure, and crystal phase of the nanoparticles (Shah et al., 2015). Using UV-vis spectrophotometry, wavelengths between 300 and 800nm are typically used when metallic nanoparticles are characterised (Shah et al., 2015). To determine the size distribution and to quantify the surface charge of nanoparticles that are in liquid suspensions, DLS can be used (Shah et al., 2015). EDX mapping allows the determination of the elemental composition of the nanoparticles (Shah et al., 2015). Examination of the nanoparticles by XRD allows the identification of the crystallite size and structure, preferred orientation of the crystals and the phases that are present in the sample (Shah et al., 2015). Surface chemistry can be investigated using FT-IR spectroscopy allowing the identification of surface residues that attach to the surface during synthesis of the nanoparticles (Shah et al., 2015). Surface residues may include functional groups such as carbonyls and hydroxyl moieties (Shah et al., 2015). Identification of the vibration signals of a compound's functional group that may have attached to the nanoparticle surface during synthesis can be measured by Raman spectroscopy (Shah et al., 2015). The different characterisation techniques used in this research are briefly discussed below.

2.3.1 UV-Vis spectroscopy

UV-Vis spectroscopy is a widely used technique for the examination of optical properties of particles that are nanosized (Talam, Karumuri, Gunnam, 2012). UV-Vis spectroscopy is based on the absorbance and reflectivity of materials at different wavelengths, allowing conclusions to be drawn about the material being studied. The average particle size can sometimes be calculated using the effective mass

model (Talam et al., 2012). UV-vis absorption spectra are a function of wavelength, and the nanoparticle size is dependent on λ_{\max} , which is indicative of the wavelength for the highest intensity band. E_g refers to the band gap energy (eV), which is characteristic for ZnO NPs, and indicates the energy difference between the valence band and conduction band (Mohammadian, Es'haghi, & Hooshmand, 2018).

2.3.2. DLS and Zeta potential measurements

Dynamic Light Scattering (DLS) can be used to investigate the size distribution of small particles in solution or suspension using a monochromatic light source such as a laser (Lin et al., 2014; Stetefeld, McKenna, & Patel, 2016). DLS monitors the temporal fluctuation of the scattering of light (Rayleigh Scattering) at a fixed scattering angle (Lin et al., 2014). Advantages of DLS include that it is a non-invasive technique requiring low amounts of sample and can give estimates of quality of a sample in a short time frame (Stetefeld et al., 2016). Drawbacks of DLS include the difficulty it presents in correlating size fractions with set composition when there is the presence of aggregates, dust particles that interfere with the scattering intensity, and the relatively small range of particle or molecule size (Lin et al., 2014). DLS is also unsuited to non-spherical nanoparticles because the analysis assumes a spherical nature of particles being measured (Lin et al., 2014, Cho et al., 2013). In DLS, the Stokes-Einstein equation is used to relate the translational diffusion coefficient to the size of the nanoparticles (Cho et al., 2013). The results from DLS are reported as mean particle size as well as the polydispersity index which refers to the homogeneity of the size distribution (Cho et al., 2013). PDI values above 0.5 are indicative of a broad distribution, whereas values from 0.1 to 0.25 are indicative of a narrow size distribution (Cho et al., 2013).

Zeta potential expresses the surface charge which is critical as it influences the interaction between the environment and the nanoparticles (Cho et al., 2013). The Stern layer is the name of the thin liquid layer formed by the surface of a charged particle being bound to oppositely charged ions in an ionic solution (Lin et al., 2014). The Stern layer is in turn encompassed by loosely associated ions in a diffuse outer layer (Lin et al., 2014). Zeta potential refers to the electric potential on the shear surface determined by measurement of the velocity of the charged species

when an external electric field is applied across the sample (Lin et al., 2014). Generally, a zeta potential value of ± 30 mV or greater is indicative of particle stability and less than 30 is indicative of tendency towards aggregation, coagulation, flocculation, and instability (Lin et al., 2014).

2.3.3. X-Ray Diffraction (XRD)

Information about the crystallinity of a sample can be obtained from powder XRD (Abd Elkodous et al., 2019). It is generally accepted that for particles below 100 – 200 nm in size, XRD can be used to calculate the average crystallite sizes by the Scherrer method (Rasmussen et al., 2018). XRD can also be used to establish that samples are amorphous and if this is the case then XRD is not appropriate for size calculation (Rasmussen et al., 2018).

2.3.4. Transmission Electron Microscopy (TEM)

Transmission electron microscopy is one of the most frequently used techniques for nanomaterial characterisation, and provides direct images as well as chemical information about the nanomaterials at very low resolution down to less than 1 nm (Lin et al., 2014). Typically, an incident electron beam transmits through a thin foil specimen, at which time the electrons that have interacted with the specimen are transformed to inelastically scattered electrons, elastically scattered electrons and electrons that are unscattered (Lin et al., 2014). Energy dispersive X-ray spectroscopy (EDX) can be used alongside TEM to investigate quantitatively the chemical composition of the nanomaterial allowing elemental analysis (Lin et al., 2014).

2.3.5. Scanning Electron Microscopy (SEM)

Beams of accelerated electrons are focused by electrostatic or electromagnetic lenses to generate images in electron microscopy (Lin et al., 2014). In SEM the incident electron beam scans across the surface of the sample to generate signals which reflect the topography of the sample and as well as the atomic composition (Lin et al., 2014). The size, shape and size distribution of nanomaterials can be obtained from SEM, although the process of preparation of the sample can alter the characteristics of the nanomaterial (Lin et al., 2014). Similar to TEM elemental analysis can be obtained from the X-rays produced during SEM.

2.3.6. *Fourier Transform Infrared (FTIR) Spectroscopy*

Infrared spectroscopy is an analytical technique that is versatile and allows qualitative analysis of a sample (Coates, 2006). The spectral bands observed in techniques that have vibrational spectra are specific to molecules. Successful interpretation of spectra is dependent on the presence of particular bands and the absence of other important bands within the spectrum (Coates, 2006). By utilising the absence of bands, entire classes of compounds can be excluded during the interpretation (Coates, 2006). As stated by Coates (2006), “the infrared spectrum is formed as a consequence of the absorption of electromagnetic radiation at frequencies that correlate to the vibration of specific sets of chemical bonds from within a molecule”. IR offers a fingerprinting of the structure of the molecule of interest by illustrating the absorption or transmission compared to the incident IR frequency (Lin et al., 2014). Different materials are unique combinations of atoms, and therefore no two compounds will produce the exact same IR spectrum allowing for qualitative analysis of materials.

2.3.7. *Thermogravimetric analysis (TGA)*

Thermal gravimetric analysis can be used to monitor the temperature-dependent weight change in bulk samples (Lin et al., 2014). Furthermore, TGA provides insight into the ratio of nanoparticle to stabiliser on a mass by mass basis (Mourdikoudis, Pallares, & Thanh, 2018). This technique involves heating the sample which leads to the decomposition and vaporisation of the sample while the mass is being recorded (Mourdikoudis et al., 2018).

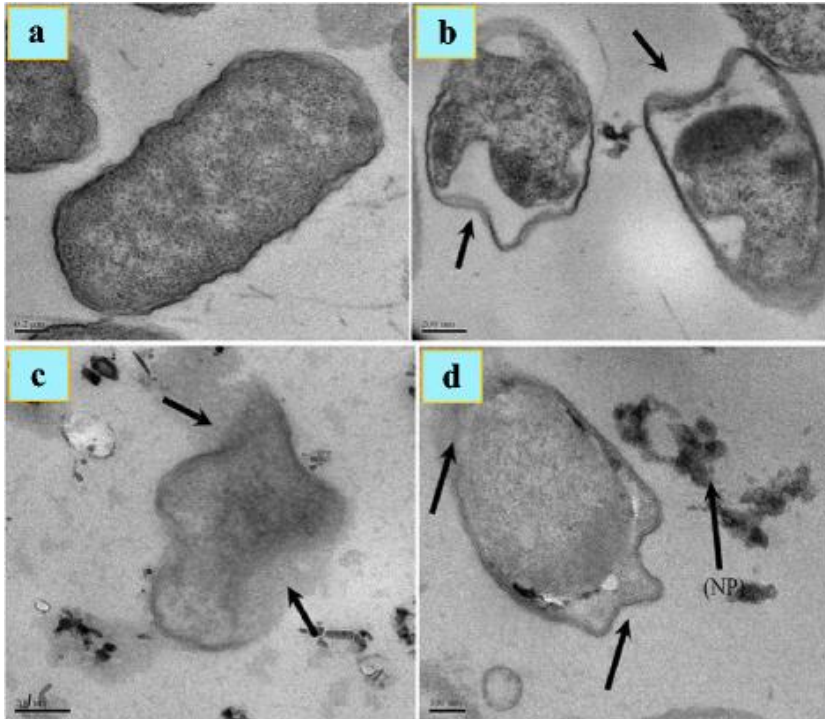
2.3.8. *Nuclear Magnetic Resonance (NMR) Spectroscopy*

This allows identification of different structural features in the samples. Purcell and Bloch discovered the phenomenon of NMR in 1946 (Mlynárik, 2017). NMR is based on the interaction between magnetic fields and the magnetic moments of the nuclei of atoms (Mlynárik, 2017). Chemical shifts obtained from NMR spectra result from the shielding effect of electrons which varies with the chemical environment, thus allowing for the identification of structural fragments of organic compounds or their substituents (Mlynárik, 2017). The HSQC NMR spectra supply

information about direct ^1H - ^{13}C correlations, which helps resolve the overlapped proton signals by the carbon signals in the second dimension.

2.4. Antimicrobial studies

Pathogenic microbes are strongly inhibited by ZnO NPs (Dobrucka & Długaszewska, 2016). Nanomaterials containing zinc reportedly have good antibacterial qualities (Vimbela et al., 2017). It is largely unknown how nanomaterials containing zinc produce antibacterial effects, but supported mechanisms of how ZnO NPs produce toxic effects include the generation of reactive oxygen species (ROS) and release of Zn^{2+} (Vimbela et al., 2017). It is reported that scanning electron microscopy (SEM) and transmission electron microscopy (TEM) images show that zinc oxide nanoparticles accumulate in the cell membrane after first damaging the bacterial cell wall and then penetrating it, as can be seen in figure 2.4 (Siddiqi et al., 2018). Once accumulated they interfere with the metabolic functions of the microbes resulting in their deaths (Siddiqi et al., 2018). Particle size, shape, concentration and exposure time to the bacterial cell all influence the antimicrobial characteristics of the zinc oxide nanoparticles (Siddiqi et al., 2018).



a TEM images of untreated normal *Salmonella typhimurium* cells. b Effects of nanoparticles on the cells (marked with arrows). c, d Micrograph of deteriorated and ruptured *S. typhimurium* cells treated with zinc oxide nanoparticles

Figure 2.4: TEM images showing effect of zinc oxide nanoparticles on *Salmonella typhimurium* cells (Siddiqi et al., 2018).

In their review, Siddiqi et al. (2018), report that lipid peroxidation leading to cell membrane alteration is most crucial in eventually leading to the disruption of vital cellular functions. Due to the amphoteric nature of zinc, it reacts both with acids and alkalis resulting in the release of Zn^{2+} ions (Siddiqi et al., 2018). Free Zn^{2+} ions bind with biomolecules, for example carbohydrates and proteins, and as a consequence the bacterial vital functions cease (Siddiqi et al., 2018). It is not however necessary for the metal oxide nanoparticles to enter the bacterial cell, the contact between cell wall and nanoparticles is enough to cause toxicity (Siddiqi et al., 2018). Due to the limited solubility of zinc oxide and its nanoparticles, it is less toxic to microbes than highly soluble zinc sulphate (Siddiqi et al., 2018).

Bacteriostatic or bactericidal activity of nanoparticles is achieved by either blocking the food supply of the bacteria or by disrupting the cell wall (Agarwal, Menon, Kumar, & Rajeshkumar, (2018). Due to the increased surface area to low volume of nanoparticles there is increased accommodation of ligands allowing specific targeting of microbes (Happy Agarwal et al., 2018).

As already mentioned, the antimicrobial activity varies according to the size of the ZnO NPs, as well as the concentration of particles used. Concentrations of ZnO NPs that have been used in antimicrobial studies vary from 100µg/ml - 5000µg/ml, with some reports showing antimicrobial activity at very low concentrations. Below is a brief review of some of these studies:

- Aleaghil et al. (2016) used ZnO NPs that were 10 – 30nm in diameter against isolated *Staphylococcus aureus*. Their results indicate MIC at 625µg/ml. MIC₅₀ was 1250µg/ml, and MIC₉₀ was 5000µg/ml.
- Khatami, Alijani, Heli, & Sharifi (2018) prepared ZnO NPs using Stevia leaves aqueous extract. Antimicrobial activity was assessed against *Staphylococcus aureus* and *Escherichia coli*. Their results show that at 1% ZnO NPs there was a significant effect on bacterial growth (MIC (µg/ml) = 2.0±1). Bactericidal effects were seen at low concentrations (MBC (µg/ml) = 4.0±1).
- Patil & Taranath (2018) synthesized ZnO NPs that were 12-53nm in size. They used *Limonia acidissima* leaf extracts for the synthesis. The authors prepared their stock solution of ZnO NPs by dispersing 1mg of zinc oxide nanopowder in 1ml 2% DMSO. These suspensions were sonicated for 30 minutes, which was followed by a 10min vortex. These stock solutions were kept in the dark at 4°C in order to prevent photo-oxidation. This stock solution was used in the preparation of the concentrations used for the antibacterial testing. The concentrations used were 100, 200 and 400µg/ml. The authors used Erythromycin (15mcg/disc) as standard control, and the other controls were 1mM ZnNO₃ and 2% DMSO. From the pictures provided in the results section by the authors the controls did not exert antimicrobial activity against *Staphylococcus aureus*.
- Gupta, Tomar, Kaushik, Mishra, & Sharma (2018) synthesized ZnO NPs using extract of *Catharanthus roseus*. The ZnO NPs were tested against *Staphylococcus aureus*, *Streptococcus pyogenes*, *Bacillus cereus*, *Pseudomonas aeruginosa*, *Proteus mirabilis* and *Escherichia coli*.

Concentrations used for antimicrobial testing reported as 700, 900, and 1500µg/ml. The authors reported that ZnO is bacteriostatic at low concentrations while bactericidal at high concentrations.

- Dobrucka and Długaszewska (2016) synthesized ZnO nanoparticles using *Trifolium pratense* flower extract and tested these against strains of *Staphylococcus aureus*, *Pseudomonas aeruginosa*, and *Escherichia coli*. The authors used concentrations of 1028, 516, 256 and 125µg/ml of the synthesized ZnO NPs against the microbes using agar well diffusion method.

2.4.1. *Staphylococcus aureus*

Staphylococcus aureus belongs to the staphylococci group of bacteria that are gram-positive spherical cells (Brooks, Carroll, Butel, & Morse, 2007, Chapter 14, page 224). Staphylococci are part of the skin's normal flora, but can cause a variety of infections opportunistically (Hanci, Ayyildiz, Igan, 2017). *Staphylococcus aureus* has an increased affinity for skin tissue and the possibility for it to invade other tissues of humans and animals is highly likely (Fit, Rapuntean, Rapuntean, Chirila, & Nadas, 2009). Many infections can be attributed to the microorganism, including eye, ear, soft tissue, skin, bone infections and associated illnesses such as meningitis, endocarditis, pneumonia, and septicaemia (Hanci et al., 2017). In the research by Fit et al. (2009) it was found that essential oil extract of Marigold (*Calendula officinalis*) performed comparatively to antibiotics ($p>0.05$). A limitation of extrapolating knowledge from this is that an essential oil was used, so the method of extraction, constituents obtained and the concentration of these constituents needs to be considered.

2.4.2. *Multidrug resistance*

Serious problems are caused by multidrug resistance in microorganisms including increased morbidity and mortality (Hanci et al., 2017). The challenge of antimicrobial resistance in the treatment of bacterial infections worldwide has existed for as long as antibiotics have been in use (Elstrøm et al., 2019). Methicillin-resistant *Staphylococcus aureus* infections (MRSA), both nosocomial and community acquired are common worldwide (Hanci et al., 2017). The choice

of the appropriate antibiotics used is important in the treatment of these infections in the face of many options for controlling and treating staphylococcal infections (Hanci et al., 2017). Empirical use of clindamycin is common in the treatment of MRSA infections (Hanci et al., 2017). However, it is important to consider inducible clindamycin resistance (Hanci et al., 2017).

Discussion

Plants have a long history of use in the treatment of ailments. *Calendula officinalis* is a plant that lends itself to biomedical applications due to its extensive history of use, as well as ease of availability. *Calendula officinalis* aqueous extract contains constituents that are potential candidates for the reduction of metal ions and capping of metallic nanoparticles using a green chemistry approach. Zinc oxide is promising in biomedical applications due to its potential antimicrobial activity and relatively low concern of toxicity. It also has a history of use in dermatological and cosmetic applications. Combining biology, chemistry, physics and nanotechnology allows the visualisation and characterisation of particles that may address concerns such as antimicrobial resistance. Various characterisation techniques such as TEM, XRD, SEM, FTIR, and NMR allow us to report on qualitative and quantitative nature of our sample. *Staphylococcus aureus* infection and multi-drug resistance are a global concern that currently requires the exploration of novel antimicrobial agents that can be considered for biomedical applications.

From the review of the literature it is evident that metallic nanoparticles, particularly zinc oxide nanoparticles, can be obtained using a phytosynthetic approach and would potentially be suitable as an antimicrobial agent. The next Chapter will discuss Research Design and Methodology and outline the hypotheses and aims of this research.

CHAPTER 3: RESEARCH DESIGN AND METHODOLOGY

3.1. Aims, objectives and hypothesis of study

The aim of this research is to synthesise ZnO NPs using an aqueous extract of *Calendula officinalis* flowers as an antimicrobial agent.

The objectives:

1. To synthesise zinc oxide nanoparticles using aqueous extracts of *Calendula officinalis* flowers, and zinc nitrate hexahydrate without the addition of any acidic or basic standard medium.
2. To characterise the synthesized nanoparticles.
3. To test the synthesised nanoparticles against methicillin resistant *Staphylococcus aureus* to ascertain antimicrobial activity using MIC (tube dilution) method.

Hypotheses:

- Phytochemicals contained in the aqueous extract of *Calendula officinalis* are involved in the reduction of zinc ions and capping to form zinc oxide nanoparticles.
- ZnO NPs synthesized from the aqueous *Calendula officinalis* extract possess antimicrobial activity against methicillin resistant *Staphylococcus aureus*.

Calendula officinalis was chosen as the herb of interest due to the long history of use, ease of access, affordability, and inherent antimicrobial properties. These have all been discussed in Chapter 2: Literature Review.

3.2. Research questions

- Does the aqueous *Calendula officinalis* extract effectively reduce zinc ions present in a zinc salt to ZnO?

- What is the minimum inhibitory concentration (MIC) of the synthesized ZnO nanoparticles against methicillin resistant *Staphylococcus aureus*?

3.3. Characterization of nanoparticles

As discussed in the previous chapter, there are a variety of techniques that can be used in the characterisation of nanoparticles. Typically, a variety of techniques are employed as each have their strengths and weaknesses, as well as characterization limitations. When results from multiple techniques are taken together it is possible to obtain more accurate results of the nanoparticles. Table 3.1 summarizes the techniques used for characterisation for the nanoparticles:

Table 3.1: Characterisation techniques and main characteristics evaluated

Technique	Characteristics evaluated
UV-vis spectroscopy	Formation of nanoparticles
X-Ray Diffraction	Confirmation of nanocrystal formation and determination of crystal structure
SEM	Morphology
TEM	Internal structure, grain size
EDX	Elemental composition
Thermogravimetric Analysis (TGA)	Thermal properties related to weight changes
FTIR	Structure and compositional analysis
NMR	Evaluation of capping agent

3.4 Materials & methods

3.4.1. Chemicals and reagents

3.4.1.1. Phytosynthesis of ZnO NPs

The materials used in this research were *Calendula officinalis* dry flowers, zinc nitrate hexahydrate (Sigma-Aldrich, 98% purity), ethanol and distilled water.

Calendula officinalis flowers were obtained from Sunrise Botanical distributed by Austral Herbs. Zinc nitrate hexahydrate (Sigma Aldrich) was purchased from Rowe Scientific. The purity of the zinc nitrate was 98% and was used without further purification. Ethanol and distilled water were supplied by the Melbourne Centre for Nanofabrication (MCN).

3.4.1.2. Antioxidant assays

The following were used in the antioxidant assays: 2,2-diphenyl-1-picrylhydrazyl (DPPH) solution, sodium carbonate (Na_2CO_3) solution, Folin–Ciocalteu (FC)-reagent, Phosphate buffer, Potassium Ferricyanide, Iron (III) Chloride hexahydrate, Trichloroacetic acid (TCA), Gallic Acid and Ascorbic Acid. All reagents were obtained from Sigma-Aldrich and used without further purification.

3.4.1.3. Antimicrobial studies

For the antimicrobial studies Tryptic Soy Broth was used for the culture. Clindamycin (1%) was used as the control. Samples were preparing using distilled water and zinc oxide nanoparticles (calcined), zinc oxide nanoparticles (uncalcined), the *Calendula officinalis* flowers aqueous extract alone and the zinc nitrate hexahydrate alone to obtain the four samples that were used for testing.

3.4.2. *Calendula officinalis* extract preparation

16.5g of dried *Calendula officinalis* flowers were weighed. These were placed in a blender for 30 seconds, shaken, and blended again for another 30 seconds. The blended plant material was placed in a 250ml conical flask, and 100ml of distilled water was added. The mixture was heated at $\sim 40^\circ\text{C}$ for 7 hours with magnetic stirring to ensure maximum extraction of any flavonoids which may enable formation of the NPs (Goktas et al., 2015). Subsequently, the mixture was covered and stored in the refrigerator overnight. The following day, the mixture was filtered using Whatman's no. 1 filter paper. The extract was kept at 4°C until further use.

3.4.3. Synthesis of zinc oxide nanoparticles

A variety of different synthesis methods were tried before the final method was decided upon as the optimized method. These are listed below.

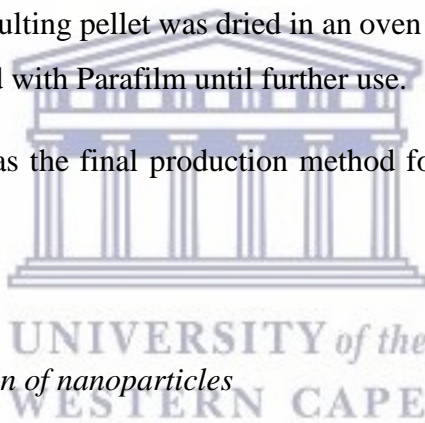
Method A was 18ml *Calendula officinalis* extract with 2ml 1mM Zn(NO₃)₂ stirred at room temperature for 3 hours.

Method B was 18ml *Calendula officinalis* extract with 2ml 1mM Zn(NO₃)₂ stirred at 80°C for 3 hours. Method B was also attempted with 9ml Witch hazel extract and 1ml Zn(NO₃)₂ stirred at 80°C for 2 hours.

Method C was 60ml *Calendula officinalis* extract with 40ml Zn(NO₃)₂, stirred at 80°C for 2 hours.

Method D was 40ml *Calendula officinalis* extract with 2g Zn(NO₃)₂, stirred at 100°C for 2 hours. The final mixture was mixed with ethanol at a ratio of 1:2 (0.5ml mixture to 1ml ethanol). The sample was spun down at 10000RPM for 5 minutes and the pellet washed with ethanol. The sample was spun down again at 10000RPM for 5 minutes. The resulting pellet was dried in an oven at 80°C for 1 hour. Store in Eppendorf tube sealed with Parafilm until further use.

Method D was used as the final production method for the particles used in this research.



3.4.4. Characterisation of nanoparticles

3.4.4.1. UV-Vis spectroscopy

UV-vis readings were taken using Agilent Technology Cary 600 UV-vis spectrophotometer. Disposable polypropylene cuvettes with 1cm pathlength were used and the spectra recorded between 800 and 300nm. It was not possible to record below 300 nm, as the cuvettes themselves absorb in this region unlike quartz cuvettes. All readings were taken in triplicate and the average reading obtained. The samples were undiluted unless otherwise specified. Raw data was obtained and graphs saved directly from the Cary software as well as data editing with Microsoft excel where needed. Readings were taken throughout synthesis of the particles at 30-minute intervals by taking a 1ml aliquots from the reaction mixture. Readings of zinc nitrate hexahydrate and *Calendula officinalis* by itself was also taken. Distilled water was used as the blank.

3.4.4.2. DLS and Zeta potential measurements

A Malvern Zeta Sizer Nano was used to obtain the DLS and Zeta potential measurements. Readings were taken using disposable capillary cuvettes at 25°C with 175° backscatter angle. Following synthesis of nanoparticles, an aliquot of each sample was used to determine the hydrodynamic size of the nanoparticle. Size readings were also taken in triplicate, followed by the measurement of zeta potential readings in triplicate. The generated reports were stored as PDF documents for further analysis.

3.4.4.3 FTIR spectroscopy

IR spectra were recorded on a Spectrum 400 FT-IR/FT-NIR spectrophotometer (Perkin Elmer, Waltham, MA, USA) equipped with an ATR accessory. FTIR was done to allow for analysis of the functional groups present in the plant extracts in order to identify what role they may have in the synthesis of the ZnO NPs. The synthesized particles were freeze-dried and then FTIR spectra were recorded.

3.4.4.4. XRD

The XRD patterns of the samples synthesised/prepared were acquired on a Bruker AXS (Rheinstetten, Germany) D8 Advance diffractometer (voltage 40 KV; current 40 mA). The XRD spectra were recorded in the range 30–90° using a CuK α (λ = 0.154 nm) monochromatic radiation X-ray source. The size of the NPs was calculated using the Debye-Scherrer (Park et al., 2016) equation below:

$$D = k\lambda\beta\cos\theta \quad \text{Equation 1}$$

where D is the size (diameter); k is the Scherrer constant (0.9); λ is the X-ray wavelength; β is the width of XRD peak at half height determined from the graph; θ is the Bragg diffraction angle.

3.4.4.5. TEM and EDX analysis

Samples were prepared for TEM and EDX analysis by drop-coating a single drop of the specimen solution onto a holey carbon coated copper/nickel grid. TEM images were collected using a Tecnai G2 20 field-emission gun (FEG, FEI, Hillsboro, OR, USA) TEM, operated in bright field mode at an accelerating voltage

of 200kV. EDX Spectra were collected using a liquid nitrogen cooled lithium doped silicon detector (EDAX, Hillsboro, OR, USA). Image J software was used to determine the size of the nanoparticles in the TEM images.

3.4.4.6. SEM

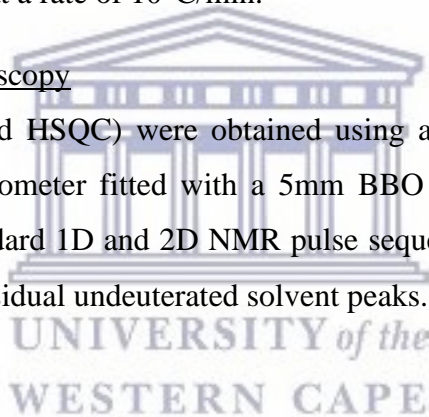
High resolution scanning electron microscopy (HRSEM) images of the surface morphology of the nanoparticles were obtained using a Zeiss Gemini Auriga Scanning Electron Microanalyser equipped with a CDU-lead detector at 25 kV with tungsten filament.

3.4.4.7. TGA

Thermogravimetric analyses of the samples were carried out using a TGA Analyser 4000 (Perkin Elmer) under a nitrogen atmosphere (at 20ml/min) in the temperature range of 50 – 850°C at a rate of 10°C/min.

3.4.4.8. NMR spectroscopy

NMR spectra (¹H and HSQC) were obtained using a Bruker 400 or 500 MHz Avance IIIHD spectrometer fitted with a 5mm BBO or TXI probe at 333K in DMSO-*d*₆ using standard 1D and 2D NMR pulse sequences. All obtained spectra were referenced to residual undeuterated solvent peaks.



3.4.5. Antioxidant studies

3.4.5.1. Determination of radical scavenging power

The method by Shyamala & Vasantha (2010) with slight modifications was used for the determination of the radical scavenging power. The method is summarised below as per Tobwala et al. (2014):

1. 3ml reaction mixture comprised of 2.9ml of DDPH (1×10^{-4} M DPPH) and 0.1ml of the sample at varying concentrations.
2. Solutions left at room temperature, in the dark, for 30 minutes
3. Resulting absorbance was measured at 520nm against blanks

4. Decreasing intensity corresponded to an increase in radical scavenging power calculated as $[(1 - A1)/A2] \times 100\%$ where A1 and A2 are the absorbance with and without the plant extract, respectively.
5. The standard used was Butylated hydroxytoluene (BHT).

3.4.5.2. Determination of total reducing power

The method by Jayanthi and Lalitha (2011) was used for the determination of the total reducing power of the extracts. The method is described below as taken from Tobwala et al. (2014):

1. 5ml solution consisting of 2.5ml 0.2M phosphate buffer (pH 6.6) and 2.5ml 1% potassium ferricyanide was added to 1ml of plant extract and gently mixed. The mixtures were incubated in a water bath for 20 minutes at 50°C
2. The mixture was then mixed with 2.5ml of 10% trichloroacetic acid (TCA) and centrifuged at 6000RPM for 10 minutes.
3. 2.5ml was transferred from the top layer to tubes containing 2.5ml distilled water and 0.5ml 0.1% ferric chloride ($\text{FeCl}_3 \cdot 6\text{H}_2\text{O}$). Resulting mixtures were mixed well and after 5 minutes the absorbance was measured at 700nm with ascorbic acid used as the standard.
4. Results were reported as μg of ascorbic acid equivalents (AAE)/mg of dried material.

3.4.5.3. Total polyphenolic content

Determination of total polyphenolic content was determined with minor modification to the technique described by Konaté et al. (2011) which relies on a bluish-grey complexing forming between Folin-Ciocalteu reagent (F-C reagent) with phenols (Tobwala et al., 2014). The steps for this method are briefly outlined below:

1. 125 μl plant extract mixed with 625 μl of 10-fold diluted F-C reagent and incubated for 5 minutes at room temperature

2. 500µl of 75mg/ml Na₂CO₃ solution added and mixture vortexed and incubated for 90minutes at room temperature in the dark.
3. Absorbance measured at 760nm against a reagent blank and gallic acid as the standard
4. Results expressed as µg of gallic acid equivalents (GAE) per mg of dried material

3.4.6. Antimicrobial studies

The antimicrobial activity of the synthesized nanoparticles was evaluated by minimum inhibitory concentration (tube dilution) method as per protocol followed by Merieux Nutrisciences. The tests were performed in duplicate. The serial dilution which achieves inhibition of the organism is deemed to be the Minimum Inhibitory Concentration. The steps are outlined briefly below:

1. Serial dilutions of aqueous solutions of ZnO NPs (calcined), ZnO NPs (uncalcined), zinc nitrate hexahydrate and *Calendula officinalis* aqueous extract were prepared in Tryptic Soy Broth (TSB)
2. Prepared dilutions were inoculated with ~10⁶ organisms of methicillin resistant *Staphylococcus aureus* (Melbourne Pathology, wild strain)
3. Samples were incubated at 37°C for 48 hours
4. Broths examined for growth by 2 individuals
5. Presence of test organisms was confirmed by subculture

3.5 Potential limitations and gaps

There are a number of limitations in the research. There were challenges in obtaining access to all of the required instrumentation, resulting in delay of obtaining some of the results. It would have been preferable for the timeline of the research to have been more concise. Due to the use of instruments from different

facilities, there is less control on concerns such as calibration of instruments, but due to the fact that the facilities used were of high calibre, it is expected that all of the instrumentation was functioning optimally. Further improvement on this research can be achieved by repeating the experiments in a variety of facilities with a variety of different researchers to allow comparative studies of the obtained results.

MIC is useful as a baseline screen for antimicrobial capacity, but further investigation is needed for more detailed and useful information about antimicrobial capacity of a substance.



CHAPTER 4: RESULTS AND DISCUSSION

The results obtained are presented in this chapter followed by the discussion.

4.1. UV-Visible spectroscopy

Figure 4.1 shows the UV-Vis spectra of the zinc salt together with the calendula extract in distilled water. The increase in absorption of the zinc salt correlates with what is expected from bulk zinc at 370nm. Amongst others, a broad absorption peak is observed between 600 nm and 365nm for the *Calendula officinalis* extract. This is typically observed and expected for compounds such as flavonoids and polyphenols which are expected in the aqueous extract. Due to the potential overlap of absorption peaks between the *Calendula officinalis* extract and the ZnO nanoparticles, UV vis spectrophotometry may not be the best suited method to determine the formation of the zinc oxide nanoparticles since an absorption peak for the ZnO NPs is expected at 355 nm.

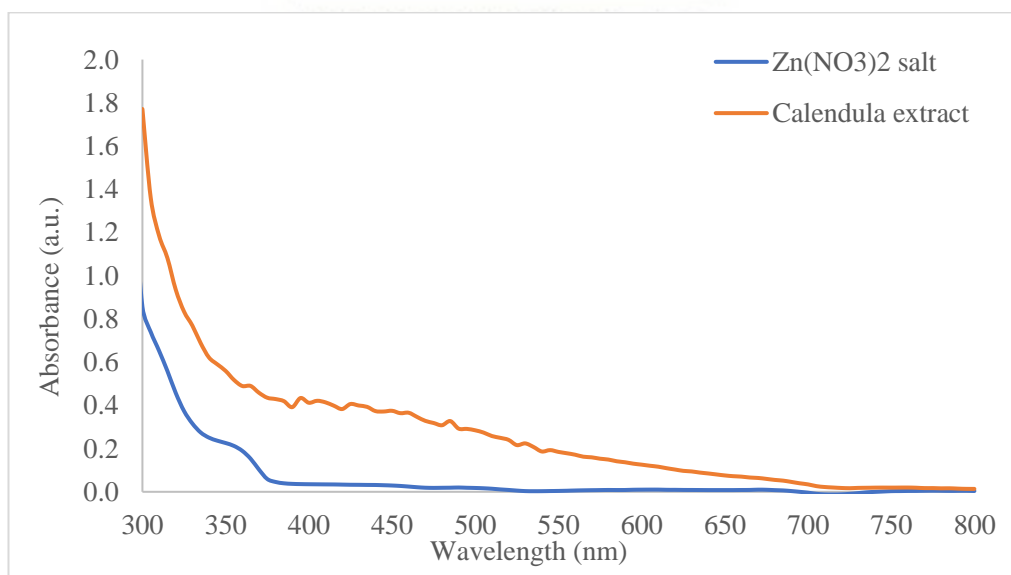
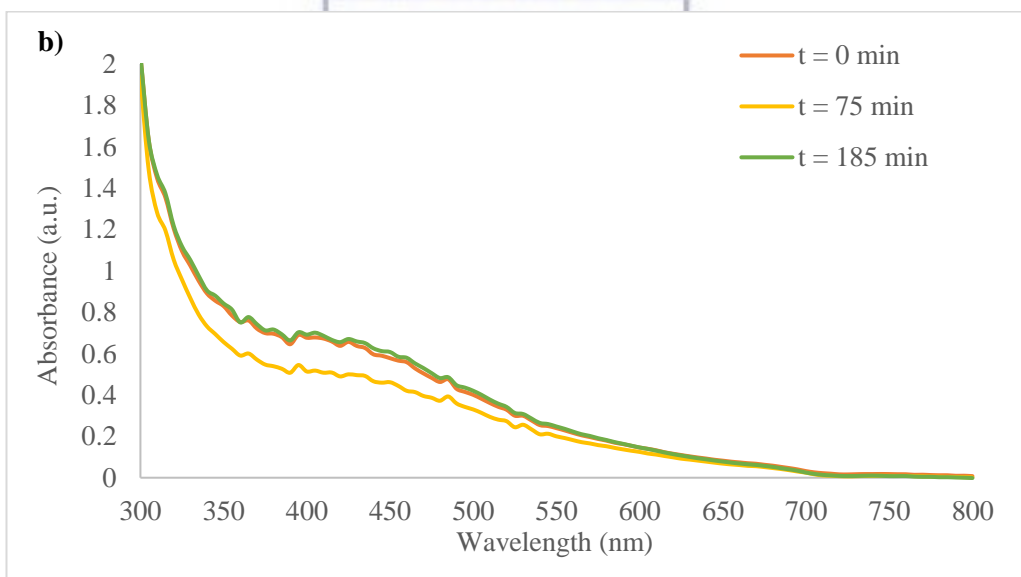
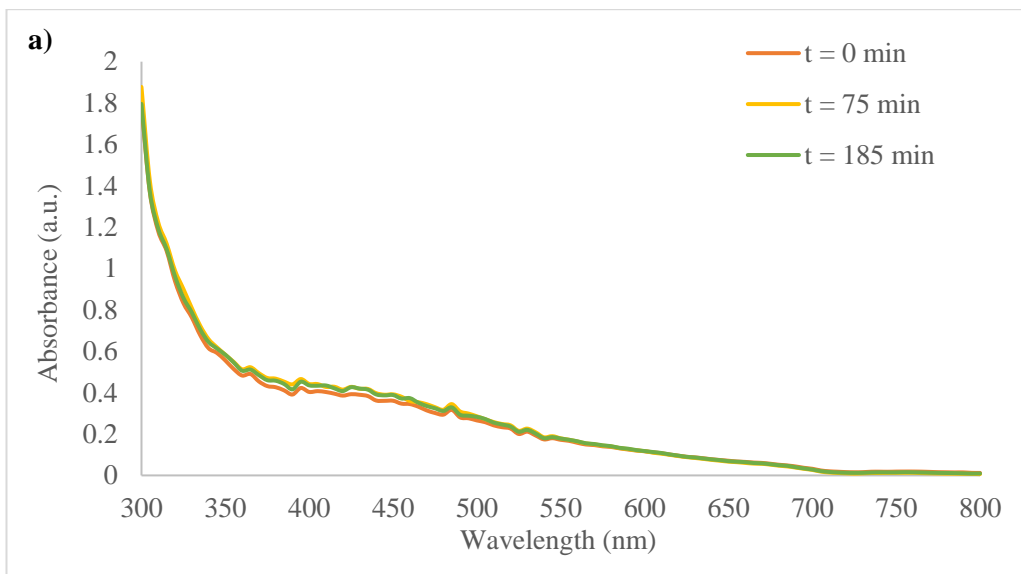


Figure 4.1: UV-Vis spectra of zinc nitrate hexahydrate and the *Calendula* aqueous extract in distilled water.

Method D was used as the final production method, however, UV-vis spectra obtained using the other methods initially explored were also included in figure 4.2 below.



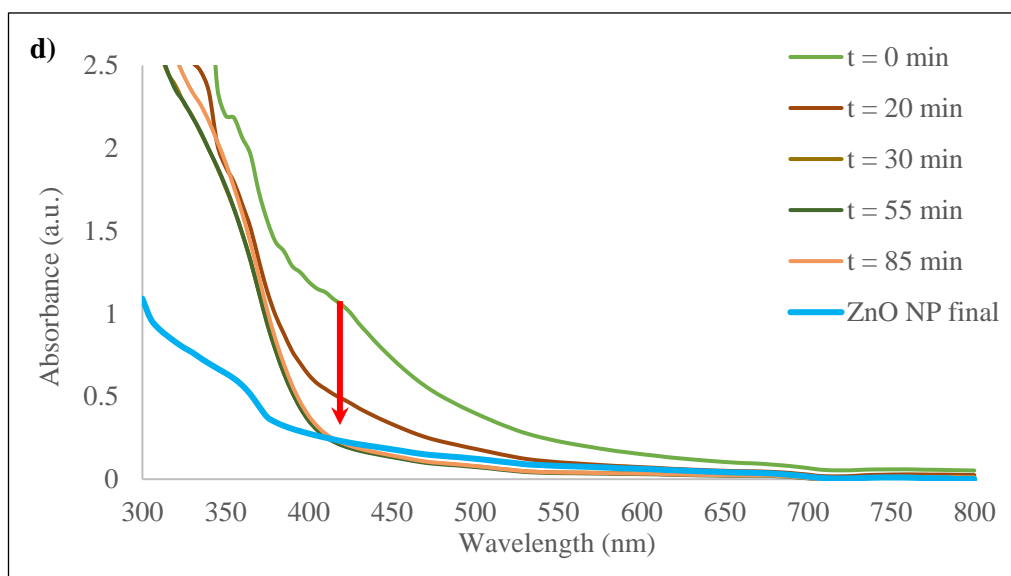
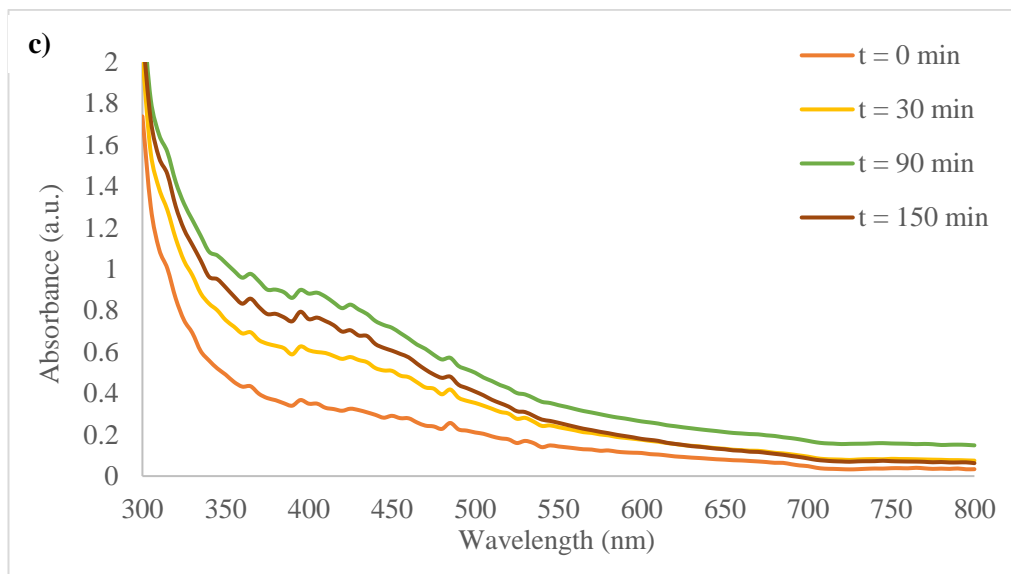


Figure 4.2: UV-Vis Spectra obtained at various time intervals for a) Method A, b) Method B, c) Method C and d) Method D in water.

From figure 4.2 it can be observed that there is a general trend towards increasing absorption as time progresses in methods A to C, however this is not consistent. This could be due to experimental error, with inconsistency in concentration of solution being used in the cuvette.

From the results for method D in figure 4.2d, the UV-vis spectra show a peak at around 360nm which is characteristic of ZnO nanoparticles. The transition of electrons from valence band to conductance band is responsible for this (Zak, Razali, Majid, & Darroudi, 2011). The good absorption of the ZnO NPs in the UV region allows for applications in sunscreen or antiseptic ointments. This however is a broad peak, and difficult to analyse the exact peak position. Use of quartz cuvettes enabling the measurement of the UV-vis spectra from 200nm – 800nm is suggested for future work. Due to the lack of a sharp absorption peak in the UV-vis spectrum it can be surmised that the synthesized nanoparticles are not spherical according to Mie’s theory (Ezealisiji, Siwe-Noundou, Maduelosi, Nwachukwu, & Krause, 2019).

4.2. Dynamic Light Scattering (DLS) and Zeta potential measurements

A Malvern Zetasizer was used for the measurement of DLS data. The data is summarised in table 4.1.

Table 4.1: Summary of DLS results

Sample	Date of reading	Z-average (d. nm)	PDI	Results quality	Range (nm)
Zinc nitrate Hexahydrate	15/06/2018	1635.0	0.6	Poor	N/A
<i>Calendula officinalis</i> extract in water	15/06/2018	527.5	0.7	Poor	43.8 – 712.4
ZnO NPs uncalcined	16/11/2018	728.9	0.3	Good	295.3- 1281.0
ZnO NPs uncalcined	15/06/2018	331.8	0.5	Good	58.8 – 955.4

No DLS readings could be obtained for the calcined sample due to the lack of solubility in the requisite solvent. From the data in table 4.1, it can be observed that there is a wide range in size of the particles. The Z-average can only be used in comparison to other techniques in instances where the sample is monomodal (has only one peak), is spherical or near spherical in shape, and is monodisperse. The polydispersity index refers to the homogeneity of the particles and PDI values above 0.5 are indicative of a broad distribution, whereas values from 0.1 to 0.25 are

indicative of a narrow size distribution (Cho et al., 2013). From the PDI values in table 4.1 it can be concluded that the uncalcined samples had a broad size distribution and lacked uniformity in size. This is to be expected, however, since calcination is considered to be a very important, final step in the synthesis of the ZnO NPs.

The results obtained for the zinc nitrate hexahydrate and *Calendula officinalis* samples did not meet the quality criteria. This could be due to a variety of factors such as the presence of large or sedimenting particles, the sample being too dark or the sample being too polydisperse for analysis of size distribution.

The Zeta potential results summarised in table 4.2 below. Since zeta potential expresses the surface charge (Cho et al., 2013), negative zeta potential values indicate the surface of the nanoparticles are coated with negatively charged compounds which was expected as *Calendula* extracts are expected to contain polysaccharides and polyphenols. Zeta potential values of $\pm 30\text{mV}$ or greater, would indicate particle stability, while values less than 30 is indicative of tendency towards aggregation, coagulation, flocculation, and instability (Lin et al., 2014). Improving the stability and solubility of the NPs therefore remains an area for future investigation.

Table 4.2: Zeta potential readings

Sample	Date of reading	Zeta potential	Results quality
ZnO NPs	11/05/2018	-20.4mV	Good
ZnO NPs	11/05/2018	-20.7mV	Good
ZnO NPs	11/05/2018	-20.6mV	Good
ZnO NPs	15/06/2018	-10.7mV	Good
<i>Calendula officinalis</i> extract in water	15/06/2018	-19.5mV	Good
<i>Calendula officinalis</i> extract in water	15/06/2018	-18.6mV	Good
<i>Calendula officinalis</i> extract in water	15/06/2018	-21.7mV	Good

4.3. X-Ray Powder diffraction

The XRD patterns for the $\text{Zn}(\text{NO}_3)_2$ salt, the *Calendula officinalis* extract, ZnO sample as is (or uncalcined), as well as the pattern obtained for the sample calcined

at 600°C were measured and are shown in figure 4.3. As expected, the XRD pattern of the zinc salt reveals its crystalline nature, while the *Calendula* extract unexpectedly revealed sylvite in its pattern. The source of KCl is unknown at this time.

The broad pattern exhibited by the uncalcined sample is indicative of amorphous behaviour (Al-Hada, Saion, Shaari, Kamarudin, & Gene, 2014). The broadened, shortened and weakened diffraction peaks observed in the uncalcined sample are due to defects in the crystals. Due to the defects the atomic arrangements are less precise, and a clear peak is not obtained. From these results we can conclude that the crystalline phase of ZnO was not been induced in the uncalcined sample. This indicated formation of crystals upon calcination. XRD can be inaccurate in calculating particle size as it takes the average of the sample NP size, and it is dependent on an assumed crystal structure.

The sample that was calcined shows narrow and sharp diffraction peaks, confirming the formation of crystalline ZnO nanoparticles (Al-Hada et al., 2014). Bragg's reflection peaks at $2\Theta = 31.74^\circ, 34.38^\circ, 36.2^\circ, 47.52^\circ, 56.54^\circ, 62.82^\circ, 67.89^\circ$ correspond to the lattice planes (100), (002), (101), (102), (110), (103), (112) respectively, for Zincite. The peaks and corresponding lattice values are summarised in table 4.3. As indicated in table 4.3, these parameters correspond well to the Zincite values (JCP2_36-1451). The XRD pattern of the calcined ZnO NPs also have a high level of agreement to the XRD pattern of phytosynthesized ZnO NPs using Neem extract by Bhuyan, Mishra, Khanuja, Prasad, & Varma (2015), as can be seen in figure 4.4. Additionally, the characteristic peaks associated with the zinc salt, are no longer visible in the patterns obtained for the uncalcined or calcined ZnO samples (figure 4.3). This is also true for the KCl originally observed in the *Calendula* extract.

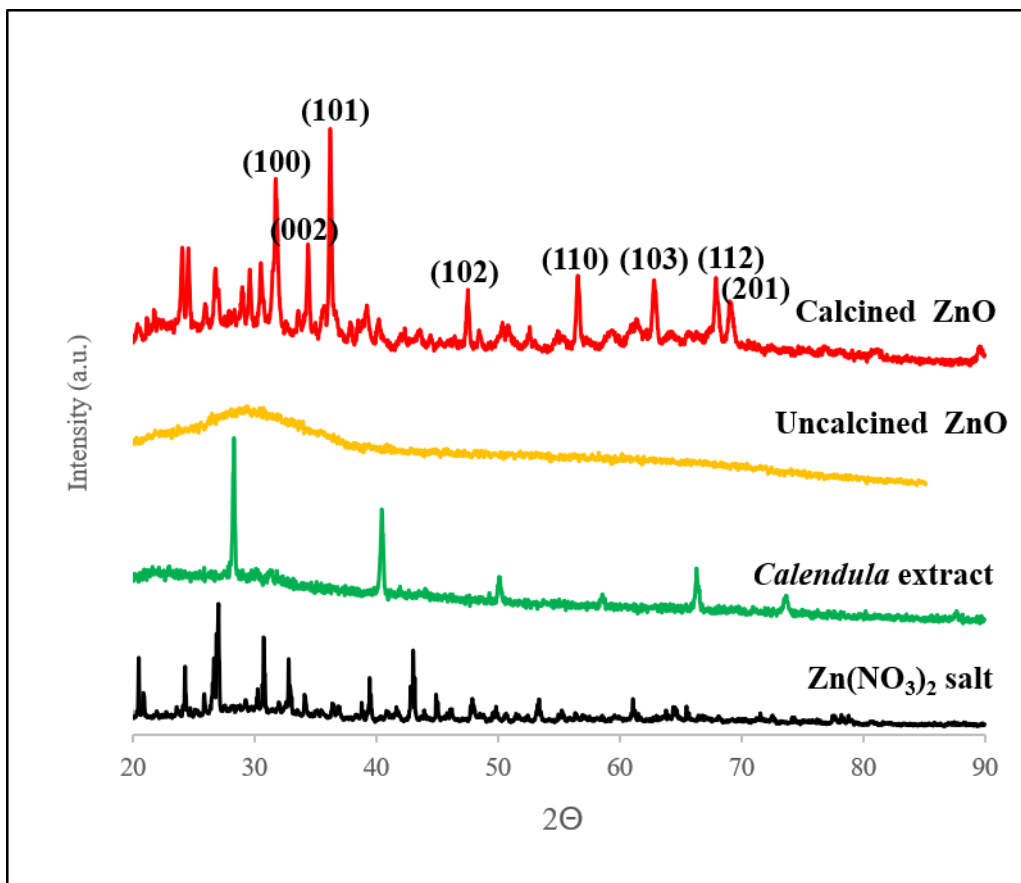


Figure 4.3: XRD diffractograms for the Zn salt, Calendula extract, uncalcined and calcined ZnO NP samples

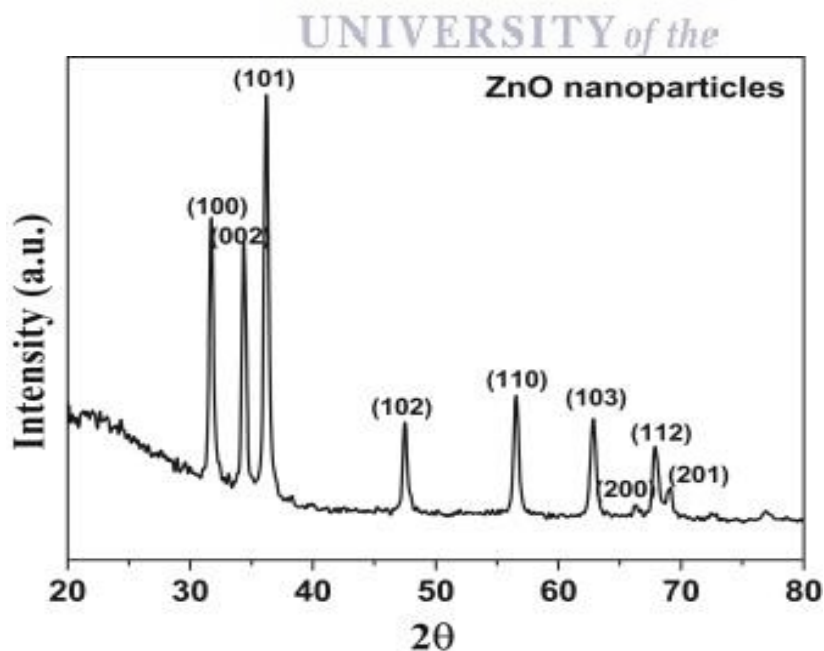


Figure 4.4 XRD pattern of ZnO nanoparticles synthesized using Neem extract ((Bhuyan, Mishra, Khanuja, Prasad, & Varma, 2015)

From the XRD pattern in figure 4.3, it can be seen that the intensity of the (101) diffraction peak is the most intense. This was thus used in the calculation of the nanoparticle sizes using the Scherrer equation. The crystallite size calculated using the Debye-Scherrer equation was 53.14nm. This was calculated using the strongest reflection at $2\Theta = 36.2^\circ$. Limitations in using this method in size determinations is that the method depends on particles that are near-spherical. As can be seen in the SEM images later in section 4.5, however, the synthesized particles are quasi-spherical tending towards agglomeration.

Table 4.3: XRD data measured compared to expected Zincite values

Peak 2Θ	Corresponding Zincite 2Θ value	Intensity	h	k	l	d-spacing* (Å)
31.74	31.77	57	1	0	0	2.82
34.38	34.42	44	0	0	2	2.61
36.20	36.25	100	1	0	1	2.48
47.52	47.53	23	1	0	2	1.91
56.54	56.60	32	1	1	0	1.63
62.82	62.86	29	1	0	3	1.48
67.89	67.96	23	1	1	2	1.38
69.06	69.10	11	2	0	1	1.36

*d-spacing was calculated using Bragg's Law and $\text{CuK}\alpha$ ($\lambda = 0.154 \text{ nm}$). This is 1.54\AA . Bragg's equation: $n\lambda = 2d\sin\theta$. d-spacing is the distance between planes of atoms that give rise to the diffraction peaks.

4.4. TEM and EDX analyses

TEM and EDX data for each of the samples were also captured, and the results can be found below.

Figure 4.5(a) shows the TEM images and lack of any identifiable particles in the *Calendula officinalis* extract, while the EDX elemental results for *Calendula officinalis* indicates the presence of N, Na, Si, S, Cl, K, Ca, Cu (figure 4.5 (b)). TEM images were obtained for the *Calendula officinalis* extract to show the lack of naturally occurring metallic nanoparticles. These data are summarised in table 4.8. N is expected as this is plant material, while Cu is present due to the holey Cu grids used in TEM analyses. Na, Si K, Cl and Ca are common elements that may

be present due to the glassware used or the plant/soil used to cultivate the *Calendula* plant.

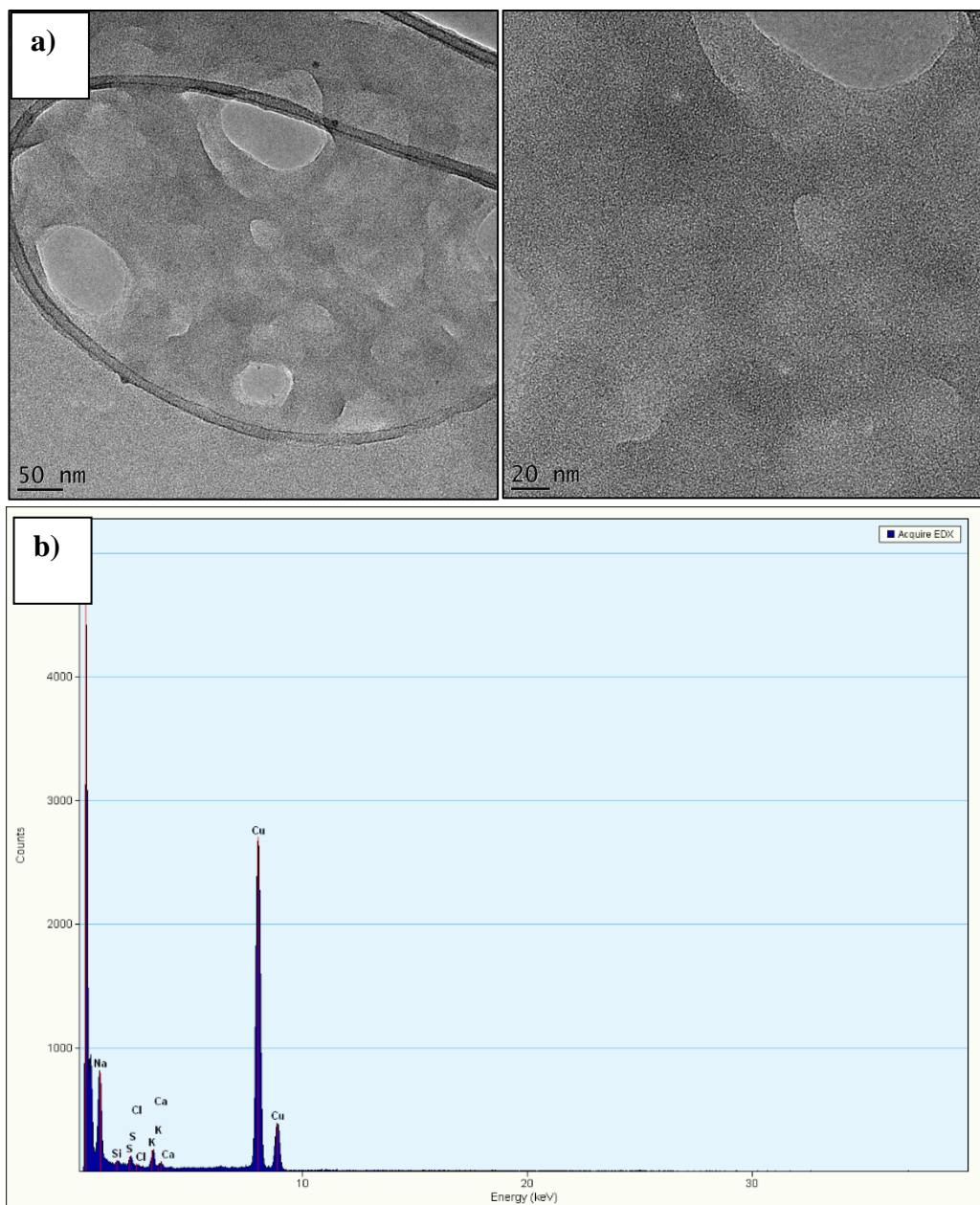


Figure 4.5: TEM images and EDX data obtained for *Calendula officinalis* extracts

Figure 4.6 shows the TEM images for the uncalcined ZnO NPs obtained at different magnifications, as well as a histogram summarising the size distributions of the particles.

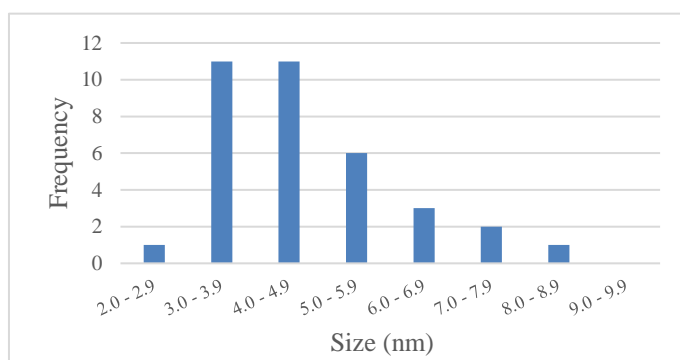
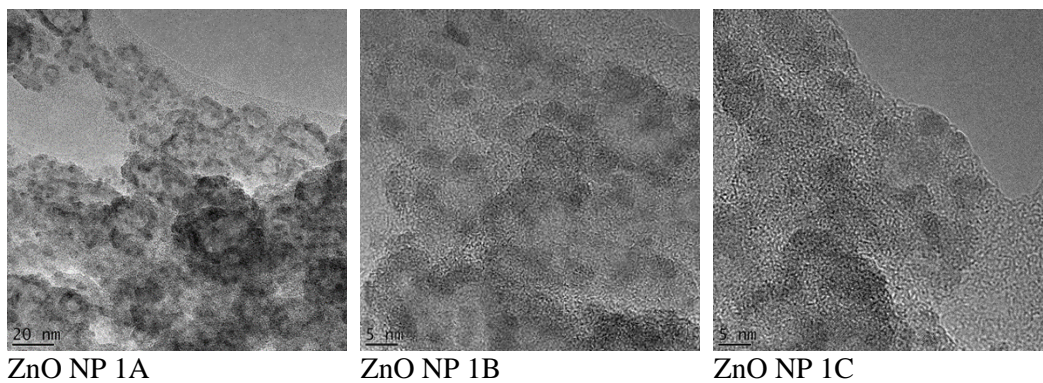


Figure 4.6: TEM images for the ZnO NPs (uncalcined) and the histogram obtained for the size distribution.

Figure 4.7 shows the TEM images at different magnifications of the ZnO NPs (calcined), as well as a histogram summarising the size distributions of the particles.

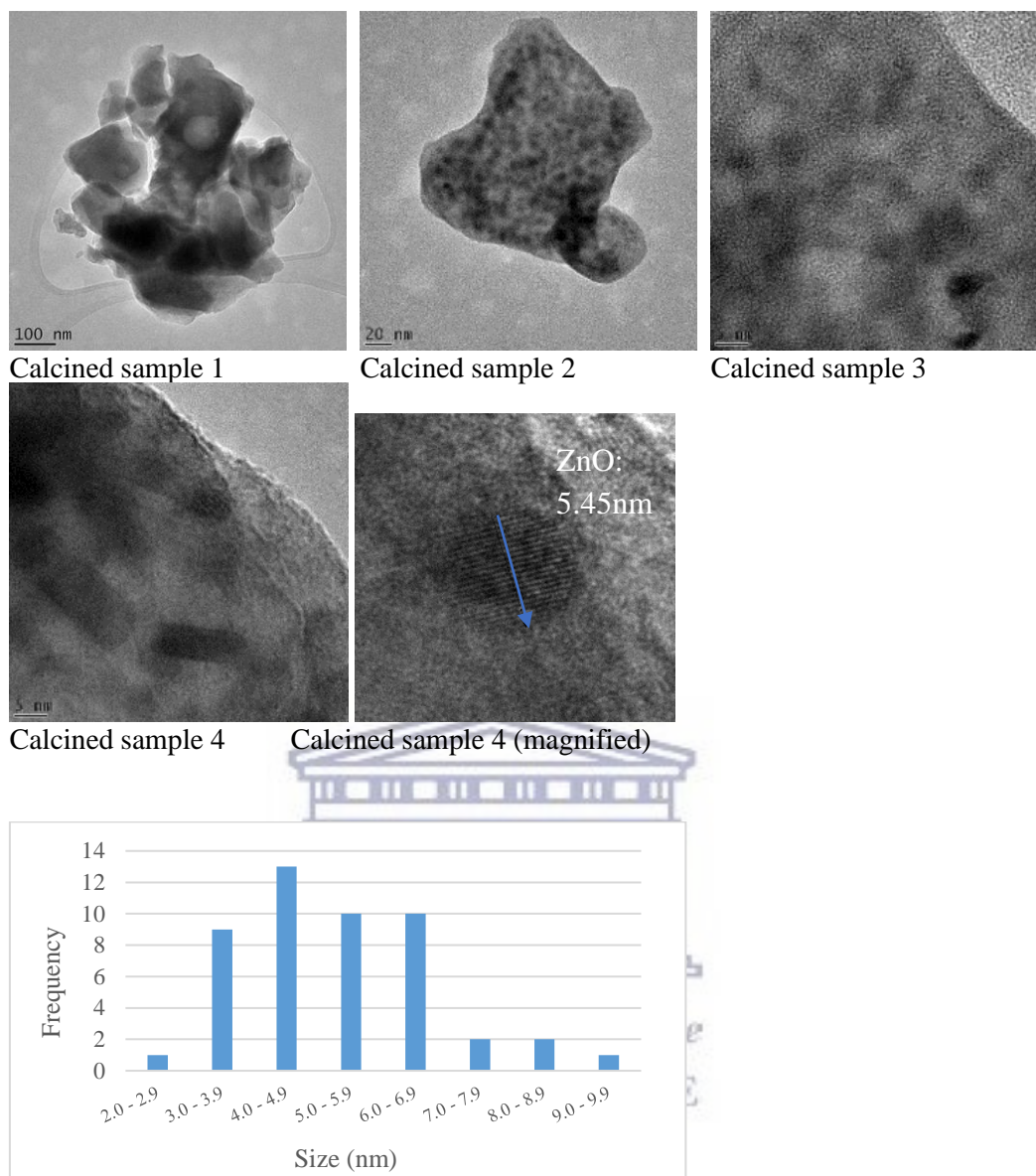


Figure 4.7: TEM Images ZnO NPs (calcined)

The EDX results of the ZnO NPs (uncalcined) sample shows the presence of C, O, Zn, P, K, Cu (figure 4.8 (a)). The EDX results of ZnO NPs (calcined) sample shows the presence of C, O, Zn, Na, Si, P, K, Ca, Cu (figure 4.8 (b)).

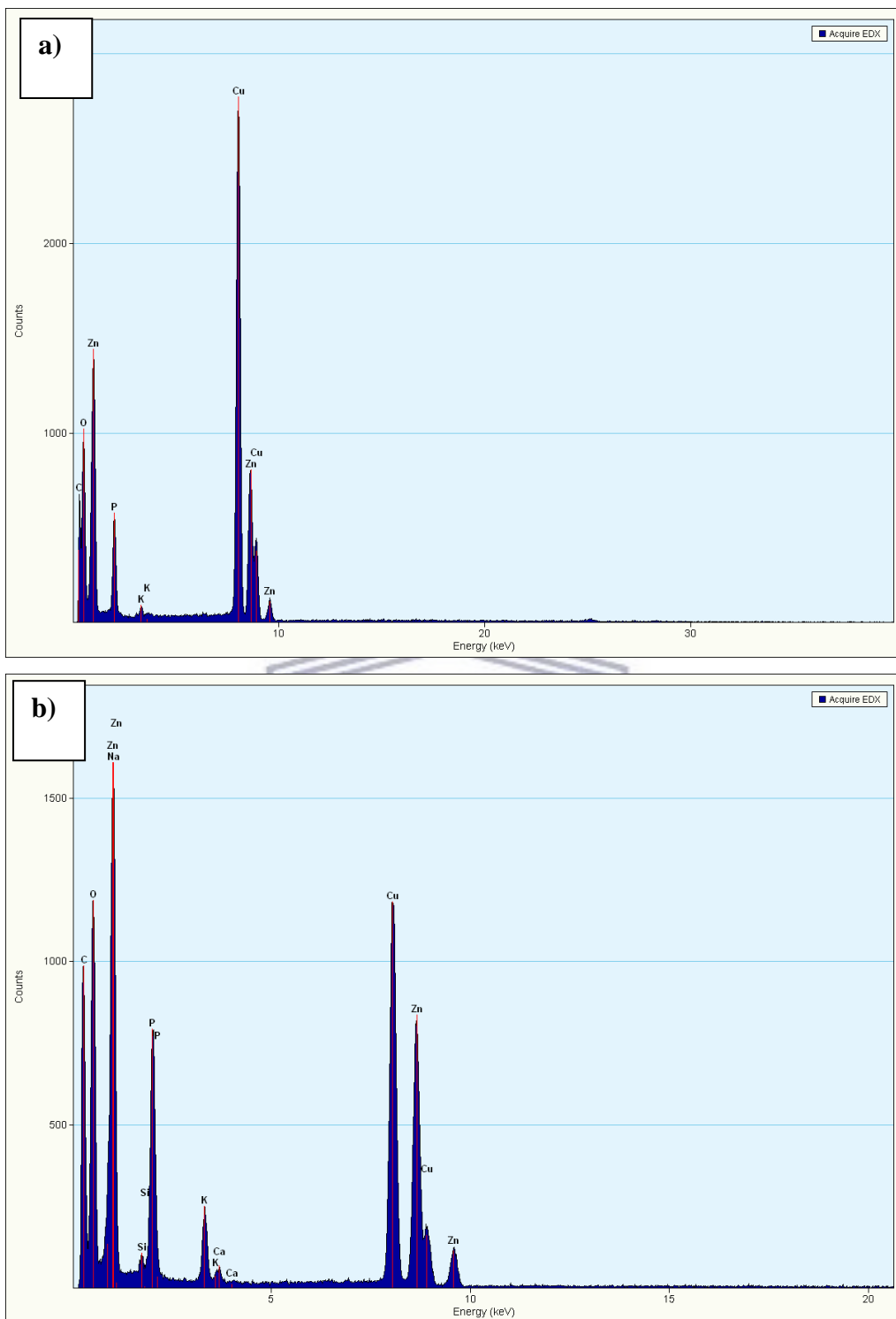


Figure 4.8: EDX ZnO NPs uncalcined a) and calcined b)

As can be seen from the results obtained via TEM and summarised in table 4.4, there is not much difference in calculated Zinc oxide core sizes between the

calcined and uncalcined sample. The TEM images reveal the varying or change in morphology, with the presence of spherical as well as rod shaped zinc oxide nanoparticles in the calcined sample. This may be due to the orientation of the particles relative to the prepared sample surface. Agglomeration of the particles can clearly be seen in the image of the TEM, especially for the uncalcined sample which has a higher level of agglomeration/less well-defined particles.

Table 4.4: ZnO NPs size summary data obtained from TEM

ZnO NPs uncalcined		ZnO NPs calcined	
<i>Average size (nm)</i>	<i>Distribution (nm)</i>	<i>Average size (nm)</i>	<i>Distribution (nm)</i>
4.71	2.59 – 8.00	5.32	2.99 – 9.24

From the TEM images obtained for the calcined sample, clearer formation of the zinc oxide nanoparticles can be observed. The d-spacing for the calcined sample was calculated manually using ImageJ software and the plot profile function. The results indicate an average spacing of 0.22nm. This is slightly less than the d-spacing calculated from the XRD data at 0.25nm. Possibilities for this may be human error introduced when calculating these results manually in ImageJ. Interestingly, the average value of the hexagonal image obtained from applying a Fast Fourier Transform (FFT) filter to the image 1_2b of the calcined sample was 0.25nm from the centre. This can be seen in figure 4.9 below.



Figure 4.9: Hexagonal image - FFT filter applied

The TEM images at varying magnifications of the zinc salt and the EDX data can be found in figure 4.10 and figure 4.11, respectively. Although these data in itself do not give much information, they do reveal the crystalline nature of the Zn salt (figure 4.10 1C) as indicated by the XRD patterns. These images also clearly show the changes taking place from the starting Zn salt material to the uncalcined sample and finally the calcined ZnO NPs formed.

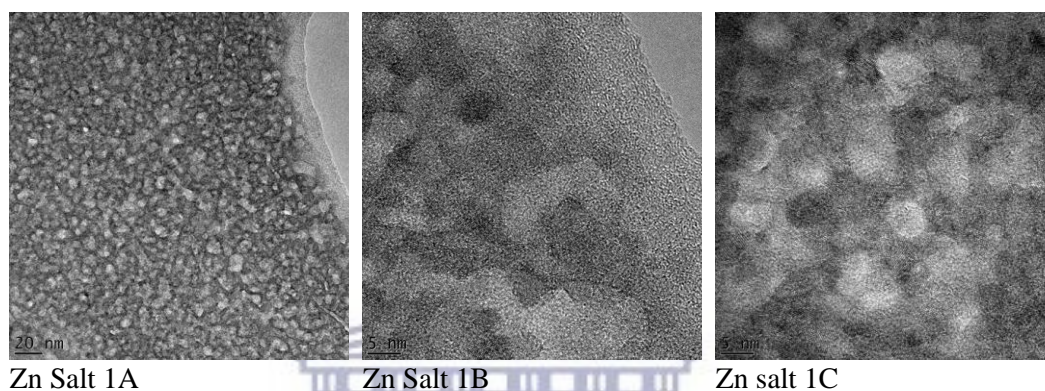


Figure 4.10: TEM images obtained from Zinc nitrate hexahydrate salt

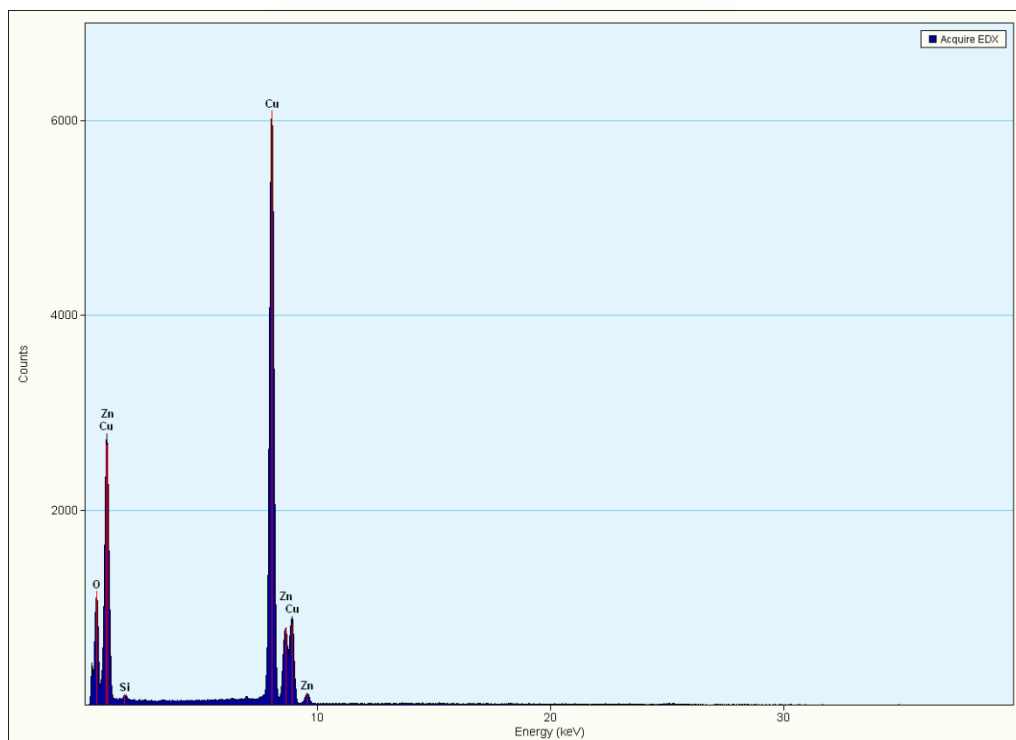


Figure 4.11: EDX data obtained from zinc nitrate hexahydrate sample

As expected, the presence of Zn, O, Si, Cu, can be observed in the zinc nitrate hexahydrate sample (figure 4.11), all of which were expected.

4.5. SEM analyses

SEM images taken on the 12th August 2018 are shown in figure 4.12 below. These are the images obtained for the uncalcined sample.

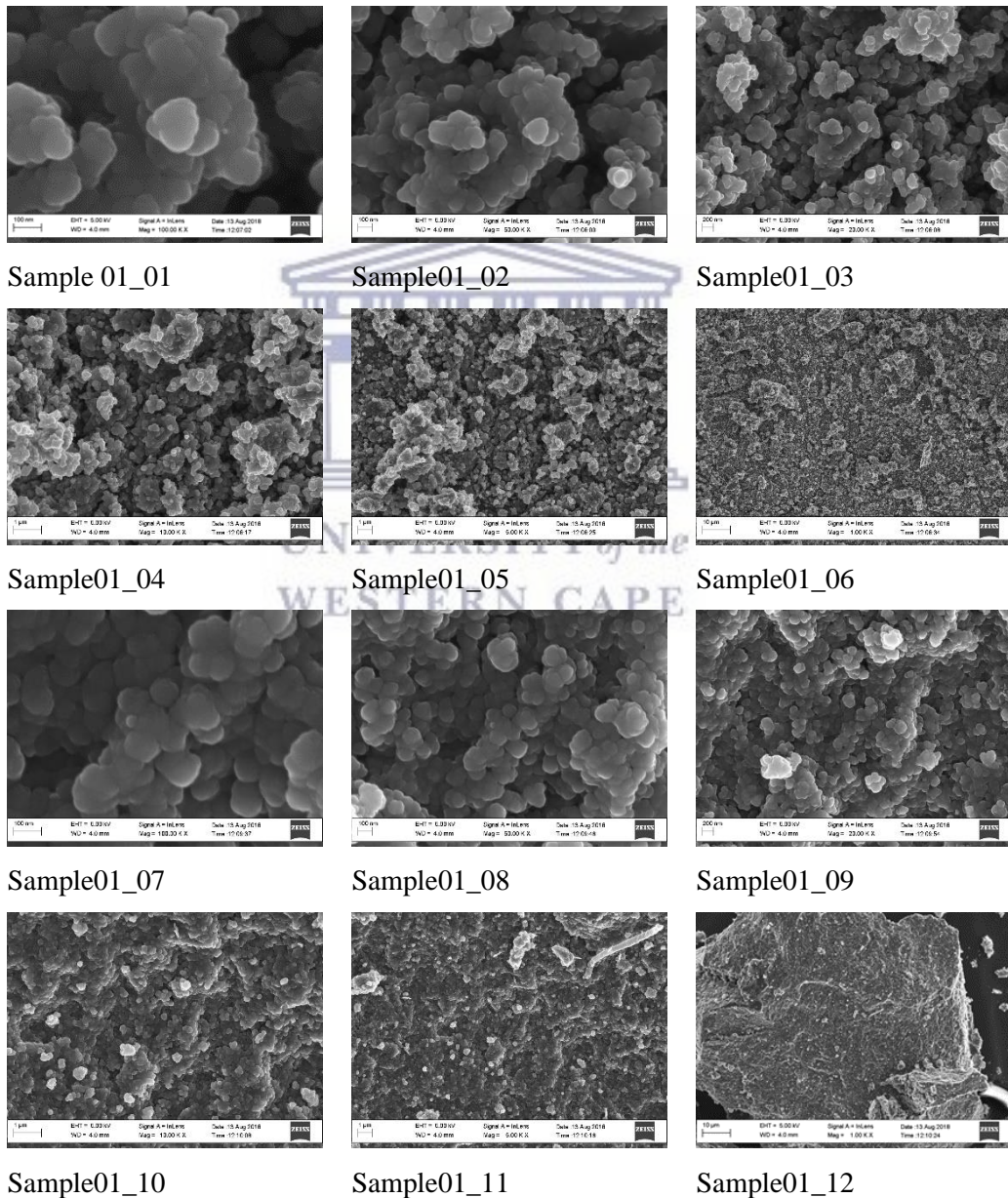


Figure 4.12: SEM images obtained for the uncalcined ZnO NPs

Quasi-spherical shaped ZnO nanoparticles that are agglomerated can be seen in the images. Causes of agglomeration may be due to insufficient quantities of the capping agent (in this case the polysaccharides present in the aqueous extract) being used. These causes need to be further explored in using this phytosynthetic approach for zinc oxide nanoparticle production in the future.

SEM images taken on the 28th August 2018 for the calcined sample can be seen in figure 4.13 below:

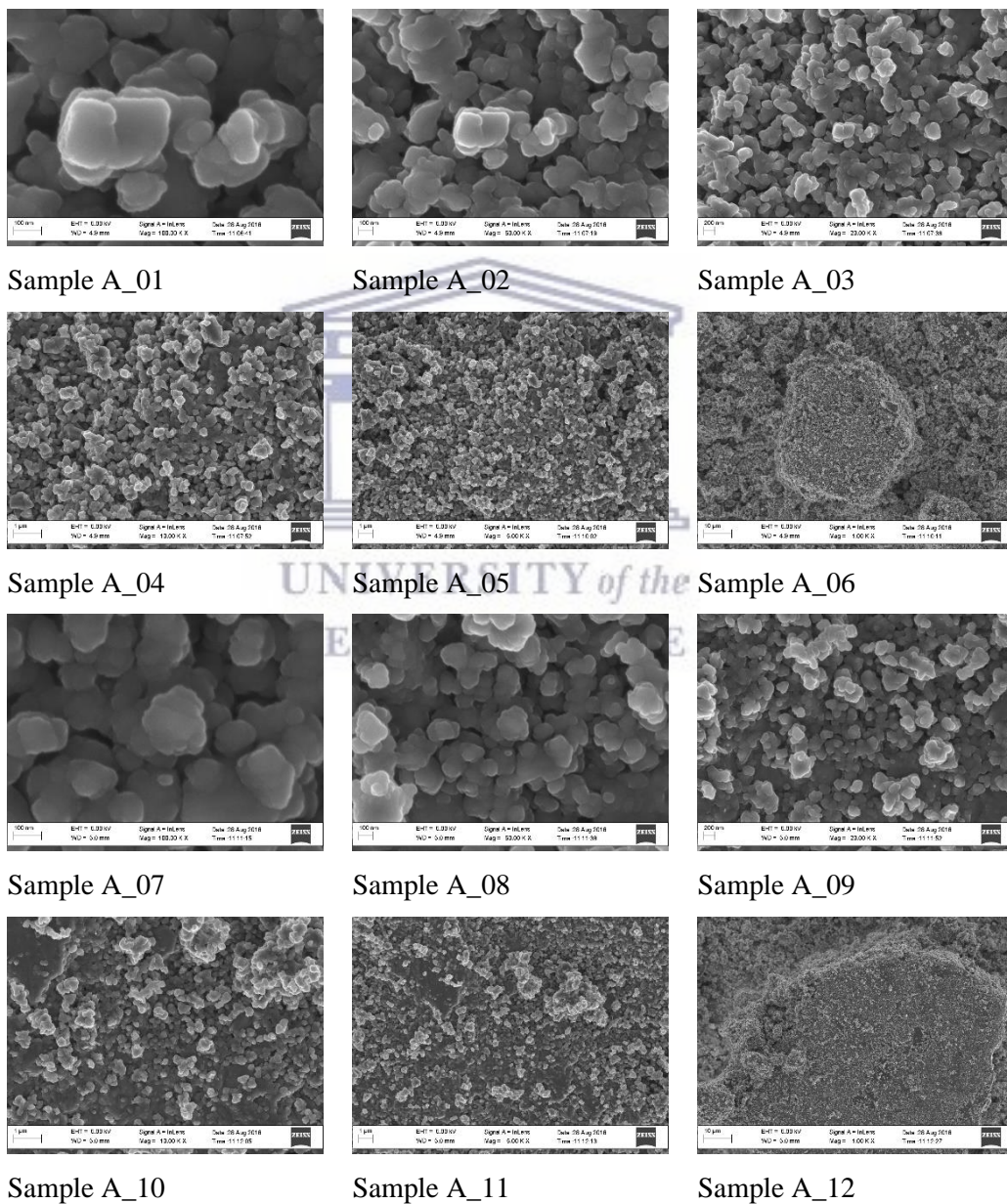


Figure 4.13: SEM images obtained for the calcined ZnO NP sample

Figure 4.14 better shows shape of the particles and approximate sizes of the calcined sample. This image shows the irregular shape of the ZnO nanoparticles, revealing a cauliflower-like agglomeration of particles. The particle shapes are more distinctive/clear for the calcined sample.

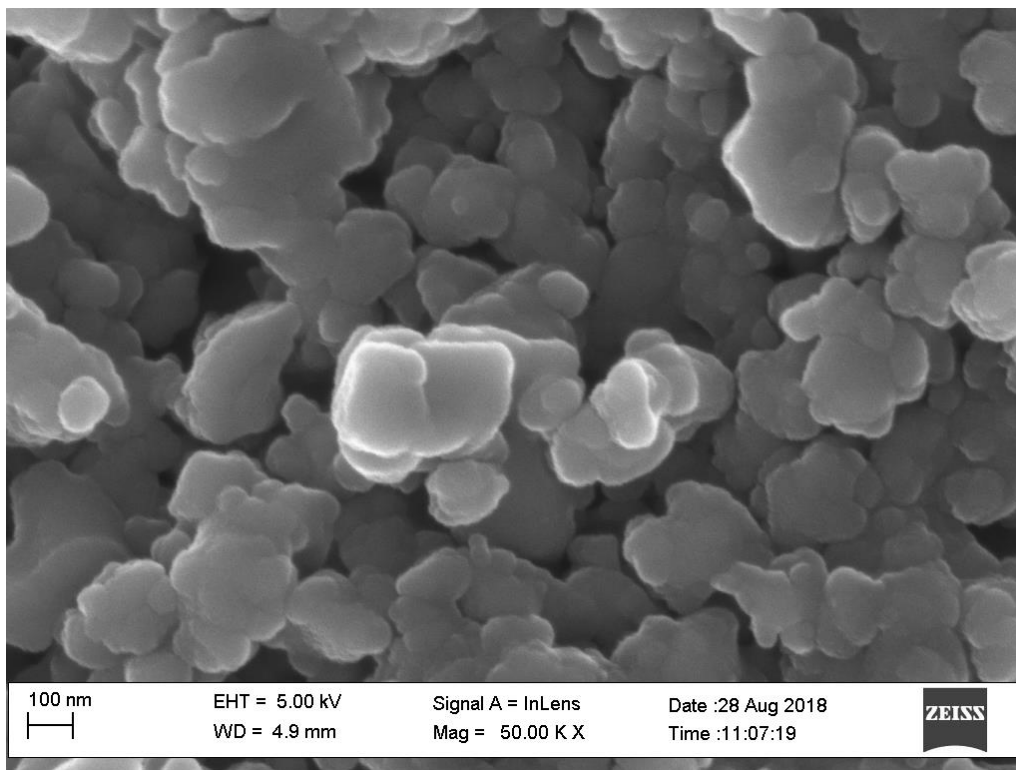


Figure 4.14: Magnified SEM image obtained for the calcined ZnO NPs

Figure 4.15 and Figure 4.16 show the SEM EDX data from the uncalcined ZnO NPs and the calcined ZnO NPs, respectively. The data for both samples confirms the presence of zinc and oxygen species. The intensity of the zinc peaks increased with calcination. The C observed is from the carbon coated grid. For the zinc there are 2 peaks in K series at ~8.6keV and 9.9keV, and 1 in L series at ~1keV.

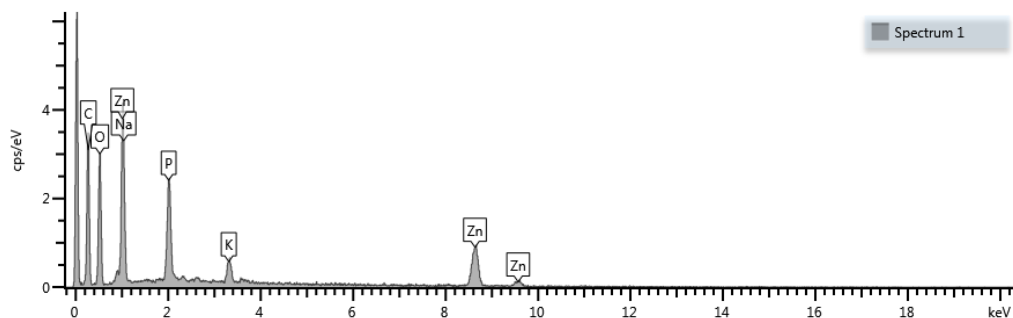


Figure 4.15: EDX data obtained for the uncalcined ZnO NPs

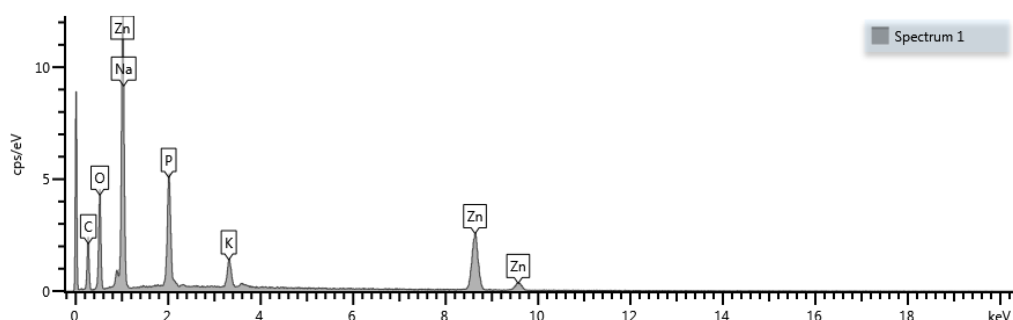


Figure 4.16: EDX data obtained for the calcined ZnO NPs

Table 4.5 provides the weight % and atomic % of the elements in the ZnO NPs samples. It can be seen that in the uncalcined sample there is a higher percentage of atomic oxygen percentage, and a lower Zinc atomic percentage. This is due to the presence of zinc hydroxide in the uncalcined sample which is converted to zinc oxide during calcination as explained by Marslin et al. (2018).

Table 4.5: Weight % and atomic % of ZnO NPs (calcined) and ZnO NPs (uncalcined)

Element	Weight % ZnO NPs (calcined)		Atomic % ZnO NPs (calcined)	Weight % ZnO NPs (uncalcined)		Atomic % ZnO NPs (uncalcined)
	Wt%	Wt% Sigma	Atomic %	Wt%	Atomic %	
O	21.6	0.36	45.6	32.3	57.4	
Na	4.79	0.51	7.04	6.89	8.53	
P	13.8	0.22	15.0	13.6	12.5	
K	3.95	0.11	3.41	3.77	2.73	
Zn	55.9	0.50	28.9	43.5	18.9	
Total	100		100	100	100	

Figure 4.17 and table 4.6 provide the data obtained from the *Calendula officinalis* extract. The data obtained are similar to that obtained for the TEM EDX data.

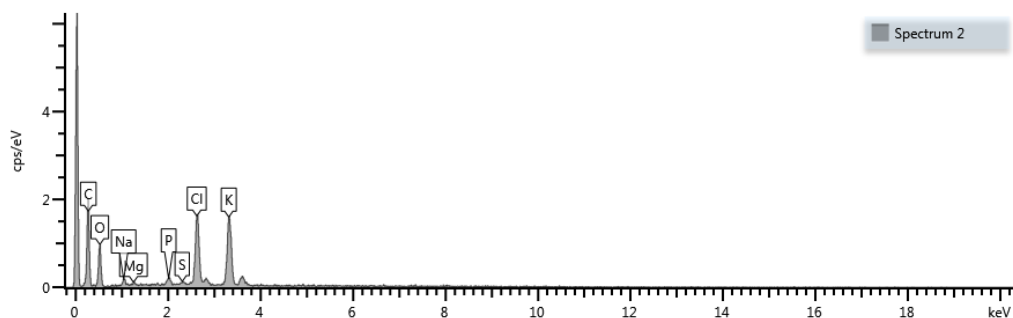


Figure 4.17: EDX *Calendula officinalis* aqueous extract

Table 4.6: EDX data obtained for the *Calendula officinalis* aqueous extract

Element	Wt%	Wt% Sigma
O	48.4	1.35
Na	2.35	0.39
Mg	0.84	0.24
P	1.67	0.25
S	0.63	0.21
Cl	18.99	0.68
K	27.11	0.88
Total:	100	

Figure 4.18 and table 4.7 provide the data for the zinc nitrate hexahydrate.

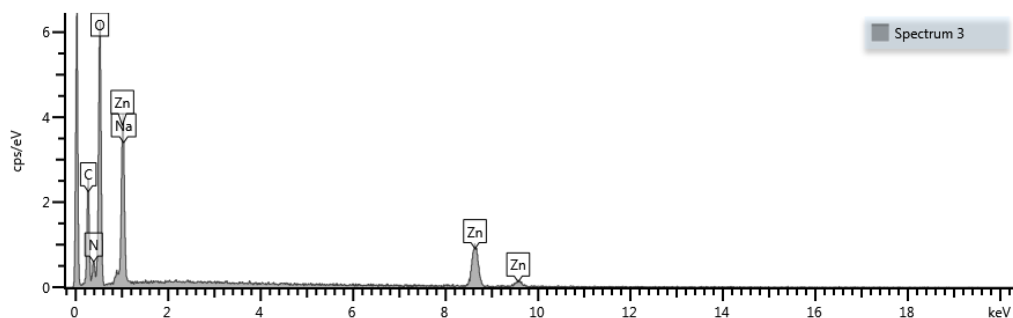


Figure 4.18: EDX data obtained for the zinc nitrate hexahydrate salt

Table 4.7: Weight % zinc nitrate hexahydrate

Element	Wt%	Wt% Sigma
N	9.19	0.97
O	47.28	0.96
Na	4.71	0.81
Zn	38.81	0.93
Total:	100	

The results from the EDX analysis from TEM and SEM are summarised in table 4.8 to enable comparison.

Table 4.8: EDX analysis summary TEM vs. SEM analysis

Sample	EDX (TEM)	EDX (SEM)
ZnO NP uncalcined	C, O, Zn, P, K, Cu	Zn, Na, C, O, P, K
ZnO NP calcined	C, O, Zn, Na, Si, P, K, Ca, Cu	Zn, Na, C, O, P, K
<i>Calendula officinalis</i>	N, Na, Si, S, K, Ca, Cu	O, Na, Mg, P, S, Cl, C, K
Zinc nitrate hexahydrate	O, Cu, Zn, Si	Zn, N, Na, O

The presence of low intensity peaks for C, P, K, Na in the ZnO samples confirms the presence of bioactive compounds from the *Calendula officinalis* extract. The carbon observed in the SEM-EDX is also due to the carbon coated grid used in the analyses. The K and P are likely from the plant extract, and interestingly remain at similar levels between the calcined and the uncalcined sample. It is assumed that these play a role in the capping of the nanoparticles.

4.6. FT-IR spectroscopy

The FTIR spectra are presented in figure 4.19 and the important peaks and possible functional groups present are summarised in table 4.9.

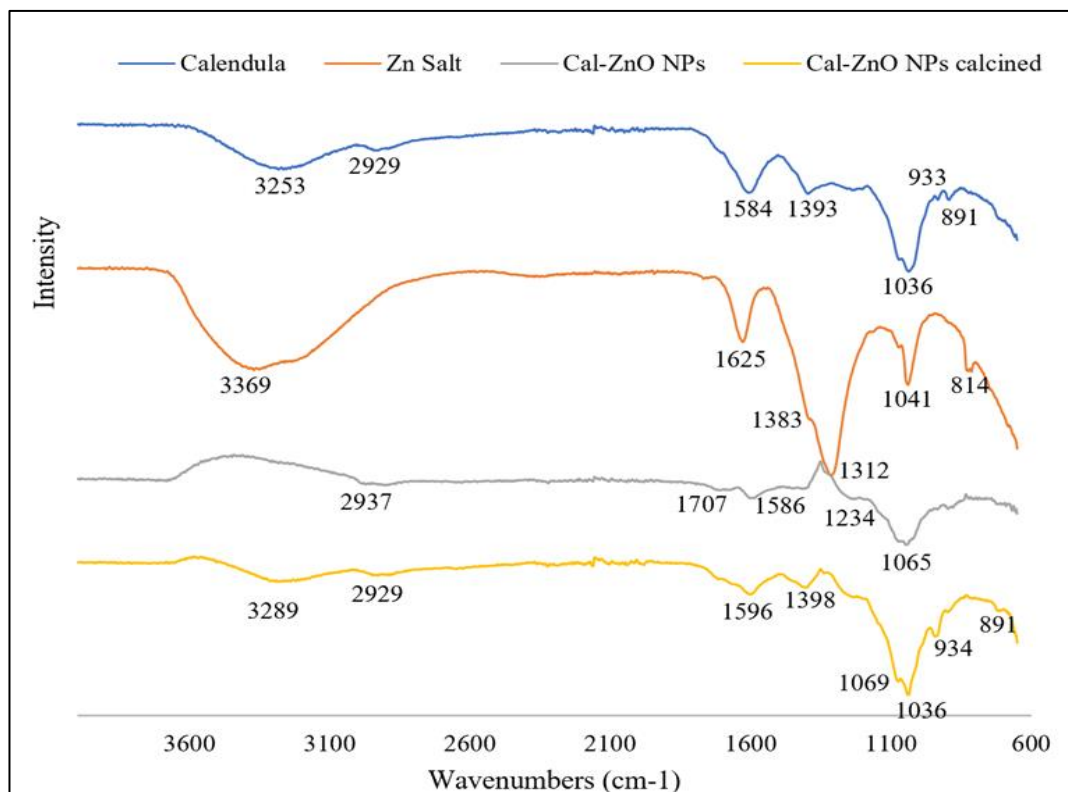


Figure 4.19: FTIR spectral data with labelled peaks

These results support the presence of aliphatic compounds, phenols and aromatic compounds in the formation of the ZnO NPs. Coates (2006) was used in the compilation of this table.

Hydroxy group is evident as a normal ‘polymeric’ OH stretch in both the calcined ZnO NPs and the *Calendula officinalis* extract with the broad band between 3200 and 3400cm⁻¹(Coates, 2006). The presence of a phenol or tertiary alcohol OH bend between 1310 and 1410cm⁻¹ is evident in both *Calendula officinalis* and calcined ZnO NPs (Coates, 2006). The peak at 891cm⁻¹ indicated a possible aromatic C-H out-of-plane bend 1,3-disubstitution (meta) group.

When comparing the FTIR results for the synthesized particles to the results of the starting materials, it can be deduced that the corresponding peaks that remain from the starting materials played a role in the reduction of zinc ions and capping of the zinc oxide nanoparticles. The spectra of the calcined and uncalcined sample were found to be similar, but more well defined for the calcined sample.

Table 4.9: FTIR Summary Table

<i>Calendula officinalis</i> extract		Cal ZnO NPs peaks - calcined	
Wavenumbers	Possible groups	Wavenumbers	Possible groups
3253	Hydroxy group: normal polymeric -OH stretch	3289	Hydroxy group: normal polymeric OH stretch
2929	C-H (Methylene)	2929	C-H (Methylene)
1584	C=C-C aromatic ring stretch (1580 – 1615)	1596	C=C-C aromatic ring stretch (1580 – 1615)
1393	O-H (phenol or tertiary alcohol)	1398	O-H (phenol or tertiary alcohol)
1036	C-H aromatic in-plane bend	1069	C-O stretch, primary alcohol
933	Methylene (cyclohexane ring vibrations)	934	Methylene (cyclohexane ring vibrations)
891	C-H aromatic out-of-plane bend (1,3 disubstitution (meta)).	891	C-H aromatic out-of-plane bend (1,3 disubstitution (meta)).

4.7. TG analysis (Thermogravimetric data)

The TGA data obtained for the four samples can be found in figure 4.20 and table 4.10.

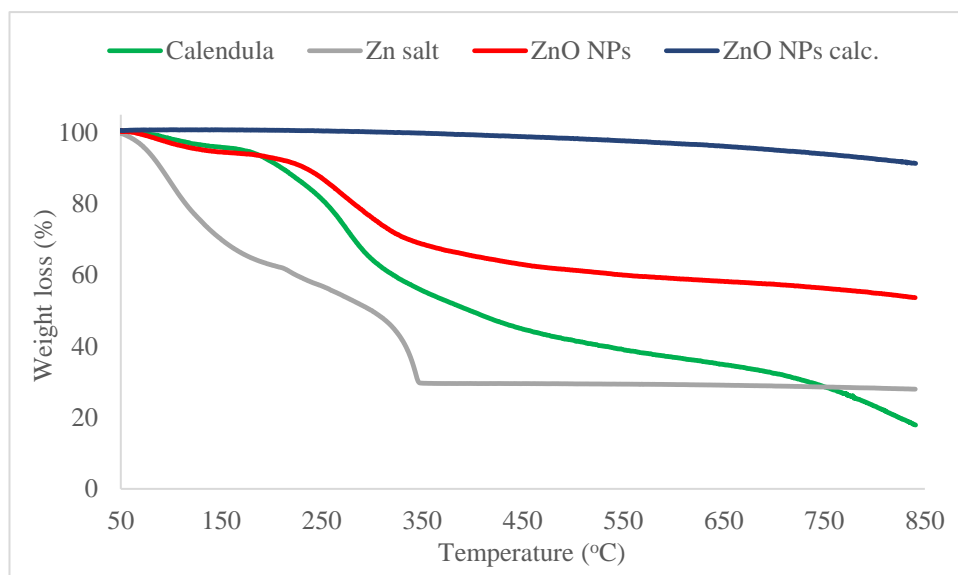


Figure 4.20: TGA data obtained for all four samples

The mass of crystal water in hydrates such as that for the zinc nitrate hexahydrate sample can be measured using thermogravimetry. Loss of crystal water often occurs in multiple dehydration steps. The zinc salt sample shows at least two steps associated with the loss of water initially from 50 to 150 °C and then a second stage from 150 to 350 °C where thermal stability is then achieved. The *Calendula officinalis* extract also shows multistage decomposition processes starting with dehydration and then carbon material decomposition at 250°C and again at around 750°C. ZnO NPs uncalcined underwent a loss of water and then a second step at around 250°C which may be attributed to the conversion of the Zinc hydroxide to Zinc oxide. One way to confirm this would be to have the TGA in tandem to an MS or FT-IR spectrometer which was not available. This further indicates the need for calcination with regards to this particular method of preparation. The calcined ZnO NPs have quite a different weight loss profile to the other samples, having only a slight decomposition, indicating high thermal stability. This is to be expected as the

calcination process would already have led to significant weight loss as carbonated material would have been removed by the calcination process at 600 °C.

From the above results we may be able to conclude that there is more residual *Calendula officinalis* extract in the uncalcined ZnO nanoparticles as compared to the calcined particles. The data is summarised in table 4.10.

Table 4.10: Tabulated TGA data for all four samples

Sample	Starting weight (mg)	End weight (mg)	Weight difference	% weight loss	% remaining
ZnO NPs Uncalcined	1.82	0.98	0.84	46.5	53.5
ZnO NPs Calcined	1.96	1.79	0.17	8.7	91.3
<i>Calendula officinalis</i> powder	1.47	0.26	1.21	82.1	17.9
Zinc nitrate hexahydrate	4.82	1.35	3.47	72.0	28.0

4.8. NMR data

Invaluable preliminary information regarding the main constituents of the *Calendula officinalis* extract may be provided by 2D HSQC NMR. Direct ¹H-¹³C bond correlations are observed in these experiments coupled with the separation or resolution offered by the second dimension. Since no further purification was carried out after obtaining the aqueous extracts, only the main structural features of the extracts were identified. A multiplicity edited HSQC experiment was employed allowing one to distinguish between methyl, methylene and methine signals. Figure 4.22 shows the HSQC NMR spectrum for the *Calendula officinalis* aqueous extract

acquired in DMSO-*d*₆ at 333K. The ¹H NMR data obtained can be found in figure 4.21 below.

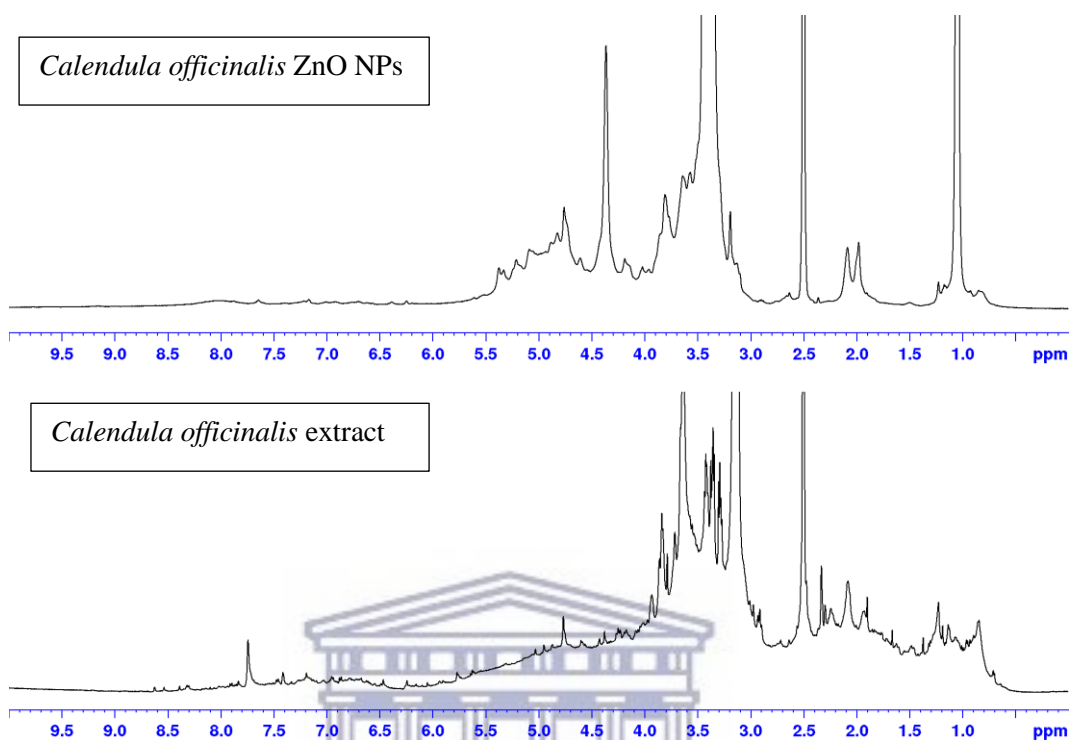


Figure 4.21: ¹H NMR data obtained for the *Calendula* extract and the calcined ZnO NPs in DMSO-*d*₆ at 333K (500 MHz)

The ¹H NMR spectrum reveals a large number of overlapping proton signals, making analysis of the ¹H NMR spectrum alone problematic. However, because a second dimension provides the ¹³C signals along the y-axis, one is able to obtain some resolution which in turn offers substantial information. The sugar oxymethine carbons between δ 60 and 80 are easily observed, together with signals visible at approximately δ 100, indicative of the presence of anomeric carbons of sugar moieties. Korzh et al. (2012), isolated acidic polysaccharides from *Calendula officinalis* flowers. The authors suggested that the different fractions they obtained from the water-soluble polysaccharide complex isolated have structures of rhamnagalacturonan I with varying degrees of branching. Additionally, characteristic, albeit far weaker, signals present at δ_C/δ_H 99/6.3 suggest the presence of polysaccharides or polyphenols as minor constituents in the aqueous extract. In addition, several signals corresponding to the aromatic signals of polyphenols may be observed at $\sim\delta_H$ 7.5- 6.5 correlating to carbon signals at 110 – 130 ppm. Danila,

Gatea, Radu (2011) found the presence of polyphenols in aqueous extract of *Calendula officinalis*, however the authors did not specify which part of the plant was used in their study. Mubashar et al. (2015) showed the presence of both flavonoids and polyphenols in aqueous extract made from *Calendula officinalis* flowers. The authors reported that the major compounds in the flower extract were chlorogenic acid, caffeic acid, rosmarinic acid, kaempferol and luteolin.

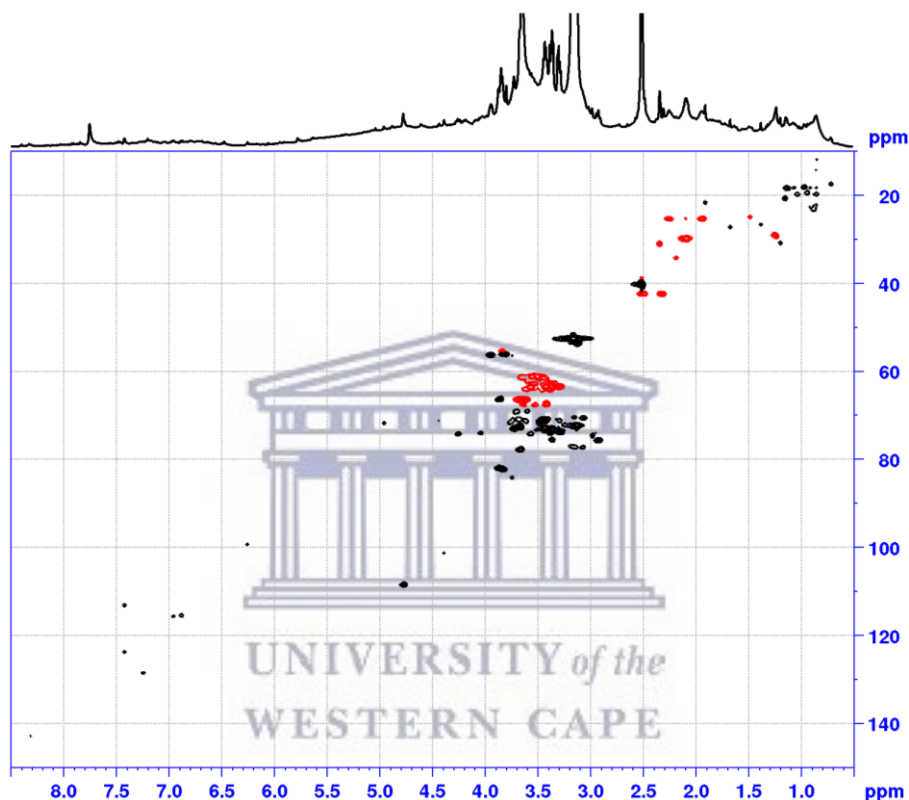


Figure 4.22: HSQC NMR (500 MHz) spectra acquired in DMSO- d_6 at 333K for the aqueous extract of *Calendula officinalis*.

Figure 4.23 shows the HSQC NMR spectrum for the ZnO NPs synthesised with *Calendula officinalis* aqueous extracts. These spectra were also acquired in DMSO- d_6 at 333K. Once again, the ^1H NMR spectrum reveals a large, similar number of overlapping proton signals. The ^{13}C spectrum along the second dimension still reveals the presence of the sugar oxymethine carbons between δ 60 and 80 and the anomeric carbons at ~ 100 ppm. The weaker signals at approximately $\delta_{\text{C}}/\delta_{\text{H}}$ 99/6.3 and the aromatic signals indicative of polysaccharides of polyphenols are now

conspicuously absent. This may be due to the polyphenols or polysaccharides being a minor constituent already in the aqueous extract - thus precluding their visibility, or because they are involved in capping the NP itself. The latter may also be supported by the observed increase in broadness of the signals in the proton spectrum. Small molecules attached to metallic nanoparticles are at the interface of a solid support and the solution (Marbella & Millstone, 2015). This may lead to line broadening, altering of the chemical shift, and there could be complete disappearance of some of the resonances (Marbella & Millstone, 2015). Ogoshi, Umeda, Yamagishi, & Nakamoto (2008) reported the disappearance of proton signals from a phenol moiety in the synthesis of polymer coated gold nanoparticles as a result of inter- and/or intra-hydrogen bonding between the gold nanoparticles and the phenol-containing moiety.

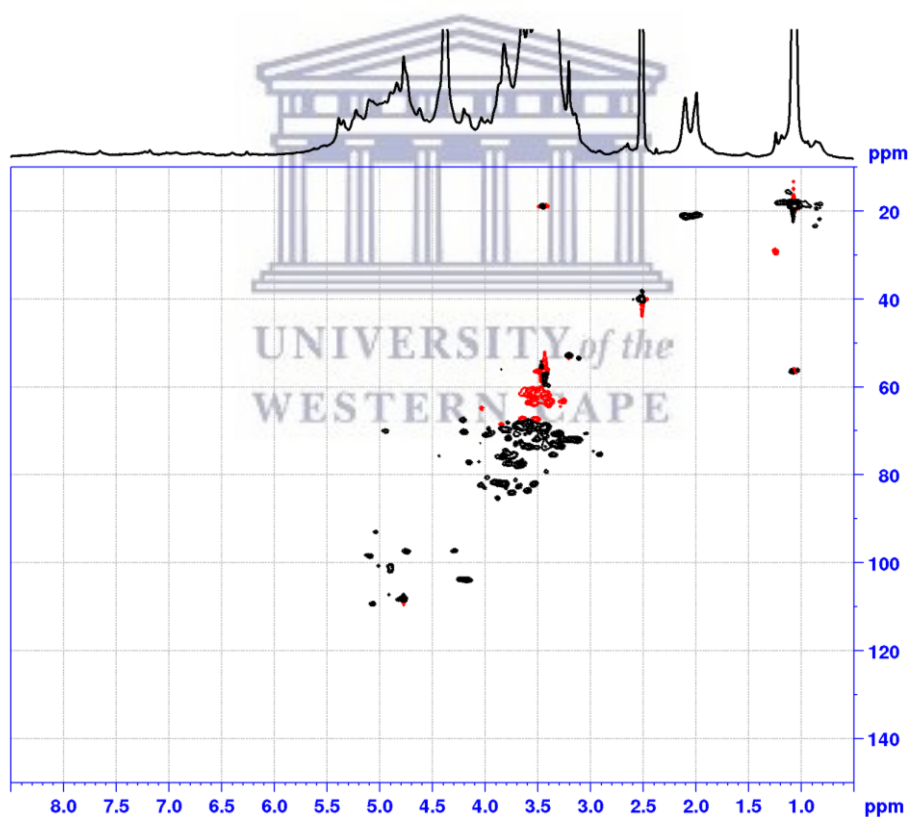


Figure 4.23: HSQC NMR (500 MHz) spectra acquired in DMSO-*d*₆ at 333K for the ZnO NPs (uncalcined sample) synthesised with the aqueous extract of *Calendula officinalis*.

Polysaccharides are water soluble and may play a part in the formation of the nanoparticles. From NMR results, the presence of sugar moieties confirm that polysaccharides may be involved in the formation of the zinc oxide nanoparticles.

4.9. Discussion of results

UV-vis spectrometry and DLS only works well with well-dispersed particles. It is evident from the results that the particles had a tendency towards agglomeration. A limitation in the interpretation and comparison of the different results relating to the size of the nanoparticles, is the lack of DLS results for the calcined particles.

Table 4.11 shows the comparative TEM and XRD size results of the ZnO NPs (calcined).

Table 4.11: ZnO NPs (calcined) TEM vs XRD mean size

Sample	TEM Size (nm)	XRD (nm)
	Mean Size	
ZnO NPs (calcined)	4.72	53.14

As can be seen in table 4.11 there is a large difference between the sizes obtained from TEM and XRD for the calcined sample. Below follows a discussion of the possible explanations for the differing sizes observed for both the calcined and the uncalcined samples.

The difference in particle size observed between TEM and DLS for the uncalcined sample may be interpreted as being due to the presence of capping agents present in the plant extract. TEM measures the zinc oxide core, whereas DLS measures the hydrodynamic radius of the particles. Capping of the NP is expected to be from the constituents contained in the *Calendula officinalis* aqueous extract which is primarily comprised of polysaccharides as revealed by the NMR data. Additionally, DLS assumes spherical particles, and, as can be seen from the SEM images, the particles are not spherical but rather quasi-spherical tending towards a cuboid shape in morphology. The difference in particle size observed between TEM and XRD may be due to methods used with the XRD data in determining the average particle size for the whole sample, TEM results are usually limited to particular sections of

the grid. Additionally, TEM data may be showing just the zinc oxide core whereas data from other techniques such as DLS pertain to the entire capped nanoparticle.

From FTIR and NMR data it is evident that constituents that may have played a role in the reduction of metal ions and capping of the zinc oxide nanoparticles and include polysaccharides, polyphenols, and aromatic compounds. There was lack of saponification on shaking the calcined sample, so it is assumed that the saponins are no longer present and they were not remaining as capping agent. There was saponification with the uncalcined sample, so it is likely that the saponins played a role in the reduction of the metal ions but, they do not remain following the calcination process.

4.10. Antioxidant assays

4.10.1. Radical scavenging

The 2,2-diphenyl-1-picrylhydrazyl (DPPH) scavenging method is based on the ability of the DPPH radical to be reduced to a more stable DPPHH form by antioxidants (Tobwala et al., 2014). The results obtained are summarised in the table 4.12 with the *Calendula officinalis* extract at 5mg/ml having the highest scavenging power.

Table 4.12: Radical scavenging results

Sample Name	Concentration	Average	Scavenging Power (%)
Cal-ZnO (calcined)	(1.00 mg/ml)	0.283	4.83
Calendula	(1.00 mg/ml)	0.249	16.16
Cal-ZnO NPs (uncalcined)	(1.00 mg/ml)	0.321	-7.97
Calendula	(5.00 mg/ml)	0.166	44.00
Cal-ZnO NPs (uncalcined)	(4.50 mg/ml)	0.265	10.66
DPPH	1.00x10 ⁻⁴ M	0.297	N/A
		Formula:	[1-(x/DPPH)]x100%

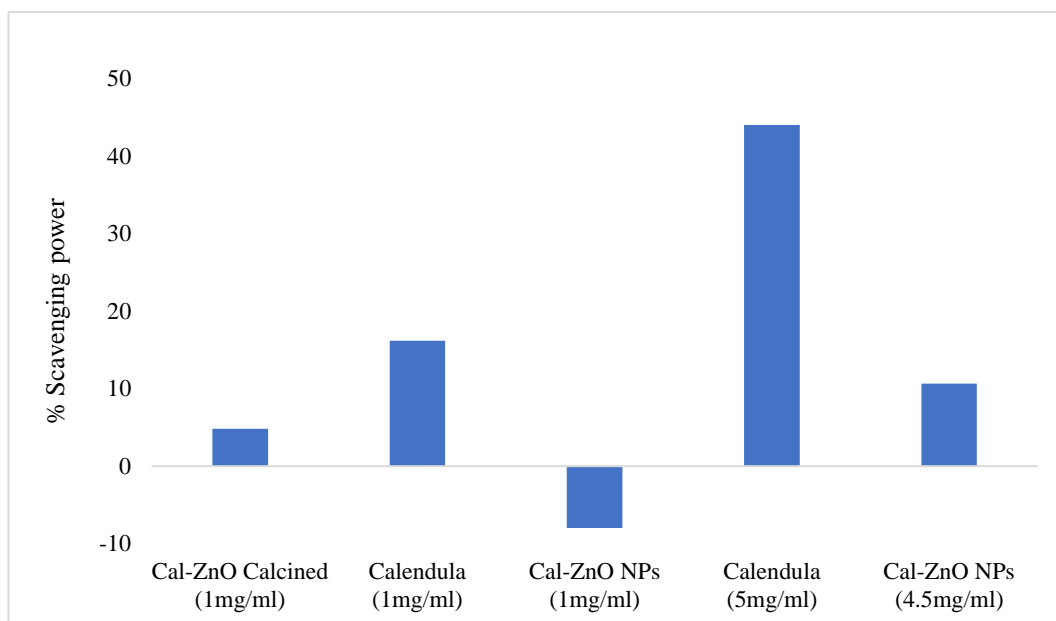


Figure 4.23: DPPH percentage radical-scavenging activity obtained for the samples analysed.

As seen in figure 4.23, all of the samples other than the 1mg/ml Cal-ZnO NPs showed DPPH radical-scavenging activity. The results indicate the presence of constituents that have antioxidant activity in the *Calendula officinalis* extract, which remain once the ZnO nanoparticles have been synthesized. The assay is based on measuring the decrease in absorbance of the DPPH (upon conversion to DPPHH) at 520 nm. The negative results obtained for 1mg/ml Cal-ZnO NPs appears to be an anomaly and may be due to experimental error, since the same sample at 4.5 mg/ml revealed 10% scavenging activity. The absorbance obtained for the 1mg/ml Cal-ZnO NPs (i.e. the NP sample before calcination step which still contains the *Calendula* extract) is higher than that obtained for the DPPH standard sample which explains the negative result. This may be due to the absorbance that the extract itself has at 520 nm, but then negative results should also have been obtained for the 4.5mg/ml Cal-ZnO NP sample and the *Calendula* extracts alone. It is our opinion then, that the negative result obtained here is due to some experimental error and the lack of solubility of the NP samples.

4.10.2. Total reducing power

A sample's reducing power can be used as an important index of antioxidant potential as it is associated with the compound's antioxidant activity (Tobwala et al., 2014). The results for total reducing power are summarised in the tables and figures that follow. The total reducing power (given as ascorbic acid equivalents (AAE), in $\mu\text{g}/\text{mg}$ of dried sample) of the samples is summarised in table 4.13. Firstly, a calibration curve was constructed using ascorbic acid and this is shown in figure 4.24. The results obtained by using the linear regression equation was then used to determine the total reducing power for each of the samples. The R^2 value is quite low at 0.8347, however. As expected, the *Calendula* extract (5mg/ml) was found to be have the greatest reducing power (figure 4.25, table 4.13) since it was clear from the DPPH studies and the NMR spectra, that antioxidants (as well as polysaccharides) are constituents of the extracts. The uncalcined ZnO NP sample (1mg/ml), followed closely by the 1mg/ml *Calendula* extract sample were shown to have moderate reducing power (figure 4.25). It is clear from figure 4.25 (and table 4.13) that the calcined NPs and the higher concentration used for the uncalcined ZnO NPs appears to have negligible to little reducing power. For the latter sample, this may stem from a decrease in solubility for the sample, while the calcined sample has been shown by TGA for example, to have little to no capping as the calcination process (which was necessary to effect the final conversion to a crystalline sample) is carried out at 600 °C.

Table 4.13: Total Reducing Power

Sample Name	Concentration	Average absorbance	Total Reducing Power (AAE, in $\mu\text{g}/\text{mg}$ of dried sample)
ZnO NPs Calcined	(1.0 mg/ml)	0.034	26.4
<i>Calendula</i>	(1.0 mg/ml)	0.188	144.6
ZnO NPs	(1.0 mg/ml)	0.192	147.7
<i>Calendula</i>	(5.0 mg/ml)	0.239	183.9
ZnO NPs	(4.5 mg/ml)	0.086	66.4

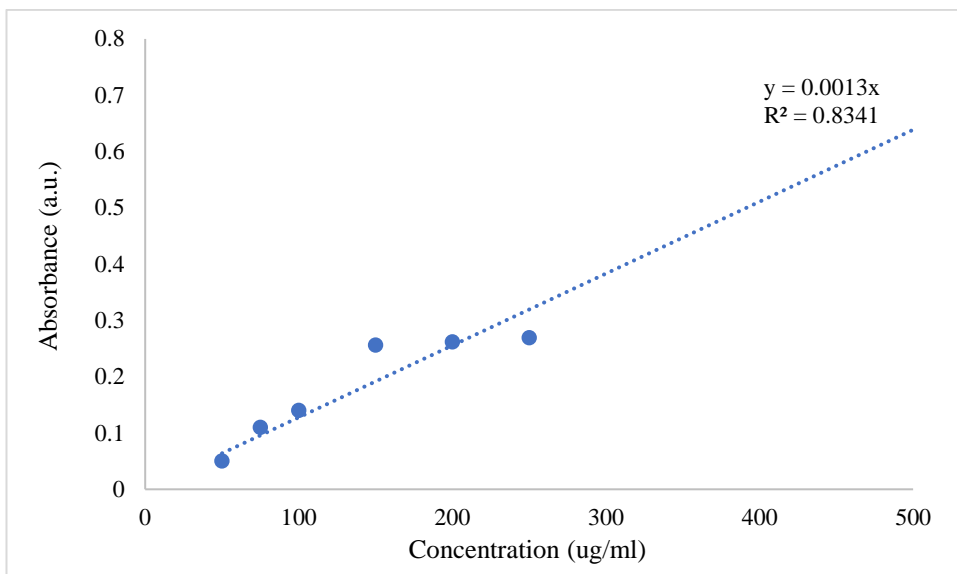


Figure 4.24: Graph plotting the reducing power (absorption) against concentration of the Ascorbic Acid.

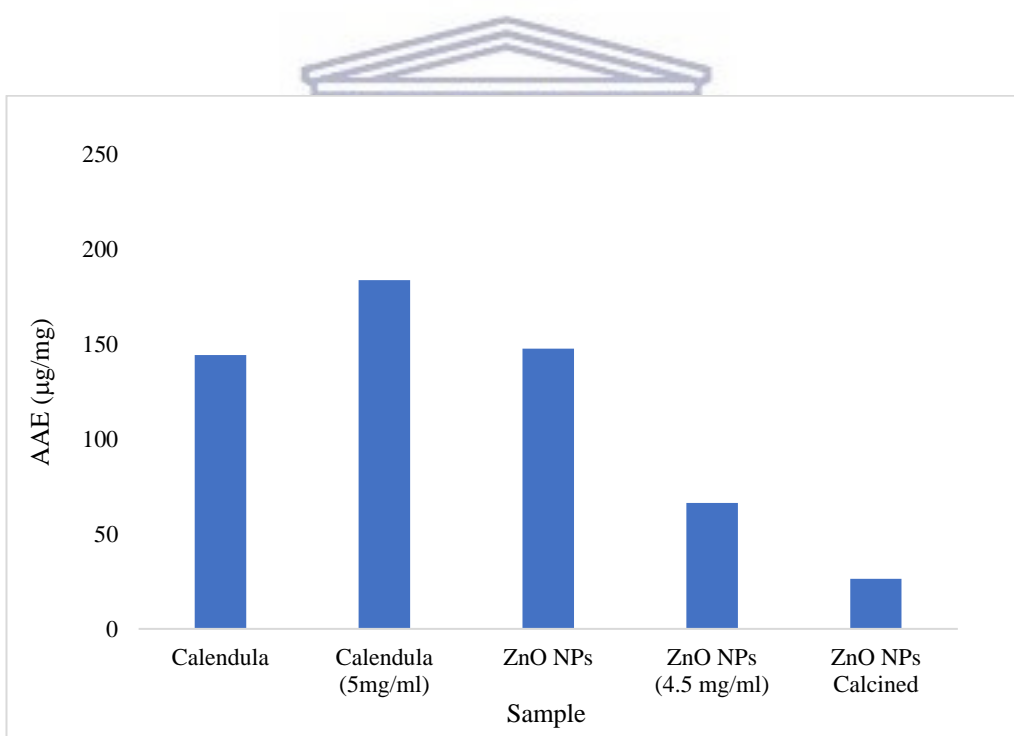


Figure 4.25: Total reducing power AAE in $\mu\text{g/mg}$ of dried sample. The concentration for the sample was 1mg/ml unless otherwise stated.

Reabsorption of the *Calendula* extract onto the calcined ZnO NP would no doubt lead to enhanced reducing power values, but due to time constraints these experiments were not conducted.

4.10.3. Polyphenolic content

The results for the polyphenolic content are summarised in table 4.14 and the polyphenolic content data was obtained from figures 4.26 and 4.27. The total phenolic content is expressed as gallic acid equivalents (GAE) μg per mg dried sample and once again a calibration curve was constructed at first (as shown in figure 4.27). The slope of the curve was then used to calculate the gallic acid equivalents for each of the samples (figure 4.26). The sample with the greatest polyphenolic content was determined to be the calendula extract (5 mg/ml) followed the 1 mg/ml *Calendula* extract sample with GAE values of 288 and 105 $\mu\text{g}/\text{mg}$, respectively. This was followed by the uncalcined samples at 4.5 mg/ml and 1 mg/ml with GAE values of 28 and 98 $\mu\text{g}/\text{mg}$ of sample. These results were obtained by forcing the intercept to go through zero, otherwise negative values would be obtained. The calcined ZnO NPs sample once again had the lowest polyphenolic content as seen in the antioxidant and total reducing power assays. From the above assays we can conclude that polyphenols are indeed present in the plant extract and that they could likely have assisted in the formation of the zinc oxide nanoparticles.

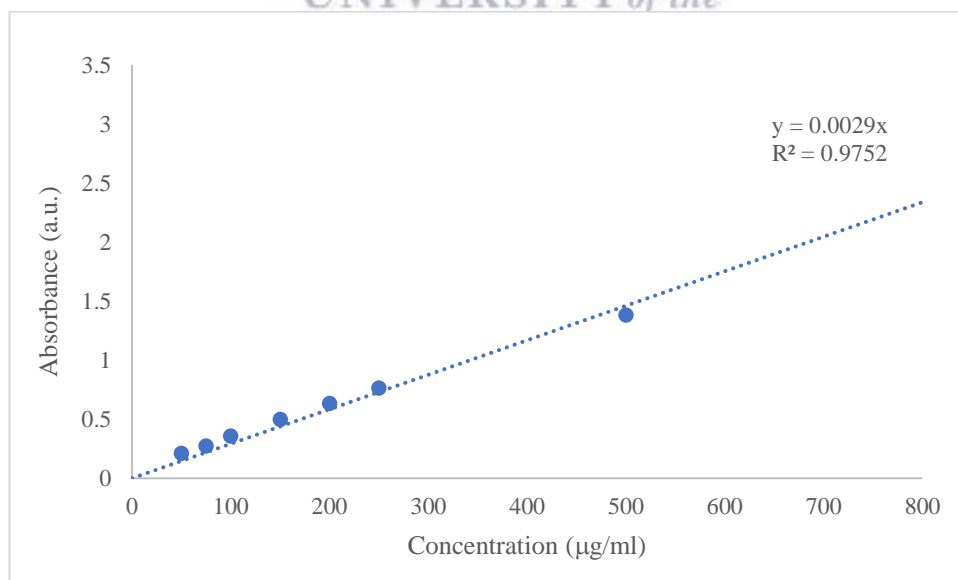


Figure 4.26: Total polyphenolic content: Gallic acid absorption vs. concentration

Table 4.14: Average results for Polyphenolic content (GAE)

Sample Name	Concentration	Average absorbance	Total Polyphenolic Content GAE, in $\mu\text{g}/\text{mg}$ of dried sample)
Calendula	(1.00 mg/ml)	0.306	105.4
Calendula	(5.00 mg/ml)	0.834	287.7
Cal-ZnO NPs	(1.00 mg/ml)	0.082	28.16
Cal-ZnO NPs	(4.50 mg/ml)	0.284	98.05
Cal-ZnO Calcined	(1.00 mg/ml)	0.061	20.92

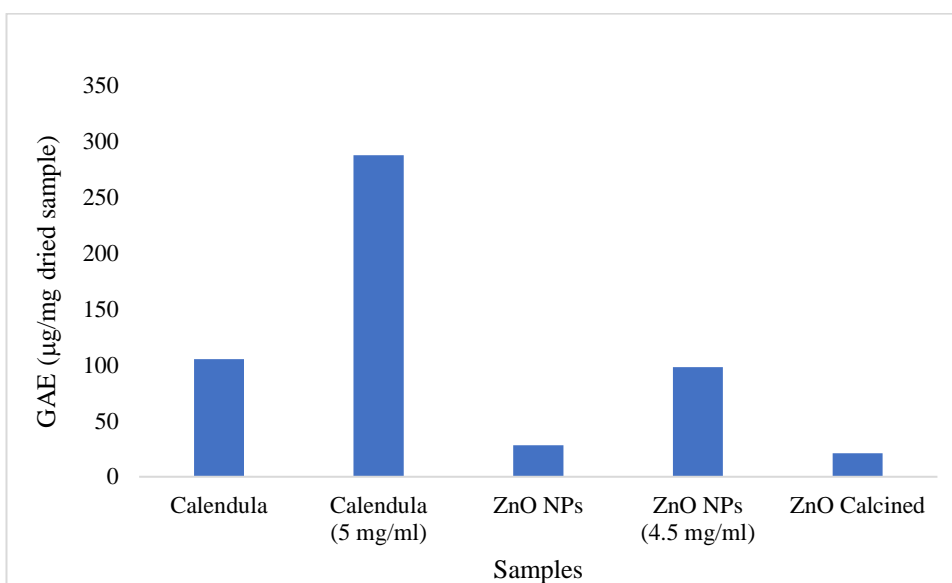


Figure 4.27: Total Polyphenolic Content (GAE) in $\mu\text{g}/\text{mg}$ of dried sample

Discussion of Antioxidant assays

Several flavonoids have the capability of chelating metal ions via formation of a stable complex through the carbonyl moiety and hydroxyl (-OH) groups (Marlin et al., 2018). It is important to consider the influence that an extraction method has on the phytochemical constituents present in the resulting aqueous extract of *Calendula officinalis*. Polar constituents would be more readily dissolved by this extraction method than non-polar constituents. As stated in Chapter 2, Goktas et al., (2015) found that different phytochemical constituents were found to be higher under different conditions. The extraction method chosen as 7 hours at 41°C was chosen to ensure maximum extraction of flavonoids in order to make use of their reducing properties.

Evidence of antioxidant activity, reducing power, and polyphenol content is apparent in the *Calendula officinalis* extract, as well as the synthesized uncalcined ZnO NPs. The constituents that provide this activity are likely responsible for the reduction of zinc ions and capping of the zinc oxide. Further investigation into the constituents of the aqueous extract would provide additional insight into constituents that are of importance in this green synthesis method. Flavonoids would be likely candidates to further explore given the chosen extraction and evidence of antioxidant activity.

4.11. Antimicrobial assays

The minimum inhibitory concentration (MIC) evaluation of the samples was prepared using Clindamycin (1%) as a control. The testing was performed against methicillin resistant *Staphylococcus aureus* (Melbourne Pathology, wild strain).

The aqueous extract of *Calendula officinalis* showed a MIC > 8.25mg/ml, while the zinc nitrate hexahydrate salt alone in distilled water had an MIC = 5.875mg/ml. Formation of the ZnO NPs (uncalcined) in distilled water revealed an MIC at a higher concentration (9.5mg/ml). Calcination of these NPs showed an MIC >7.75mg/ml. Comparatively, Clindamycin had an MIC of 0.5% at 5mg/ml.

Further testing is needed to investigate whether higher concentrations have effective antimicrobial activity. As the samples were prepared in distilled water, solubility is an area warranting further investigation as ZnO has limited solubility in water. UV-Vis spectroscopy and DLS results indicated agglomeration and the antimicrobial activity observed was likely due to the effect of particle agglomerates. Investigating whether different solvents make a difference would be worthwhile in future work. Interestingly, the uncalcined sample showed MIC of 9.5mg/ml. This sample still had presence of polysaccharides and polyphenols, which the calcined sample did not appear to have (based on visual observation of foaming ability). Due to the lack of availability of results of higher concentrations of the calcined ZnO NPs, it is not possible to say whether the constituents may be playing a role in the

release of the ZnO. Considering that the *Calendula officinalis* extract did not show antimicrobial activity at the given dose, it is unlikely that the constituents exerted antimicrobial activity, but rather that they possibly played a role in the solubility of the ZnO nanoparticles in the distilled water, or the delivery of the ZnO nanoparticles to exert an antimicrobial effect on the bacteria. Supported mechanisms revealing how ZnO NPs produce toxic effects include the generation of ROS and release of Zn²⁺ (Vimbela et al., 2017), therefore the solubility and delivery of the zinc ions is important to consider when investigating the antimicrobial activity of ZnO NPs. Due to the limited solubility of zinc oxide and its nanoparticles, it is less toxic to microbes than the highly soluble zinc sulphate (Siddiqi et al., 2018). Addressing solubility concerns may be a way to increase the toxicity of zinc oxide to microbes. In the study by Patil & Taranath (2018), the zinc salt alone did not appear to exert antimicrobial activity against *Staphylococcus aureus*, but this may be related to the concentration used.



CHAPTER 5: CONCLUSIONS AND FUTURE RECOMMENDATIONS

To answer the research question “Does the aqueous *Calendula officinalis* extract effectively reduce zinc ions present in zinc salt to ZnO?” Yes, from the plethora of techniques and data obtained, the zinc ions were reduced to ZnO, but further calcination is needed to finish the conversion of remaining Zn(OH)₂ to ZnO.

Successful synthesis of ZnO NPs was achieved using a novel one-pot green chemistry method. Calcination of the nanoparticles improved the crystallinity of the zinc oxide by final conversion of remaining zinc hydroxide to zinc oxide. The particles had varying morphology with quasi-spherical and rod-like structures evident. They tended towards agglomeration resulting in a cauliflower like the images revealed by SEM. TEM results indicated a zinc oxide core <10nm in size. The phytochemicals present in the aqueous *Calendula officinalis* extract contributed to the reduction of the metallic ions and the subsequent capping. Potential for further work to identify the constituents contained within the extract by liquid chromatography, and the subsequent testing of formation of nanoparticles with isolated versions of the constituents may provide further insight into the constituents responsible for the formation of the particles. Even though this would be interesting, oftentimes the complexity and interaction of the various components within a plant extract is what leads to the reduction, and studying this complexity is complicated. From the FTIR and NMR spectra and antioxidant studies results, it is likely that polyphenols, flavonoids, aromatic compounds and sugars are responsible for the reduction of the zinc ions and capping of zinc oxide nanoparticles. Polyphenols could possibly be responsible for the reduction of Zn²⁺ to ZnO. The presence of polyphenolic compounds is confirmed by the antioxidant assays, FTIR, and NMR. From the FTIR spectra, the presence of phenols were observed, as well as the presence of aromatic compounds, while the antioxidant assays showed that *Calendula officinalis* can be used as an effective reducing agent.

Characterisation of the particles revealed differences in sizes between TEM and XRD. This may be due to TEM giving an indication of the metallic zinc oxide core, and not the surrounding organic capping layer. XRD gives an indication of the

average size of particles in the sample and is more suited to spherical particles which might explain the larger size obtained compared to TEM results. Irrespective of the size differences, these particles are worthy of further investigation. Due to the wide availability of *Calendula officinalis* and the history of use in the biomedical field, it would be worthwhile researching the feasibility of production of ZnO NPs using the reported method. However, preceding this, investigation into stabilisation of the particles and prevention of agglomeration is warranted. Particles of predictable size would also be important to focus on in future research.

Future antimicrobial testing should be done in detail. Antimicrobial resistance is dependent on a variety of factors with biofilm formation playing an important role. Future work should include MIC testing at higher concentrations to establish whether there is antimicrobial activity at higher concentrations, and then testing should be focused on bactericidal studies and biofilm inhibition studies. Investigating the impact of reabsorbing the plant extract onto the ZnO NPs following calcination could also be investigated to see if this improves antimicrobial activity by potentially enhancing delivery of the ZnO NPs via penetrating of the cell wall of the microbes. Due to zinc's photocatalytic ability, it is also worthwhile investigating whether inhibition of microbes differs markedly under irradiation.

Limitations encountered during this research include working between multiple laboratories to obtain the data. Reproduction of the results by another researcher would further support the results and the subsequent potential for the application of these particles in the biomedical field. Further limitations include the lack of sample stability studies, and the lack of extensive investigation into the constituents present in the aqueous extract of *Calendula officinalis*.

REFERENCES

- Abd Elkodous, M., El-Sayyad, G. S., Abdelrahman, I. Y., El-Bastawisy, H. S., Mohamed, A. E., Mosallam, F. M., ... El-Batal, A. I. (2019). Therapeutic and diagnostic potential of nanomaterials for enhanced biomedical applications. *Colloids and Surfaces B: Biointerfaces*, 180, 411–428. <https://doi.org/10.1016/j.colsurfb.2019.05.008>
- Agarwal, H., Menon, S., Kumar, V.S., & Rajeshkumar, S. (2018). Mechanistic study on antibacterial action of zinc oxide nanoparticles synthesized using green route. *Chemico-Biological Interactions*, 286, 60–70. <https://doi.org/10.1016/j.cbi.2018.03.008>
- Akhtar, M. S., Panwar, J., & Yun, Y.-S. (2013). Biogenic Synthesis of Metallic Nanoparticles by Plant Extracts. *ACS Sustainable Chemistry & Engineering*, 1(6), 591–602. <https://doi.org/10.1021/sc300118u>
- Aleaghil, S. A., Fattahy, E., Baei, B., Saghali, M., Bagheri, H., Javid, N., & Ghaemi, E. A. (2016). Antibacterial activity of Zinc oxide nanoparticles on *Staphylococcus aureus*. *International Journal of Advanced Biotechnology and Research*, 7(3), 1569–1575.
- Al-Hada, N. M., Saion, E., Shaari, A. H., Kamarudin, M. A., & Gene, S. A. (2014). The Influence of Calcination Temperature on the Formation of Zinc Oxide Nanoparticles by Thermal-Treatment. *Applied Mechanics and Materials*, 446–447, 181–184. <https://doi.org/10.4028/www.scientific.net/AMM.446-447.181>
- Arora, D., Rani, A., & Sharma, A. (2013). A review on phytochemistry and ethnopharmacological aspects of genus *Calendula*. *Pharmacognosy Reviews*, 7(14), 179–187. <https://doi.org/10.4103/0973-7847.120520>
- Azizi, S., Mohamad, R., & Mahdavi Shahri, M. (2017). Green Microwave-Assisted Combustion Synthesis of Zinc Oxide Nanoparticles with *Citrullus colocynthis* (L.) Schrad: Characterization and Biomedical Applications. *Molecules: A Journal of Synthetic Chemistry and Natural Product*

Chemistry, 22(2), 301 (13 pages). <https://doi.org/10.3390/molecules22020301>

- Azizi, S., Mohamad, R., Bahadoran, A., Bayat, S., Rahim, R. A., Ariff, A., & Saad, W. Z. (2016). Effect of annealing temperature on antimicrobial and structural properties of bio-synthesized zinc oxide nanoparticles using flower extract of *Anchusa italica*. *Journal of Photochemistry and Photobiology B: Biology*, 161, 441–449. <https://doi.org/10.1016/j.jphotobiol.2016.06.007>
- Binnig, G., & Rohrer, H. (1987). Scanning tunneling microscopy---from birth to adolescence. *Reviews of Modern Physics*, 59(3), 615–625. <https://doi.org/10.1103/RevModPhys.59.615>
- Brooks, G. C., Carroll, K. C., Butel, J. S., & Morse, S. A. (2007). *Jawetz, Melnick & Adelberg's Medical Microbiology, 24th ed. The McGraw-Hill Companies, USA*. USA: The McGraw-Hill Companies.
- Bhuyan, T., Mishra, K., Khanuja, M., Prasad, R., & Varma, A. (2015). Biosynthesis of zinc oxide nanoparticles from *Azadirachta indica* for antibacterial and photocatalytic applications. *Materials Science in Semiconductor Processing*, 32, 55–61. <https://doi.org/10.1016/j.mssp.2014.12.053>
- Chaudhary, A., Kumar, N., Kumar, R., & Salar, R. K. (2018). Antimicrobial activity of zinc oxide nanoparticles synthesized from *Aloe vera* peel extract. *SN Applied Sciences*, 1(1), 136. <https://doi.org/10.1007/s42452-018-0144-2>
- Cho, E. J., Holback, H., Liu, K. C., Abouelmagd, S. A., Park, J., & Yeo, Y. (2013). Nanoparticle Characterization: State of the Art, Challenges, and Emerging Technologies. *Molecular Pharmaceutics*, 10(6), 2093–2110. <https://doi.org/10.1021/mp300697h>
- Coates, J. (2006). Interpretation of Infrared Spectra, A Practical Approach. In *Encyclopedia of Analytical Chemistry*. American Cancer Society. <https://doi.org/10.1002/9780470027318.a5606>

- Danila, A.O., Gatea, F., Radu, G.L. (2011). Polyphenol composition and antioxidant activity of selected medicinal herbs. *Chemistry of Natural Compounds* 47(1), 22–26. <https://doi.org/10.1007/s10600-011-9822-7>
- Datta, A., Patra, C., Bharadwaj, H., Kaur, S., Dimri, N., Khajuria, R. (2017). Green Synthesis of Zinc Oxide Nanoparticles Using *Parthenium hysterophorus* Leaf Extract and Evaluation of their Antibacterial Properties *Journal of Biotechnology & Biomaterials*, 7(3), 1–5. <https://doi.org/10.4172/2155-952X.1000271>
- Diebold, U., Koplitz, L. V., & Dulub, O. (2004). Atomic-scale properties of low-index ZnO surfaces. *Applied Surface Science*, 237(1–4), 336–342.
- Dobrucka, R., & Długaszewska, J. (2016). Biosynthesis and antibacterial activity of ZnO nanoparticles using *Trifolium pratense* flower extract. *Saudi Journal of Biological Sciences*, 23(4), 517–523. <https://doi.org/10.1016/j.sjbs.2015.05.016>
- Efstratiou, E., Hussain, A. I., Nigam, P. S., Moore, J. E., Ayub, M. A., & Rao, J. R. (2012). Antimicrobial activity of *Calendula officinalis* petal extracts against fungi, as well as Gram-negative and gram-positive clinical pathogens. *Complementary Therapies in Clinical Practice*, 18, 173 - 176.
- Elstrøm, P., Astrup, E., Hegstad, K., Samuelsen, Ø., Enger, H., & Kacelnik, O. (2019). The fight to keep resistance at bay, epidemiology of carbapenemase producing organisms (CPOs), vancomycin resistant enterococci (VRE) and methicillin resistant *Staphylococcus aureus* (MRSA) in Norway, 2006 - 2017. *PloS One*, 14(2), e0211741–e0211741. <https://doi.org/10.1371/journal.pone.0211741>
- Ezealisiji, K. M., Siwe-Noundou, X., Maduelosi, B., Nwachukwu, N., & Krause, R. W. M. (2019). Green synthesis of zinc oxide nanoparticles using *Solanum torvum* (L) leaf extract and evaluation of the toxicological profile of the ZnO nanoparticles–hydrogel composite in Wistar albino rats.

International Nano Letters, 9(2), 99-107. <https://doi.org/10.1007/s40089-018-0263-1>

Fierascu, I., Bunghez, I.-R., Fierascu, R.-C., Ion, R.-M., Dinu-Pîrvu, E., & Nuță, D. (2014). Characterization and antioxidant activity of phytosynthesised silver nanoparticles using *Calendula officinalis* extract. *Farmacologia*, 62(1), 129–136.

Fit, N. I., Rapuntean, G., Rapuntean, S., Chirila, F., & Nadas, G. C. (2009). Antibacterial Effect of Essential Vegetal Extracts on *Staphylococcus aureus* Compared to Antibiotics. *Notulae Botanicae Horti Agrobotanici Cluj-Napoca*, 37(2), 117–123. <https://doi.org/10.15835/nbha3723183>

Ghobadi, N. (2013). Band gap determination using absorption spectrum fitting procedure. *International Nano Letters*, 3(1), 2. <https://doi.org/10.1186/2228-5326-3-2>

Goktas, F.M., Sahin, B., & Yigitarslan, S. (2015) “Production of Sterilizing Agents from *Calendula officinalis* Extracts Optimized by Response Surface Methodology,” *International Journal of Analytical Chemistry*, vol. 2015, Article ID 789732. <https://doi.org/10.1155/2015/789732>.

Gomes Honório, I. C., Giardini Bonfim, F. P., Montoya, S. G., Dias Casali, V. W., Viana Leite, J. P., & Cecon, P. R. (2016). Growth, development and content of flavonoids in calendula (*Calendula officinalis* L.). *Crescimento, Desenvolvimento e Teor de Flavonoides Em Calêndula (Calendula Officinalis L.)*, 38(1), 69–75. <https://doi.org/10.4025/actasciagron.v38i1.25976>

Guo, T., Yao, M.-S., Lin, Y.-H., & Nan, C.-W. (2015). A comprehensive review on synthesis methods for transition-metal oxide nanostructures. *CrystEngComm*, 17(19), 3551–3585. <https://doi.org/10.1039/C5CE00034C>

Gupta, M., Tomar, R. S., Kaushik, S., Mishra, R. K., & Sharma, D. (2018). Effective Antimicrobial Activity of Green ZnO Nano Particles of

- Catharanthus roseus. *Frontiers in Microbiology*, 9, 2030. <https://doi.org/10.3389/fmicb.2018.02030>
- Hanci, H., Ayyildiz, A., Igan, H. (2017). Investigation of inducible clindamycin resistance in methicillin resistant Staphylococcus aureus strains. *Marmara Pharmaceutical Journal* 21, 1–5.
- Hashemi, S., Asrar, Z., Pourseyedi, S., & Nadernejad, N. (2016). Green synthesis of ZnO nanoparticles by Olive (*Olea europaea*). *IET Nanobiotechnology*, 10(6), 400–404. <https://doi.org/10.1049/iet-nbt.2015.0117>
- Heinrich, M., Barnes, J., Prieto Garcia, J.M., Williamson, E.M. (2018). *Fundamentals of Pharmacognosy and Phytotherapy*. Elsevier.
- Huang, Y.-W., Wu, C., & Aronstam, R. S. (2010). Toxicity of Transition Metal Oxide Nanoparticles: Recent Insights from in vitro Studies. *Materials*, 3(10), 4842–4859. <https://doi.org/10.3390/ma3104842>
- Ickrath, P., Wagner, M., Scherzad, A., Gehrke, T., Burghartz, M., Hagen, R., ... Hackenberg, S. (2017). Time-Dependent Toxic and Genotoxic Effects of Zinc Oxide Nanoparticles after Long-Term and Repetitive Exposure to Human Mesenchymal Stem Cells. *International Journal of Environmental Research and Public Health*, 14(12), 1590. <https://doi.org/10.3390/ijerph14121590>
- Jamdagni, P., Khatri, P., & Rana, J. S. (2018). Green synthesis of zinc oxide nanoparticles using flower extract of *Nyctanthes arbor-tristis* and their antifungal activity. *Journal of King Saud University - Science*, 30(2), 168–175. <https://doi.org/10.1016/j.jksus.2016.10.002>
- Jayanthi, P., & Lalitha, P. (2011). Reducing Power of the solvent extracts of *eichhornia crassipes* (Mart.) solms. *Int J Pharmacy Pharmaceutical Sci*, 3(3), 126-128.

- Jiang, J., Pi, J., Cai, J. (2018). The Advancing of Zinc Oxide Nanoparticles for Biomedical Applications. *Bioinorganic Chemistry and Applications*, vol. 2018, Article ID 1062562, 18 pages <https://doi.org/10.1155/2018/1062562>
- Khatami, M., Alijani, H. Q., Heli, H., & Sharifi, I. (2018). Rectangular shaped zinc oxide nanoparticles: Green synthesis by Stevia and its biomedical efficiency. *Ceramics International*, 44(13), 15596–15602. <https://doi.org/10.1016/j.ceramint.2018.05.224>
- Kołodziejczak-Radzimska, A., & Jesionowski, T. (2014). Zinc Oxide—From Synthesis to Application: A Review. *Materials*, 7(4), 2833–2881. <https://doi.org/10.3390/ma7042833>
- Konaté, K., Kiendrébéogo, M., Ouattara, M.B., Souza, A., Lamien-Meda, A., Nongasida, Y., Barro, N., Millogo-Rasolodimby, J. and Nacoulma, O.G. (2011). Antibacterial Potential of Aqueous Acetone Extracts From Five Medicinal Plants used Traditionally to Treat Infectious Diseases in Burkina Faso. *Current Research Journal of Biological Sciences*, 3(5): 435-442
- Korzh, A., Gur'ev, A., Belousov, M., Yusubov, M., & Belyanin, M. (2012). Composition of water-soluble polysaccharides from *Calendula officinalis* L. flowers. *Pharmaceutical Chemistry Journal*, 46(4), 219–221. <https://doi.org/10.1007/s11094-012-0765-5>
- Kumar, A., Chopra, E. K., Mukherjee, M., Pottabathini, R., & Dhull, D. K. (2015). Current knowledge and pharmacological profile of berberine: An update. *European Journal of Pharmacology*, 761, 288 - 297.
- Kumar, B., Smita, K., Cumbal, L., & Debut, A. (2014). Biogenic synthesis of iron oxide nanoparticles for 2-arylbenzimidazole fabrication. *SI: Nanomaterials for Energy and Environmental Applications*, 18(4), 364–369. <https://doi.org/10.1016/j.jscs.2014.01.003>

- Kumar, R., Umar, A., Kumar, G., & Nalwa, H. S. (2017). Antimicrobial properties of ZnO nanomaterials: A review. *Ceramics International*, 43(5), 3940–3961.
- Kumar, S., Chaudhury, K., Sen, P., & Guha, S. K. (2005). Atomic force microscopy: a powerful tool for high-resolution imaging of spermatozoa. *Journal of Nanobiotechnology*, 3, 9–9. <https://doi.org/10.1186/1477-3155-3-9>
- Lin, P.-C., Lin, S., Wang, P. C., & Sridhar, R. (2014). Techniques for physicochemical characterization of nanomaterials. *Biotechnology Advances*, 32(4), 711–726. <https://doi.org/10.1016/j.biotechadv.2013.11.006>
- Manokari, M. S. (2016). Green synthesis of zinc oxide nanoparticles using plant extracts of *Leucas aspera*. *International Journal of Biological Papers*, 1, 22 - 27.
- Marbella, L. E., & Millstone, J. E. (2015). NMR Techniques for Noble Metal Nanoparticles. *Chemistry of Materials*, 27(8), 2721–2739. <https://doi.org/10.1021/cm504809c>
- Marslin, G., Siram, K., Maqbool, Q., Selvakesavan, R. K., Kruszka, D., Kachlicki, P., & Franklin, G. (2018). Secondary Metabolites in the Green Synthesis of Metallic Nanoparticles. *Materials*, 11(6), 940. <https://doi.org/10.3390/ma11060940>
- Matinise, N., Fuku, X. G., Kaviyarasu, K., Mayedwa, N., & Maaza, M. (2017). ZnO nanoparticles via *Moringa oleifera* green synthesis: Physical properties & mechanism of formation. *Applied Surface Science*, 406, 339–347. <https://doi.org/10.1016/j.apsusc.2017.01.219>
- Mlynárik, V. (2017). Introduction to nuclear magnetic resonance. *Introduction to in Vivo Magnetic Resonance Spectroscopy (MRS): A Method to Non-*

Invasively Study Metabolism, 529, 4–9.
<https://doi.org/10.1016/j.ab.2016.05.006>

Mohammadian, M., Es'haghi, Z., & Hooshmand, S. (2018). Green and chemical synthesis of zinc oxide nanoparticles and size evaluation by UV-vis spectroscopy. *J Nanomed Res*, 7(1), 52–58.

Morkoç, H., & Özgür, Ü. (2009). *Zinc Oxide: Fundamentals, Materials and Device Technology*. Weinheim: WILEY-VCH Verlag GmbH & Co. KGaA.

Mourdikoudis, S., M. Pallares, R., & K. Thanh, N. T. (2018). Characterization techniques for nanoparticles: Comparison and complementarity upon studying nanoparticle properties. *Nanoscale*, 10(27), 12871–12934.
<https://doi.org/10.1039/C8NR02278J>

Mubashar Sabir, S., Khan, M. F., Rocha, J. B. T., Boligon, A. A., & Athayde, M. L. (2015). Phenolic Profile, Antioxidant Activities and Genotoxic Evaluations of *Calendula officinalis*. *Journal of Food Biochemistry*, 39(3), 316–324. <https://doi.org/10.1111/jfbc.12132>

Ogoshi, T., Umeda, K., Yamagishi, T., & Nakamoto, Y. (2008). Synthesis of Phenolic Polymer-Coated Gold Nanoparticles. *Polymer Journal*, 40(10), 942–943. <https://doi.org/10.1295/polymj.PJ2008069>

Park, S., Cha, S.-H., Cho, I., Park, S., Park, Y., Cho, S., & Park, Y. (2016). Antibacterial nanocarriers of resveratrol with gold and silver nanoparticles. *Materials Science and Engineering: C*, 58, 1160–1169.
<https://doi.org/10.1016/j.msec.2015.09.068>

Patil, B. N., & Taranath, T. C. (2018). *Limonia acidissima* L. leaf mediated synthesis of silver and zinc oxide nanoparticles and their antibacterial activities. *Microbial Pathogenesis*, 115, 227–232.
<https://doi.org/10.1016/j.micpath.2017.12.035>

Rajeshkumar, S., Kumar, S. V., Ramaiah, A., Agarwal, H., Lakshmi, T., & Roopan, S. M. (2018). Biosynthesis of zinc oxide nanoparticles using *Mangifera*

indica leaves and evaluation of their antioxidant and cytotoxic properties in lung cancer (A549) cells. *Enzyme and Microbial Technology*, 117, 91–95. <https://doi.org/10.1016/j.enzmictec.2018.06.009>

Rasmussen, K., Rauscher, H., Mech, A., Riego Sintes, J., Gilliland, D., González, M., ... Bleeker, E. A. J. (2018). Physico-chemical properties of manufactured nanomaterials - Characterisation and relevant methods. An outlook based on the OECD Testing Programme. *Regulatory Toxicology and Pharmacology*, 92, 8–28. <https://doi.org/10.1016/j.yrtph.2017.10.019>

Ross, M. B., Mirkin, C. A., & Schatz, G. C. (2016). Optical Properties of One-, Two-, and Three-Dimensional Arrays of Plasmonic Nanostructures. *The Journal of Physical Chemistry C*, 120(2), 816–830. <https://doi.org/10.1021/acs.jpcc.5b10800>

Sabir, S., Arshad, M., & Chaudhari, S. K. (2014). Zinc Oxide Nanoparticles for Revolutionizing Agriculture: Synthesis and Applications. *The Scientific World Journal*, vol. 2014, Article ID 925494, 8 pages. <https://doi.org/10.1155/2014/925494>

Sadatzadeh, A., Charati, F. R., Akbari, R., & Moghaddam, H. H. (2018). Green biosynthesis of zinc oxide nanoparticles via aqueous extract of cottonseed. *Journal of Materials and Environmental Sciences*, 9(10), 2849–2853.

Safdar, W., Majeed, H., Naveed, I., Kayani, W. K., Ahmed, H., Hussain, S., & Kamal, A. (2010). Pharmacognostical study of the medicinal plant *Calendula officinalis* L. (Family Compositae). *International Journal of Cell & Molecular Biology*, 1(2), 108–116.

Santhoshkumar, J., Kumar, S. V., & Rajeshkumar, S. (2017). Synthesis of zinc oxide nanoparticles using plant leaf extract against urinary tract infection pathogen. *Resource-Efficient Technologies*, 3(4), 459–465. <https://doi.org/10.1016/j.refffit.2017.05.001>

- Schaming, D., & Remita, H. (2015). Nanotechnology: From the ancient time to nowadays. *Foundations of Chemistry*, 17(3), 187–205. <https://doi.org/10.1007/s10698-015-9235-y>
- Shah, M., Fawcett, D., Sharma, S., Tripathy, S. K., & Poinern, G. E. J. (2015). Green Synthesis of Metallic Nanoparticles via Biological Entities. *Materials*, 8(11), 7278–7308. <https://doi.org/10.3390/ma8115377>
- Shyamala, S., & Vasantha, K. (2010). Free radical scavenging and antioxidant activity of leaves from Agathi (*Sesbania grandiflora*) (L.) Pers. *Am Eurasian J Sci Res*, 5(6).
- Siddiqi, K. S., ur Rahman, A., Tajuddin, & Husen, A. (2018). Properties of Zinc Oxide Nanoparticles and Their Activity Against Microbes. *Nanoscale Research Letters*, 13, Article number: 141 (2018) <https://doi.org/10.1186/s11671-018-2532-3>
- Stetefeld, J., McKenna, S. A., & Patel, T. R. (2016). Dynamic light scattering: A practical guide and applications in biomedical sciences. *Biophysical Reviews*, 8(4), 409–427. <https://doi.org/10.1007/s12551-016-0218-6>
- Supraja, N. P. (2016). Synthesis, characterization, and evaluation of the antimicrobial efficacy of *Boswellia ovalifoliolata* stem bark-extract-mediated zinc oxide nanoparticles. *Applied Nanoscience*, 6(4), 581 - 590.
- Talam, S., Karumuri, S. R., & Gunnam, N. (2012). Synthesis, Characterization, and Spectroscopic Properties of ZnO Nanoparticles. *ISRN Nanotechnology*, vol. 2012, Article ID 372505. <https://doi.org/10.5402/2012/372505>
- Tillhon, M., Ortiz, L. M., Lombardi, P., & Scovassi, I. (2012). Berberine: New perspectives for old remedies. *Biochemical Pharmacology*, 84, 1260 - 1267.
- Tobwala, S., Fan, W., Hines, C. J., Folk, W. R., & Ercal, N. (2014). Antioxidant potential of *Sutherlandia frutescens* and its protective effects against oxidative stress in various cell cultures. *BMC Complementary and Alternative Medicine*, 14, 271. <https://doi.org/10.1186/1472-6882-14-271>

- US EPA, O. (2013, February 12). Basics of Green Chemistry [Overviews and Factsheets]. Retrieved April 10, 2019, from US EPA website: <https://www.epa.gov/greenchemistry/basics-green-chemistry>
- Verma, P. K., Raina, R., Agarwal, S., & Kour, H. (2018). Phytochemical ingredients and pharmacological potential of *Calendula officinalis* Linn. *Pharmaceutical & Biomedical Research*, 4(2), 1–17.
- Villinski, J. R., Dumas, E. R., Chai, H.-B., Pezzuto, J. M., Angerhofer, C. K., & Gafner, S. (2003). Antibacterial Activity and Alkaloid Content of *Berberis thunbergii*, *Berberis vulgaris* and *Hydrastis canadensis*. *Pharmaceutical Biology*, 41(8), 551 - 557. <https://doi.org/10.1080/13880200390500768>
- Vimbela, G. V., Ngo, S. M., Frazee, C., Yang, L., & Stout, D. A. (2017). Antibacterial properties and toxicity from metallic nanomaterials. *International Journal of Nanomedicine*, 12, 3941–3965. <https://doi.org/10.2147/IJN.S134526>
- Zak, A. K., Razali, R., Majid, W. H. A., & Darroudi, M. (2011). Synthesis and characterization of a narrow size distribution of zinc oxide nanoparticles. *International Journal of Nanomedicine*, 6, 1399–1403. <https://doi.org/10.2147/IJN.S19693>
- Zhang, Y., Nayak, T. R., Hong, H., & Cai, W. (2013). Biomedical Applications of Zinc Oxide Nanomaterials. *Current Molecular Medicine*, 13(10), 1633–1645.